UNIVERSITÀ DEGLI STUDI DI MILANO

SCUOLA DI DOTTORATO IN SCIENZE E TECNOLOGIE CHIMICHE

DIPARTIMENTO DI CHIMICA INORGANICA, METALLORGANICA E ANALITICA "L. MALATESTA"

CORSO DI DOTTORATO IN CHIMICA INDUSTRIALE (XXIV CICLO)

TESI DI DOTTORATO DI RICERCA

03/B1

NEW POLYNUCLEAR LUMINESCENT TRICARBONYL RE(I) COMPLEXES CONTAINING MULTI-NITROGEN HETEROCYCLIC LIGANDS

Ph.D. student:
Alessio **RAIMONDI**

Tutor:
Prof. Giuseppe D'ALFONSO

Coordinatore:
Prof.ssa Dominique ROBERTO

ANNO ACCADEMICO 2010/2011

alla mia famiglia

ai miei amici

a me

Table of Contents

Table of Contents **I**

Chapter 1: Summary **1**

1.1 Luminescent dirhenium-pyridazine complexes containing bridging OR or SR anions (Chapter 3) 2

1.2 Dinuclear rhenium(I) complexes containing triazole and tetrazole ligands (Chapter 4) 12

1.3 Luminescent hydrido-carbonyl clusters of rhenium with square geometry (Chapter 5) 19

Chapter 2: Introduction **25**

2.1 Photophysics: general considerations 26

2.2 Luminescent transition metal complexes 31

2.2.1 Rhenium(I) complexes 36

Chapter 3: Luminescent dirhenium-pyridazine complexes containing bridging OR or SR anions **45**

3.1 Introduction 46

3.2 Results and discussion 47

3.2.1 Synthesis 47

3.2.2 Solid state structures 53

3.2.3 Computational study 555

3.2.4 Electrochemical characterization 60

3.2.5 Photophysical characterization 70

3.3 Conclusions 76

Chapter 4: Dinuclear rhenium(I) complexes containing triazole and tetrazole ligands **81**

4.1 Introduction 82

4.2 Results and discussion 85

4.2.1 Synthesis 85

4.2.2 Computational study 97

4.2.3 Electrochemical characterization 98

4.2.4 Photophysical characterization 101

4.3 Conclusions 105

Chapter 5: Luminescent hydrido-carbonyl clusters of rhenium(I) with square geometry **109**

5.1 Introduction 110

5.2 Results and discussion 114

5.2.1 Synthesis 114

5.2.1.1 Reaction of $[Re_4(\mu_3\text{-}H)_4(CO)_{12}]$ with 4,5-bis(trimethylsilyl)pyridazine 115

5.2.1.2 Reaction of $[Re_4(\mu_3\text{-}H)_4(CO)_{12}]$ with 6,7-dihydro-5*H*-cyclopentapyridazine 117

5.2.1.3 Reaction of $[Re_4(\mu_3\text{-}H)_4(CO)_{12}]$ with 1,8-naphthyridine 120

5.2.2 Preliminary photophysical characterization 122

5.3 Conclusions 124

Chapter 6: Experimental section **127**

6.1 Experimental techniques 128

6.1.1 Steady-state absorption and emission spectroscopy 128

6.1.2 Time-resolved fluorescence spectroscopy 131

6.1.3 Electrochemical measurements 132

6.1.4 Other techniques 134

6.2 Experimental section of Chapter 3 135

6.3 Experimental section of Chapter 4 141

6.4 Experimental section of Chapter 5 154

Chapter 1

SUMMARY

A brief summary of chapters 3-5 is here presented. The main results are discussed, and the properties of the investigated systems are also reported.

1.1 Luminescent dirhenium-pyridazine complexes containing bridging OR or SR anions (Chapter 3)

Rhenium carbonyl-diimine complexes, $[Re(CO)_3(N,N)L]$, exhibit photoluminescence from triplet Metal-to-Ligand-Charge Transfer (^{3}MLCT) excited states, which can be widely tuned by variations of the ancillary L ligands or of the substituents on the diimine ligand,[1] attaining very high photoluminescence quantum yields (PLQY) in the case of some cationic species.[2]

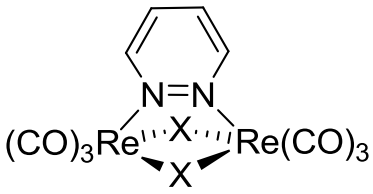

Chart 1.

A new family of luminescent rhenium(I) complexes, of general formula $[Re_2(\mu\text{-}X)_2(CO)_6(\mu\text{-}1,2\text{-diazine})]$ (Chart 1, X = hydrides[3] or halides[4,5]) has been recently developed. Wavelengths, lifetimes and quantum yields of the emission dramatically vary on varying the diazine substituents and the ancillary ligands X.[3,4,5] The derivatives with X = Cl and two alkyl groups in the β positions of the 1,2-diazine give the highest PLQYs, up to 0.53 in toluene solution at room temperature.[5] By contrast, the presence of substituents in the α positions nearly zeroes the emission, due to steric hindrance with the carbonyl ligands, which reduces the stiffness of the complex, promoting non-radiative deactivation pathways.[4] The replacement of chlorides by bulkier bromides and iodides freezes the emission too (in solution at room temperature),[4] in

agreement with the decreased rigidity of the coordination sphere on increasing the bulkiness of the bridging ligands.

We decided to investigate the photophysical properties of diazine complexes bearing polyatomic bridging ligands, with a twofold aim. Firstly we were interested in learning how to exploit the change of the ancillary ligands for controlling the HOMO-LUMO gap, and then modulating position and intensity of the emission. Secondly, the replacement of chlorides by polyatomic ligands might also provide other sites, besides the diazine ring, for functionalizing the dirhenium complexes, which might be useful for application as luminescent bio-probes, where the linking to suitable biomolecules is most often required.

The synthesis of a series of neutral dinuclear rhenium complexes of general formula $[Re_2(\mu\text{-}ER)_2(CO)_6(\mu\text{-pydz})]$ (E = S, R = C_6H_5, **2**; E = O, R = C_6F_5, **3**; C_6H_5, **4**; CH_3, **5**; H, **6**) has been performed. The method used for the preparation of the previously reported $[Re_2(\mu\text{-}X)_2(CO)_6(\mu\text{-diaz})]$ complexes (X = Cl, Br, I) cannot be followed in the present case, since $[Re(CO)_5(OR)]$ complexes are unstable and elusive species.[6] We therefore developed several alternative routes, using different starting materials, as summarized in Scheme 1.

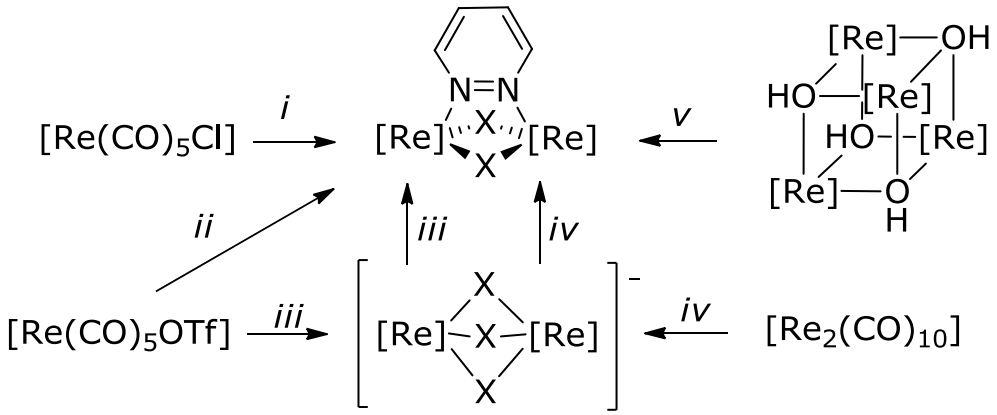

X = Cl (**1**); = SC_6H_5 (**2**); = OC_6F_5 (**3**); = OC_6H_5 (**4**); = OCH_3 (**5**); = OH (**6**)

[Re] = $Re(CO)_3$; *i*: **1**; *ii*: **2**, **4**; *iii*: **3**; *iv*: **5**; *v*: **6**

Scheme 1. The different synthetic routes *i-v* leading to complexes **1**-**6**.

The new rhenium complexes **2**-**6** have been studied by means of density functional and time-dependent density functional (TD-DFT) computations by Dr. Pierluigi Mercandelli of the Department of Structural Chemistry and Inorganic Stereochemistry of the Università degli Studi di Milano. Partial orbital diagrams and views of the isodensity surface plots of the HOMOs are reported in Figure 1.

The substitution of halides by ER groups does not modify significantly the nature of the frontier orbitals and of the absorption/emission processes, which maintain the previously described Metal-Ligand-to-Ligand Charge Transfer character. As already found for **1**,[4,5] LUMO and LUMO+1 are the two lowest-lying π^* orbitals of the coordinated pyridazine. The following four MO (from LUMO+2 to LUMO+5) are the e_g set of the two Re atoms, showing in addition a large C≡O π^* character. For species **5** and **6** the six HOMOs are the t_{2g} set of the two Re atoms in a pseudo-octahedral environment. In particular, the three highest lying orbitals show a strong Re–(μ-O) π^* character, in close analogy

with the halogenated derivatives previously described.[4] The bridging ER groups are deeply involved in the HOMO set, whose energy progressively rises on increasing the ER donor power (a part the deviant behavior of the OH derivative), with consequent easier oxidation of the complex and reduced band gap. Accordingly a progressively red shifted and weakened emission is observed on going from OC_6F_5 to OC_6H_5 to OCH_3 (and OH) and to SC_6H_5.

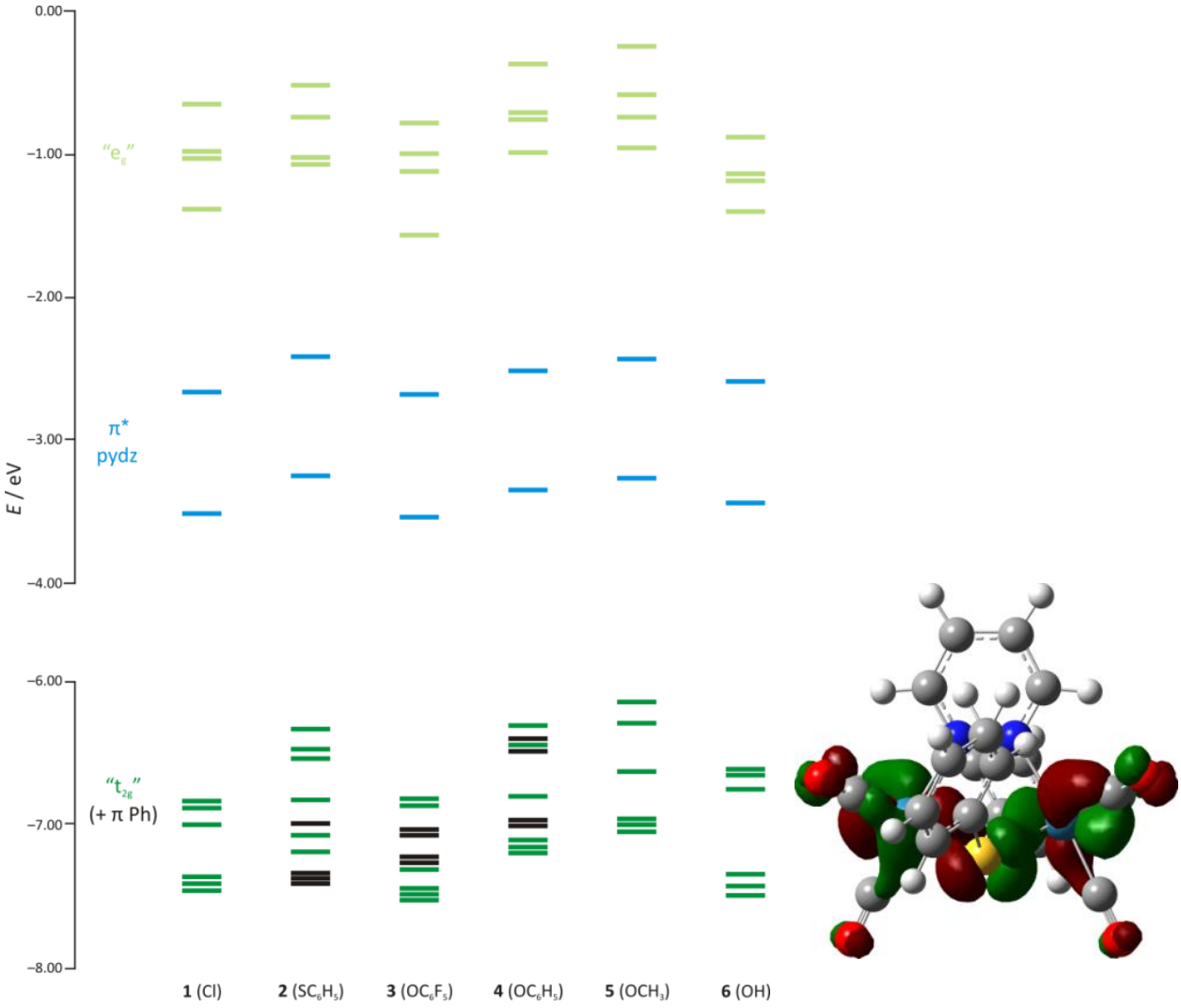

Figure 1. Left: partial molecular orbital diagram for the complexes **1**-**6**. The black lines are referred to the π orbitals of the phenyl groups in complexes **2**-**4**. Right: frontal views of the isodensity surface plots of the highest occupied molecular orbital (HOMO) of complex **2**.

Figure 2 shows the results of cyclic voltammetry (CV) analyses of complexes **2**-**6** in MeCN solution (in collaboration with Prof. Patrizia Mussini of the Department of Physical Chemistry and Electrochemistry of the Università degli Studi di Milano), including, for comparison, the previously published data concerning the dichloro complex **1** and the analogous dibromo and diiodo derivatives **1'** and **1"**.[4]

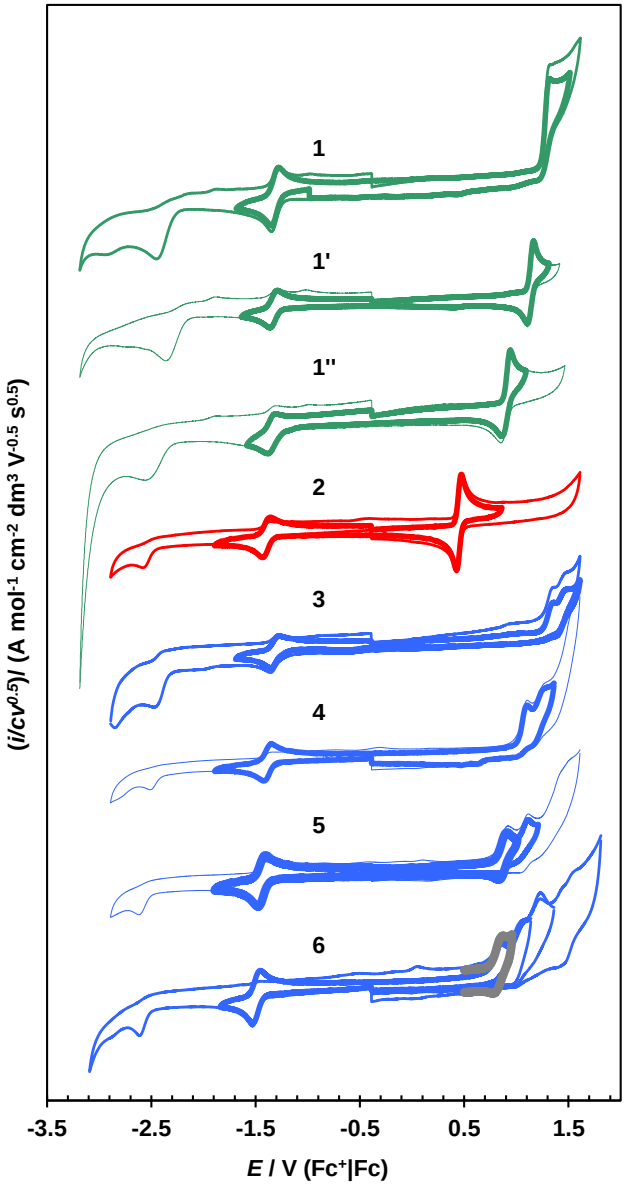

Figure 2. Normalized CV features for complexes **1**-**6** and the three complexes with halide ligands previously investigated **1**, **1'**, **1''** (green lines), recorded on GC electrode at 0.2 V s^{-1} in MeCN solution. The gray line for **6** refers to a scan at 2 V s^{-1}.

The first reduction peaks are monoelectronic and reversible, and must be localized for all complexes on their common pyridazine ligand, consistently with previous work.[4] Accordingly such peaks are quite similar for all complexes. As to the oxidation, in the series of the OR derivatives **3**-**6**, a close sequence of two monoelectronic peaks is observed, differently from the thio derivative **2**, which shows the bielectronic and reversible oxidation peak already observed in the halide cases. Another surprising feature of **2** is the value of its oxidation potential (0.47 V), much lower than that of the phenolato derivative **4** (1.1 V), in spite of the close similarity of their HOMO energies (Figure 1).

Figure 3a shows a plot of the E_p values (for compounds **2**-**6** and the related halide derivatives **1**, **1'**, and **1"**[4]) vs. the energies computed for the HOMO in vacuo. Two trends can be clearly recognized. The sulphur derivative **2** perfectly fits with the trend of the complexes bearing halide ancillary ligands, whilst the phenolato **4** agrees with the trend of the OR derivatives.

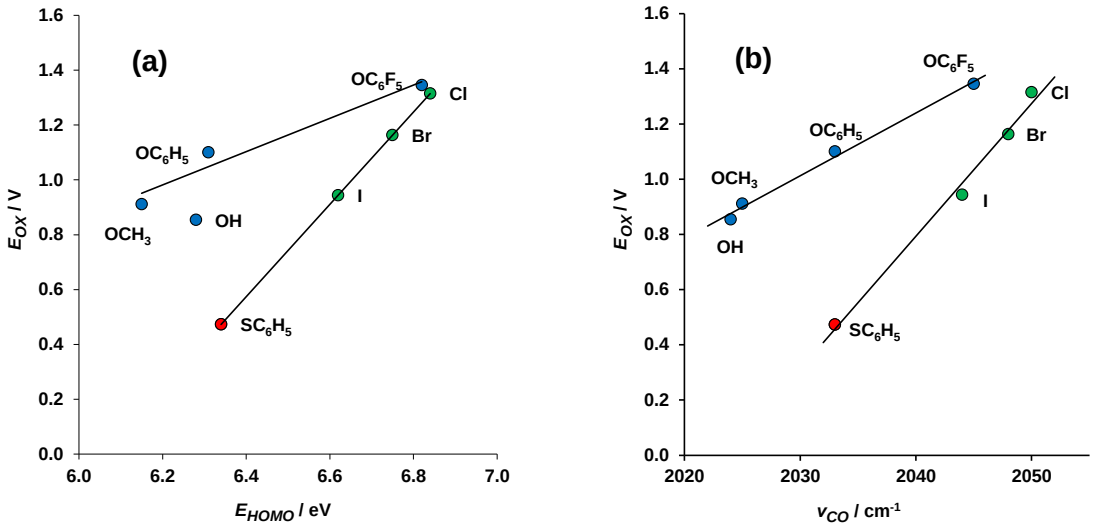

Figure 3. Plot of the first oxidation E_p values (measured in MeCN solution) vs. (a) the vacuum computed HOMO energies, and (b) the wavenumbers of the highest energy (totalsymmetric) ν(CO) band (MeCN solution).

An impressively similar two-trend plot (Figure 3b) is obtained by correlating the measured oxidation potentials with the ν(CO) values of the stretching modes, which are reliable indicators of the electron density on the metal atom. These findings fully support the view that the oxidation process is markedly different in the case of the oxygen-bridged derivatives (which show two monoelectronic oxidation steps) with respect to the other four complexes, which exhibit a single bielectronic oxidation step.

In the UV-Vis region all the complexes show spectra dominated by two main absorption features (Figure 4). On the basis of TD-DFT computations, the bands at higher energy, whose position (ca. 270 nm) is independent of the polarity of the solvent, can be attributed to the superposition of many singlet *d-d* excitations from the t_{2g} set to the e_g set of the two Re atoms.

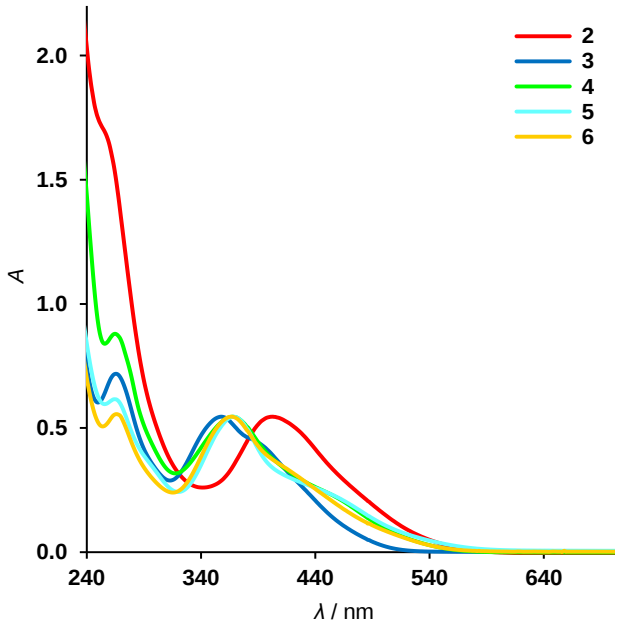

Figure 4. UV-Vis absorption spectra of complexes **2**-**6** in CH_2Cl_2 solution at room temperature.

The lower energy absorption bands, can be assigned to Metal-Ligand-to-Ligand Charge Transfer (MLLCT) transitions, taking into account the significant contribution of the bridging ancillary ligands to the metal-centered HOMO set.

The charge-transfer character of such transitions is supported by their strong solvent dependence:[7] indeed, a blue shift is observed upon increasing solvent polarity (e.g. from 363 nm in toluene to 335 nm in MeCN for **3**, see Figure 5).

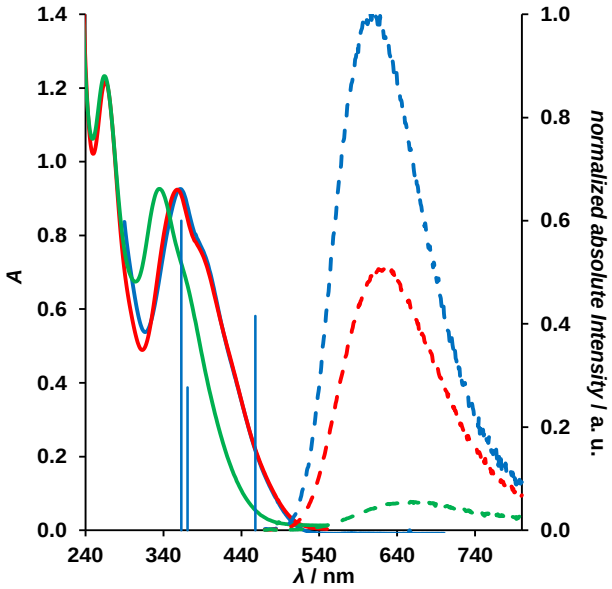

Figure 5. Solvent effect on the absorption (**—**) and emission (---) spectra of **3**. A comparison with excitation energies and oscillator strengths (vertical blue lines) computed in toluene is reported. Blue: toluene; red: dichloromethane; green: acetonitrile.

All the complexes with bridging OR groups show broad, featureless photoluminescence in the red region of the visible spectrum (range 608 ÷ 708 nm). The photoluminescence spectra for complexes **3**-**6** are shown in Figure 6 and the data are summarized in Table 1.

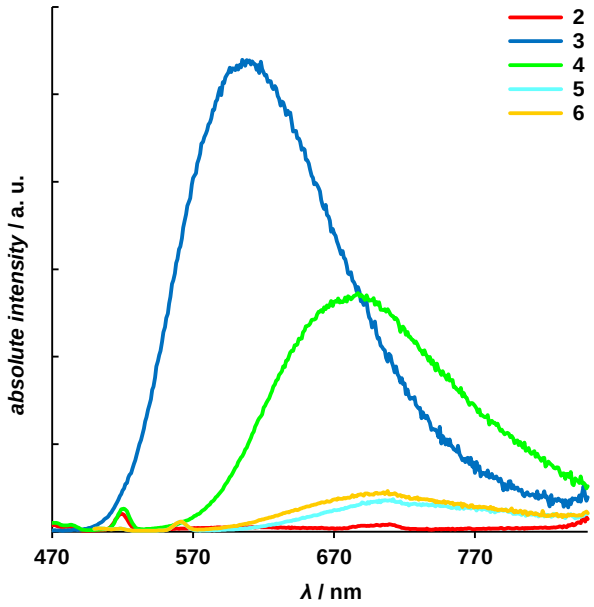

Figure 6. Effect of the ancillary OR or SR ligands on the emission spectra, recorded at room temperature in deoxygenated toluene solution, upon excitation at 450 nm (for **2**-**4**) or 480 nm (for **5** and **6**). The emission intensity of the OC_6F_5 derivative **3** has been decreased 5 times with respect to the other complexes.

Complex	**X**	λ_{abs} ($\varepsilon \times 10^{-3}$) [nm, $M^{-1}cm^{-1}$]	λ_{em} [nm]	Φ_{em} [a] × **10^2**	τ [a] [ns]	k_r x **10^{-5}** [s^{-1}]	k_{nr} x **10^{-5}** [s^{-1}]
1	Cl	379 (8.1)	603	7.0	800	0.88	11.6
2	SC_6H_5	403 (7.0)	-	-	-	-	-
3	OC_6F_5	362 (7.6)	608	5.5	550	1.0	17.2
4	OC_6H_5	374 (6.9)	680	0.55	37	1.5	270
5	OCH_3	372 (8.7)	708	0.07	8.6	0.81	1160
6	OH	369 (8.0)	702	0.09	9.2	0.98	1090

Table 1. Photophysical data of complexes **1**-**6** in toluene solution. [a] In deoxygenated toluene at room temperature.

These results confirm that it is possible to modulate the photophysical properties of the Re_2-diazine complexes in a two-fold manner: the variation of the substituents on the chromophoric moiety (the diazine ring) affects the LUMO level (as observed in the series of the dichloro derivatives[4]), while the

variation of the ancillary ligands modifies the HOMO level. The photoluminescence quantum yields of the synthesized complexes **3**-**6** agree with the Energy Gap Law, and the non-radiative rate constants (k_{nr}) values roughly lie on the same line as the previously reported dichloro derivatives.[4] This indicates that the nature of the excited states and the pathways responsible for their non-radiative deactivation are little affected by the nature of the bridging ancillary ligands X, provided that these ones do not perturb the stiffness of the [Re_2(μ-X)$_2$(μ-diazine)] core. The behavior of the bis-pentafluorophenolato derivative **3** is comparable to that of the dichloro complex **1**.

1.2 Dinuclear rhenium (I) complexes containing triazole and tetrazole ligands (Chapter 4)

A new family of neutral dinuclear complexes of rhenium containing bridging 1,2,4-triazoles has been synthesized, in which either electron-donor or electron-withdrawing substituents are bound to the 4 position of the triazole (Chart 2).

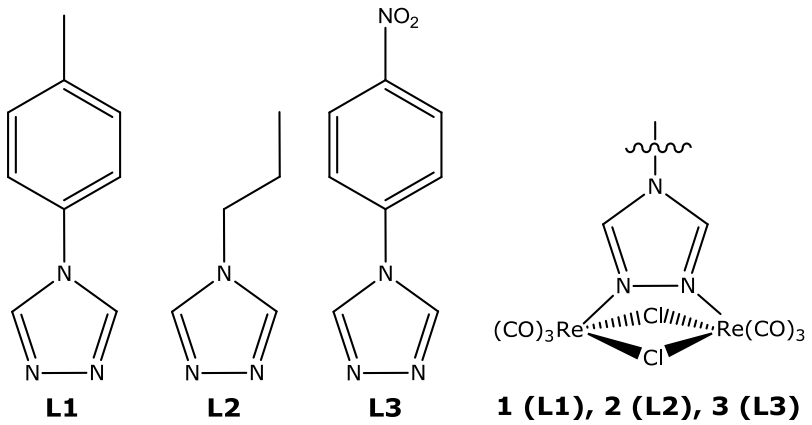

Chart 2. The synthesized ligands **L1**-**L3** and the corresponding rhenium complexes **1**-**3**.

The synthesis of ligands **L1**-**L3** involves reaction between N,N'-diformylhydrazine, (obtained by N-formylhydrazine and triethyl orthoformate in MeOH), and the appropriate primary amine. The corresponding Re(I) complexes **1**-**3** were obtained in acceptable yields by refluxing the appropriate triazole and two equivalents of $[Re(CO)_5Cl]$ in toluene solution.

Cyclic voltammetric analyses of complexes **1**-**3** are reported in Figure 7. The first reduction peak centered on the triazole is observed around -2.5 V (vs. $Fc^+|Fc$), indicating a much easier reduction than the free ligand (coordination stabilizes LUMO).

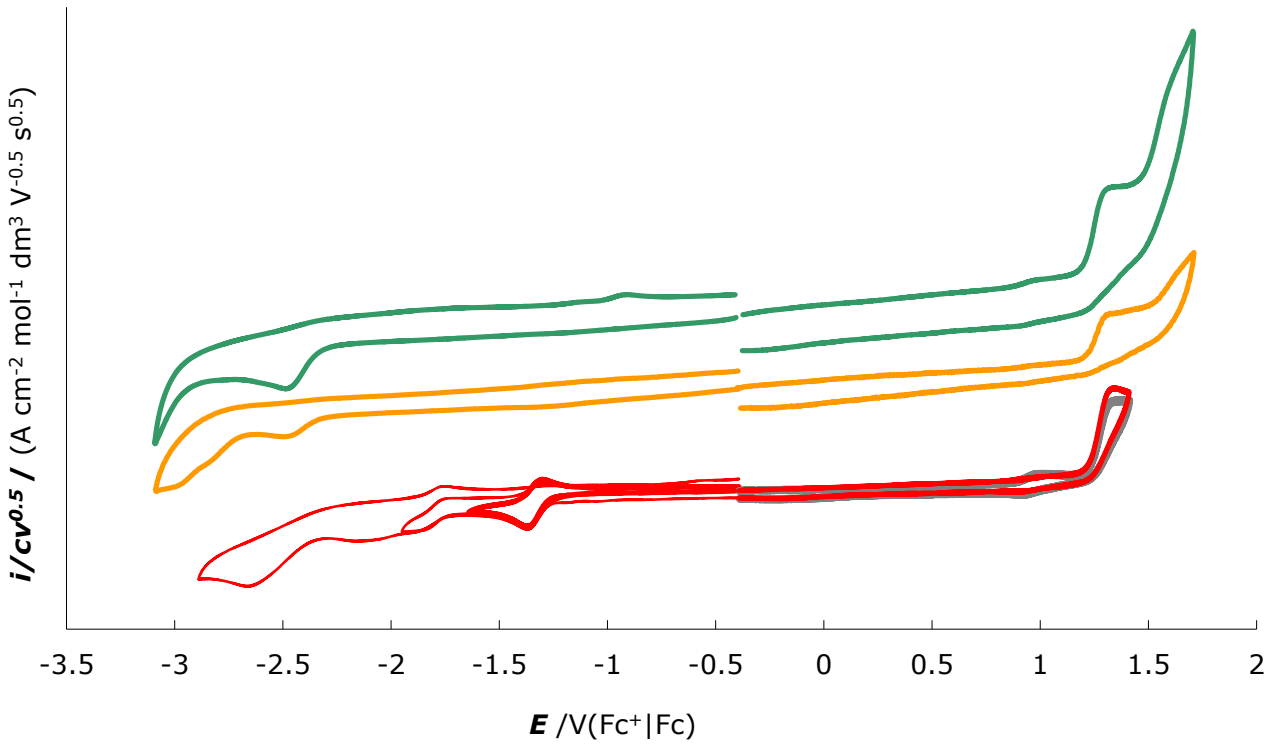

Figure 7. Cyclovoltammetric analysis of complexes **1** (yellow line), **2** (green line) and **3** (red line) recorded in MeCN solution at room temperature. The gray superimposed curve in complex **3** refers to apparent solvolysis process.

All complexes show a bielectronic oxidation peak at ca. +1.3 V (vs. $Fc^+|Fc$), similar to the ones observed in the corresponding diazine complexes,[4,5] clearly indicating that the oxidation is metal centered. The presence of a more electron-withdrawing ligand (the triazole) makes the oxidation more difficult with respect to the complex with 1,2-diazines. As in the case of the oxadiazole derivative,[8] both the oxidation and the reduction processes are chemically and electrochemically irreversible.

In the case of complex **3** the LUMO is more stabilized and is localized on the nitro group; accordingly, the monoelectronic first reduction happens at a remarkably less negative potential. As a consequence, the electrochemical HOMO-LUMO gap is much narrower (of about 1 eV).

The strong withdrawing character of the nitro group in derivative **3** is probably responsible for the slow solvolysis by the acetonitrile solvent (gray superimposed curve recorded after about half an hour), possibly yielding a monomeric rhenium complex species, as in our formerly studied 3,6-dichloropyridazine case.[4] The insertion of strong electron attractor groups on the diazine or triazole ligand decreases the electron donating ability of the two nitrogen atoms bridging the two rhenium atoms, and therefore destabilizes the complex, especially in a solvent like MeCN, highly competitive in cation coordination.

DFT calculations showed that the HOMO sets of complexes **1**-**3** are essentially constituted by combinations of the t_{2g} orbitals of the two metals, with a contribution, in the higher energy levels, of the *p* orbitals of the ancillary ligands, while the LUMO levels are localized on the triazole and phenyl ring π^* orbitals (Figure 8).

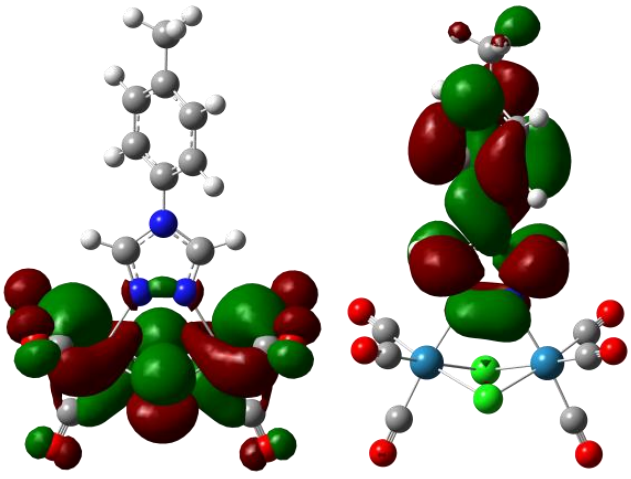

Figure 8. Views of the isodensity surface plots of the HOMO (left) and LUMO (right) of **1**.

The free ligands show two absorption bands in the UV region (Figure 9). The lower energy band is attributable to a n-π* transition, with a contribution of the π-π* transition of the phenyl group in the 4 position as confirmed by the shift of the relative band from 232 to 282 nm going from to **L1** to **L3**, due to the electron-withdrawing character of the nitro group, which decreases the π* level. Moreover, for both the ligands, the position of the band is slightly solvent-dependent, in accord with the weak charge transfer character of such n-π* transitions. The band at higher energy (~ 190 nm) is mainly ascribed to a π-π* transition. The third weaker band in the spectrum of **L3** (~ 217 nm) is due to transitions involving the nitro group.

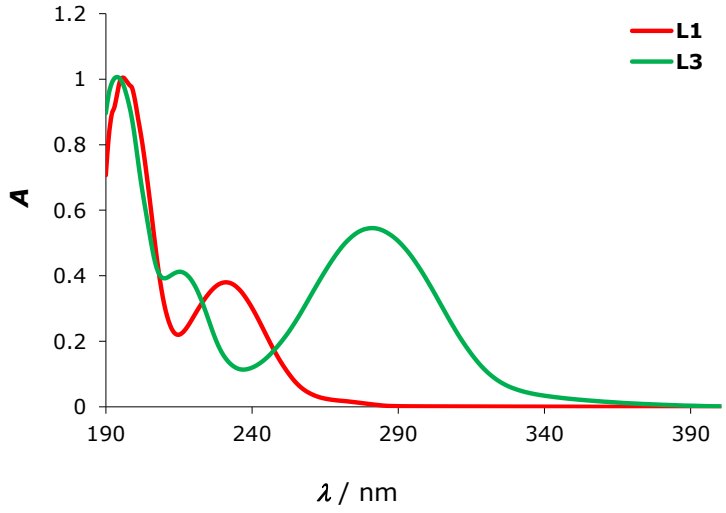

Figure 9. Absorption spectra of **L1** and **L3** in MeCN solution at room temperature.

All the complexes show an absorption band at 195 nm (Figure 10) attributed to π-π* transitions of both aromatic and heterocyclic rings, and at least two very broad absorption at lower energy assigned mainly to ^{1}MLCT transitions, on the basis of DFT calculations.

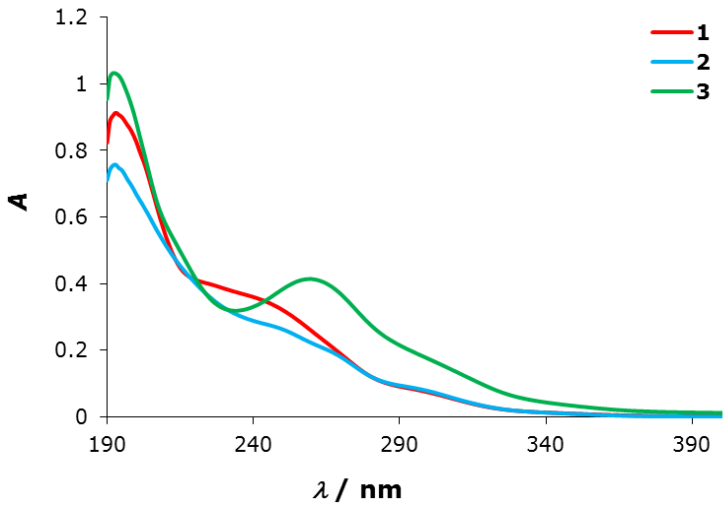

Figure 10. Absorption spectra of complexes **1**-**3** in MeCN solution at room temperature.

The ^{1}MLCT bands are blue-shifted by ca. 50 nm with respect to the corresponding diazine complexes, in line with the raising of the LUMO levels and the higher HOMO-LUMO gap (about 3.8 eV for **1** and **2** vs. 2.66 for the dichloro-pydz derivative[4]). As far as the substituent effect is concerned, the MLCT bands of **3** are shifted to lower energy, as expected for the presence of the electron-withdrawing nitro group.

All the complexes resulted to be bad emitters, as the oxadiazole derivative:[8] very weak bands in the range 350-450 nm were observed after excitation at 300 nm. In the case of the oxadiazole derivative, the lack of emission had been attributed to the poor stiffness of the complex, due to the low basicity of oxadiazole and the significant steric hindrance determined by the presence of two phenyl substituents in ortho position. This should not be the case for the complexes here presented, since the lack of substituents in ortho position and the better σ-donor proprieties of the ligand should improve the stiffness of the complexes. Therefore, the lack of emission might be

attributed to photoinstability or to LUMO destabilization, which allows the overlap between the potential energy surfaces of MLCT triplet states and those of d^{π}-$d^{\sigma*}$ type states, whose decay to the ground state is spin forbidden.

Also the synthesis of neutral dinuclear rhenium complexes containing as bridging ligands one 1,2-diazine and one or two 1,2,4-triazolate anions has been tried, in order to obtain luminescent complexes, thanks to the presence of the pyridazine chromophore. Moreover, these compounds are expected to be potential building blocks for the assembly of mono or two dimensional coordination polymers, due to the third donor nitrogen atom on the triazolate ligands.[9] Preliminary experiments suggest that the formation of the desired complex is actually feasible, provided the optimization of a purification procedure from the many (albeit in low concentration) byproducts. Noteworthy is the obtainment of the new anion $[Re_2(\mu\text{-triazolate})_3(CO)_6]^-$, from $[Re_2(\mu\text{-}OCH_3)_3(CO)_6]^-$ and molten triazole. The formation of dinuclear complex in which two metal centres are linked by three double bridging triazolates is rare and was never reported before for complexes of metals in low oxidation state.[10]

The synthesis of complexes with tetrazole ligands was performed in collaboration with Dr. Stefano Stagni of the Inorganic and Physical Chemistry Department of the Università di Bologna, who provided us the ligand 2-(*t*-butyl)-5-phenyl-2*H*-tetrazole (**L4**) (Chart 3). An alkyl-tetrazole was chosen in order to obtain neutral complexes. The reaction with $[Re(CO)_5Cl]$, performed in

the same conditions as before described, afforded a mixture of at least three dinuclear species.

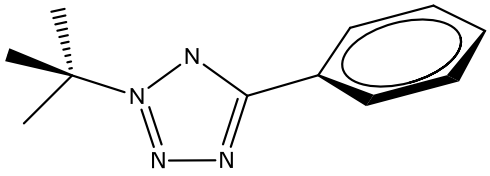

L4

Chart 3.

The best characterized product is the anion [{$Re_2(\mu\text{-}Cl_2)(CO)_6$}$_2$(μ-5-phenyl-5*H*-tetrazolate] (**4**), in which a single tetrazolate anion acts as a bridging ligand towards the to two Re(μ-Cl)$_2$Re units using all its four nitrogen atoms. This coordination, shown in Figure 11, is rather unusual, at least for rhenium complexes, although in the literature examples of tetrazolate anions acting as tetradentate ligands are known.[11]

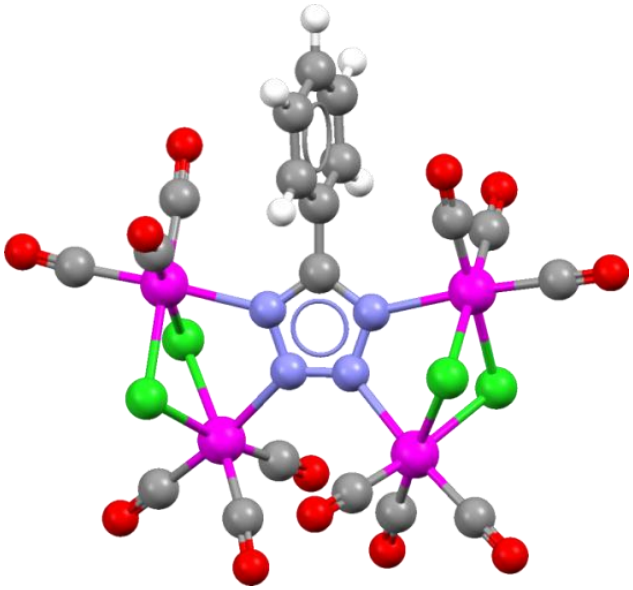

Figure 11. ORTEP view of complex **4**.

1.3 Luminescent hydrido-carbonyl clusters of rhenium with square geometry (Chapter 5)

A large number of electronically unsaturated hydrido-carbonyl clusters of rhenium have been synthesized and characterized in the past,[12,13] much larger than for any other transition metal. In a previous work of my group[3] the reactivity of the unsaturated tetranuclear complex $[Re_4(\mu_3\text{-}H)_4(CO)_{12}]$ (**1**) towards pyridazine and phtalazine was deeply investigated. Different reaction paths have been identified (Scheme 2), and the photophysical properties of the main products have been determined.

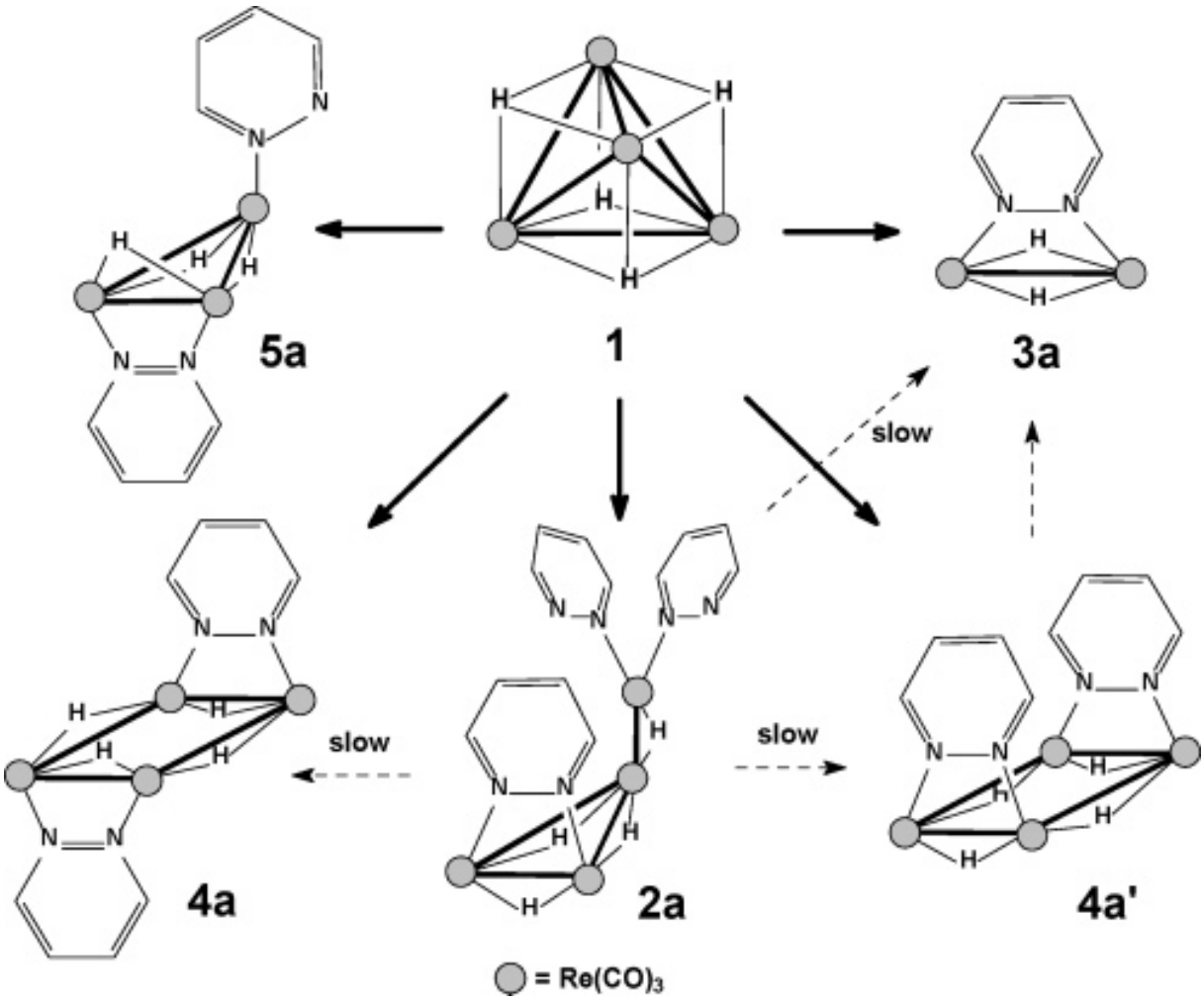

Scheme 2. Reaction paths of $[Re_4(\mu_3\text{-}H)_4(CO)_{12}]$ (**1**) in presence of pyridazine.

We were interested in understanding how the photophysical properties of these clusters can be affected using different 1,2-diazines. We choosed 4,5-bis(trimethylsylil)pyridazine (**L5**) and 6,7-dihydro-5*H*-cyclopentapyridazine (**L6**) (Chart 4) because their corresponding dichloro complexes show very high PLQYs, in solid (**L5**) or in solution (**L6**).[5,14] Moreover, the presence of bulky substituents in the 4 and 5 positions could influence the fragmentation path of the parental clusters **1**.

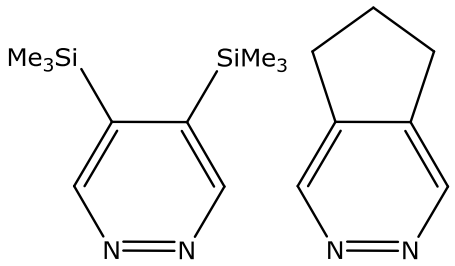

L5 **L6**

Chart 4.

The reaction of **1** with **L5** has been monitored by ^{1}H NMR spectroscopy (Figure 12, these species are noted by letter b): at the beginning of the reaction the prevalent species is the spiked triangle **2b**, that rapidly converts mainly into the dimer **3b** (that is soluble) and in the *trans*-square **4b**, that is partially soluble and slowly precipitates as an orange microcrystalline solid.

Noteworthy, the *cis*-square **4b'** is not formed, due to the steric hindrance of the $SiMe_3$ groups on the pyridazine ring. Also the triangular specie **5b** is negligible. The reaction of **1** with **L2** has a similar trend (noted by letter c), but in this case the *trans*-square species **4c** is almost insoluble in the reaction solvent, and precipitates as a yellow powder.

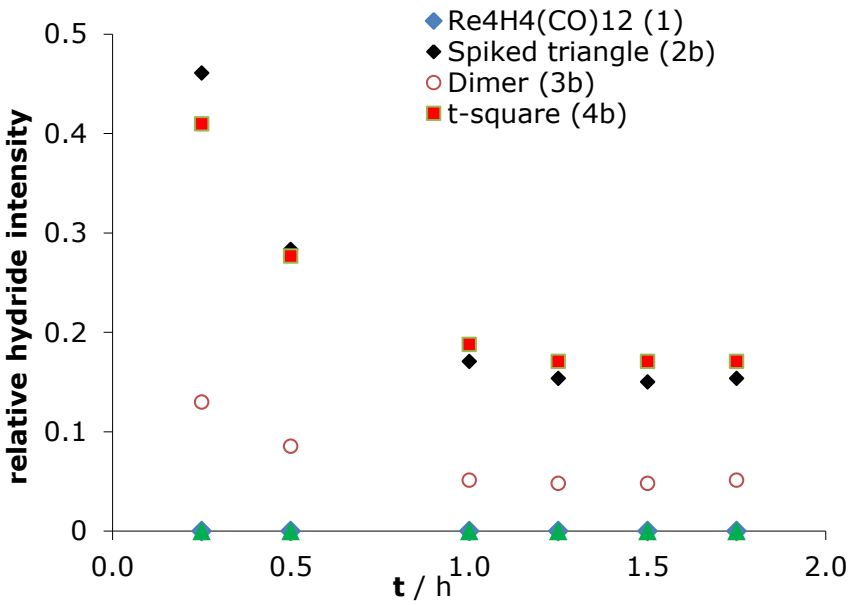

Figure 12. ^{1}H NMR monitoring of the course of the reaction of **1** with 2 equivalents of **L5** (CD_2Cl_2, 298 K). In the ordinate, the fraction of the overall hydride intensity for each species is reported.

The experimental (electrochemical, photophysical) and computational characterization of these new complexes is still in progress. The available spectroscopic data are summarized in Table 2. The *trans*-square complexes **4b** and **4c** are weaker emitters than the corresponding *trans*-square with pyridazine.[3] Therefore the observed variation of luminescence does not follow the same trend of the $[Re_2(\mu\text{-}Cl)_2(CO)_6(\mu\text{-}1,2\text{-diazine})]$ compounds, indicating that no straightforward transfer of information from one class to another is possible, since the factors affecting the photophysical properties are well different in the two classes of complexes.

Complex	X	λ_{abs} [nm]	λ_{em} [nm]	$\Phi_{em} \times 10^2$
4b	**L5**	412	644	0.80
4c	**L6**	397	601	0.20
4a	**pydz**	401	611	1.7

Table 2. Preliminary absorption and emission data of *trans*-square complexes **4b**, **4c** and **4a** in (deoxygenated) CH_2Cl_2 solution at room temperature.

Finally, also the reaction of **1** with 1,8-naphthyridine (**L3**) has been investigated, in order to understand how a different steric hindrance and the capability to act both as bridging and chelating ligand could influence the reaction pathways as well as the photophysical properties of the reaction products.

(1) See for instance a) Kumar, A.; Sun, S.-S.; Lees, A. J. *Top. Organomet. Chem.* **2010**, *29*, 1-35; b) Yam, V. W.-W., Wong, K. M.-C. *Chem. Commun.* **2011**, *47*, 11579-11592;

(2) See for instance a) Villegas, J. M.; Stoyanov, S. R.; Huang, W.; Rillema, D. P. *Inorg. Chem*. **2005**, *44*, 2297-2309; b) Tseng, Y.-H.; Bhattacharya, D.; Lin, S.-H.; Thanasekaran, P.; Wu, J.-Y.; Lee, L.-W.; Sathiyendiran, M.; Ho, M.-L.; Chung, M.-W.; Hsu, K.-C.; Chou, P.-T.; Lu, K.-L. *Inorg. Chem.* **2010**, *49*, 6805-6807;

(3) Panigati, M.; Donghi, D.; D'Alfonso, G.; Mercandelli, P.; Sironi, A.; Mussini, P.; D'Alfonso, L. *Inorg. Chem.* **2006**, *45*, 10909-10921;

(4) Donghi, D.; D'Alfonso, G.; Mauro, M.; Panigati, M.; Mercandelli, P.; Sironi, A.; Mussini, P.; D'Alfonso, L. *Inorg. Chem.* **2008**, *47*, 4243-4255;

(5) Mauro, M.; Quartapelle Procopio, E.; Sun, Y.; Chien, C.H.; Donghi, D.; Panigati, M.; Mercandelli, P.; Mussini, P.; D'Alfonso, G.; De Cola, L. *Adv. Funct. Mater*. **2009**, *19*, 2607-2614;

(6) See Lucenti, E.; D'Alfonso, G.; Macchi, P.; Maranesi, M.; Roberto, D.; Sironi, A.; Ugo, R. *J. Am. Chem. Soc.* **2006**, *128*, 12054-12055, and refs therein;

(7) Giordano, P. J.; Wrighton, M. S. *J. Am. Chem. Soc.* **1979**, *101*, 2888-2897;

(8) Mauro, M.; Panigati, M.; Donghi, D.; Mercandelli, P.; Mussini, P.; Sironi, A.; D'Alfonso, G. *Inorg. Chem.* **2008**, *47*, 11154-11165;

(9) Barea, E.; Rodriguez-Diéguez, A.; Navarro, J. A. R.; Sironi, A.; D'Alfonso, G. *Dalton Trans.* **2008**, 1825-1827;

(10) Aromí, G.; Barrios, L. A.; Roubeau, O.; Gamez, P. *Coord. Chem. Rev*. **2011**, *255*, 485-546;

(11) Zhao, H.; Qu, Z.-R.; Ye, H.-Y.; Xiong, R.-G. *Chem. Soc. Rev.* **2008**, *37*, 84-100;

(12) Horng, H. C.; Cheng, C. P.; Yang, C. S.; Lee, G.-H. *Organometallics* **1996**, *15*, 2543-2547;

(13) Beringhelli, T.; D'Alfonso, G. *J. Chem. Soc., Chem. Commun*. **1994**, 2631-2632;

(14) Quartapelle Procopio, E.; Mauro, M.; Panigati, M.; Donghi, D.; Mercandelli, P.; Sironi, A.; D'Alfonso, G.; De Cola, L. *J. Am. Chem. Soc*. **2010**, *132*, 14397-14399.

Chapter 2

INTRODUCTION

General considerations about photophysics are here presented. A brief presentation of Re(I) compounds is also present, with particular attention to the families that have been studied in this thesis.

2.1 Photophysics: general considerations

Electromagnetic radiation and matter can interact each other in different way, prevalently dependent on the energy of the involved photons. In a molecule, the most important interaction is the conversion of the energy of a photon in electronic energy, and the subsequent transfer of an electron to an orbital of higher energy (generally, from a bonding or non-bonding orbital to an anti-bonding orbital). In this way, the molecule goes from the ground, non-excited, electronic state to an higher energy excited state. Due to the higher energy as well as the different electronic configuration respect to the ground state, the excited states of a chemical specie possess different chemical and physical properties, as for instance different reactivity, geometry and dipolar moment. For these reasons, an excited species should be considered chemically different with respect to the non-excited one.

A photon can be absorbed by a molecule with the subsequent promotion of an electron in an excited state only if its energy, $h\nu$, exactly corresponds to the energy difference between the initial and final states (equation 1).

$$A + h\nu \rightarrow A^* \qquad \text{(eq. 1)}$$

It is important to note that the absorption of a photon is an extremely fast process (10^{-15} s) with respect to the all other processes and even to the nuclei motion (*Frank-Condon principle*). Hence, the nuclei are considered at their ground state position immediately after generation of the excited state.

So, the excited specie is unstable and relaxes in different times and in competitive ways: 1) conversion to the ground state, with only production of heat (non radiative decay); 2) conversion to the ground state, with emission of a photon (radiative decay), process called *photo-luminescence*; 3) transformation in other chemical species (photochemical reaction).[1]

A simple method to depict the molecule-light interaction relies on a state energy diagram (Figure 1), usually called "Jablonski diagram", which schematically describes all the possible photophysical processes, where photon absorption, internal conversion, fluorescence, intersystem crossing, phosphorescence and vibrational relaxation are the most common. Each state is usually labeled by its *spin multiplicity* and a number according to the relative energy. For example, S_0, S_1 and S_2 represent *singlet* states of increasing energy and a total spin quantum number equal to zero. On the other hand, the excited states which have a total spin of 1 and possess multiplicity of 3, are *triplet* states (T_1, T_2, T_3…). The latter have a lower energy than the singlet states in the same configuration. Furthermore, vibrational levels are associated with each electronic state, thus we actually consider transitions that lead to different *vibronic* states. Transitions within vibronic states can be due to radiative processes (straight lines in Figure 1) if an absorption/emission of electromagnetic radiation occurs, or to non-radiative processes (wavy lines), with only production of heat.

Theory as well as experience have proved that the major photophysical -phenomena take place from the lowest vibrational state of the first excited state of a species (*Kasha's rule*), therefore, after the absorption process, a fast

internal conversion followed by vibrational relaxations brings the species to the S_1 state.

A set of "selection rules" (electronic, vibrational and spin) governs the transition probabilities. Transitions between states with identical spin multiplicity are allowed, thus singlet-singlet and triplet-triplet processes are the most favorite and give rise to intense bands in the absorption and emission spectra. Singlet–triplet and triplet–singlet transitions are usually forbidden.

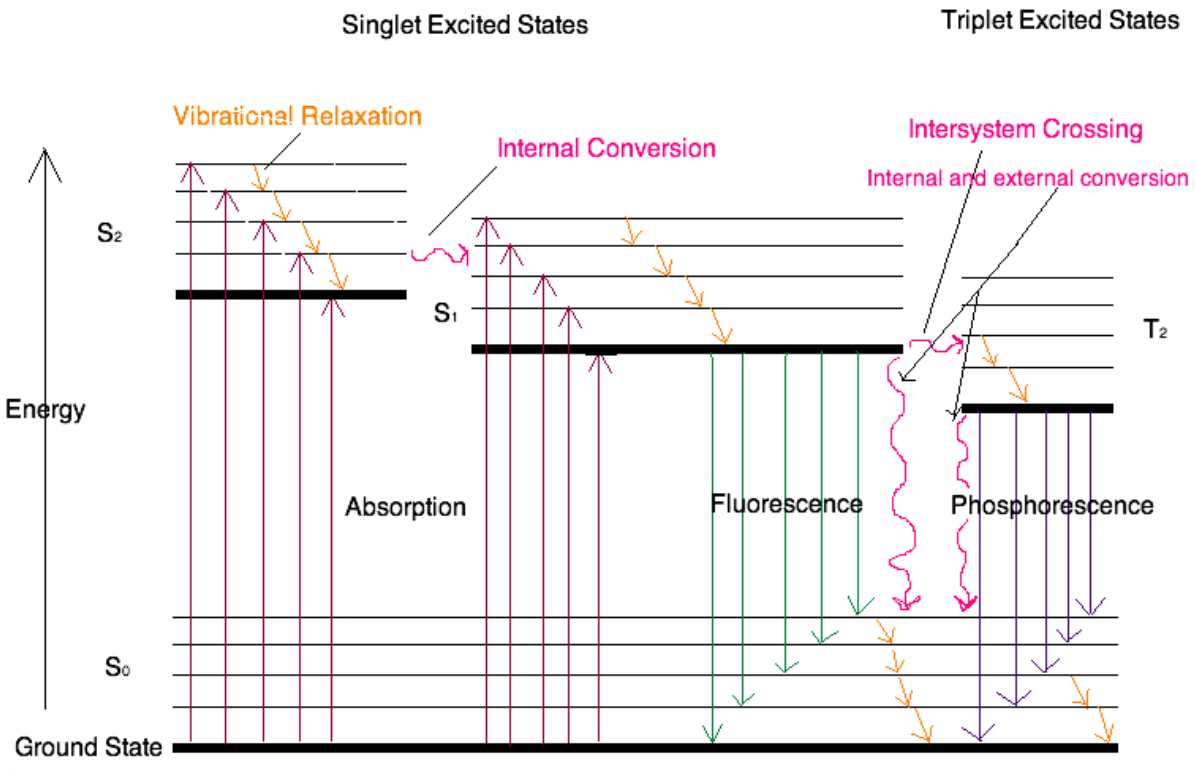

Figure 1.1. Simplified Jablonski diagram. The main electronic transitions and their corresponding rate constants are depicted.

The emission of a photon is called photoluminescence and is typically divided into two categories, depending on the nature of the emitting excited state: *fluorescence* ($S_1 \rightarrow S_0$, equation 2) and *phosphorescence* ($T_1 \rightarrow S_0$,

equations 1.2 and 1.3, where A indicates a chemical species in its ground state and A* in an excited state).

$$^1A^* \rightarrow {}^1A + h\nu' \qquad \text{(eq. 2)}$$

$$^3A^* \rightarrow {}^1A + h\nu'' \qquad \text{(eq. 3)}$$

It is worth to note that in solution at room temperature, phosphorescence is a spin-forbidden process, as above stated, thus triplet states decay non radiatively to the ground state. However, there is often an interaction between wavefunctions of different multiplicities via spin–orbit coupling (i.e. coupling between the orbital magnetic moment and the spin magnetic moment). The efficiency of this coupling varies with the fourth power of the atomic number (Z), which explains why the above mentioned rule is not obeyed in the case of complexes of heavy metals (see below). In some case, the spin-orbit coupling can be large enough to make intersystem crossing (ISC) possible.

Another consequence of the Kasha's rule is that the mentioned processes involving S_1 and T_1 states are all in direct competition. The physico-chemical nature of the excited species, as well as the environmental and experimental conditions (temperature, media, concentration…) determine whether fluorescence, phosphorescence or non-radiative transitions dominates the deactivation path.

The most important parameters for describing an emitting excited state are the lifetime, τ, and the emission quantum yield, Φ_{em}. The excited-state lifetime is equal to the mean time during which molecules remain in the excited state. Since the emission process is kinetically a first order process (equations 2 and 3), the lifetime is defined as

$$\tau = \frac{1}{\Sigma_i k_i} = \frac{1}{k_{em} + k_{ic} + k_{isc} + k_{nr}} \qquad \text{(eq. 4)}$$

where k_{em} is the sum of the emission rate constants, k_{ic} of internal conversion, k_{isc} of intersystem crossing and k_{nr} the sum of non radiative decays. In general, the lifetime of a singlet excited state ranges from tens picoseconds to several nanoseconds, whereas triplet lifetimes are much longer (microseconds to seconds) due to their spin-forbidden nature.

On the other hand, the emission quantum yield is the number of emitted photons relative to the number of absorbed photons and it can be also expressed in terms of kinetic rate constant, as in the equation 5:

$$\Phi_{em} = \frac{emitted\ photons}{absorbed\ photons} = \frac{k_r}{k_r + k_{nr}} \Rightarrow 0 \leq \Phi_{em} \leq 1 \qquad \text{(eq. 5)}$$

2.2 Luminescent transition metal complexes

The photophysical properties of transition metal complexes exhibit a number of interesting features due to their more complex structure compared to a general organic molecule. As already mentioned, the presence of a heavy metal atom could induce a considerable degree of spin-orbit coupling, to such an extent that spin-forbidden electronic transitions may become sufficiently allowed. This effect is particularly evident for metals belonging to the second and third row of the transition metals block. In particular, d^6 transition metal complexes as Ru(II), Re(I) and Ir(III) have a closed-shell ground state electronic configuration and the ground state has a singlet spin multiplicity (S_0). In these complexes, the strong spin-orbit coupling leads to efficient ISC from the lowest singlet excited state (S_1) to the lowest triplet manifold (T_1). Furthermore the same effect induces a mixing between the singlet and triplet excited states, eliminating the spin-forbidden nature of the $T_1 \rightarrow S_0$ transition and resulting in phosphorescent complexes. Differently from fluorescent organic molecules, the efficiency of ISC in such complexes can be close to unity, providing emission only as phosphorescence, even at room temperature.

A simplified method to describe the electronic structure of metal complexes is illustrated by the crystal field theory.[2] In this approach, ligands are treated as negative point charges which set up an electrostatic field. It results that, in an octahedral complex, the five metal *d* orbitals (which are normally degenerate) are split into two sets, because of their different spatial orientation which makes them not equivalent. One set consists of three

equivalent orbitals labelled t_{2g}, and the second one of two equivalent orbitals labelled e_g. The e_g orbitals, which point directly toward the ligands, are higher in energy than the t_{2g} orbitals, which point between the ligands. The magnitude of splitting between these two sets is generally denoted as Δ. Its value varies on varying the central ion, and usually increases with the principal quantum number in the periodic table (i.e. Δ increases as follows: Ru(II) (4*d*) < Re(I) (5d) < Ir(III) (5*d*)) . It is also dependent on the field strength of the ligands, that can be ordered along the so called "spectrochemical series".[3]

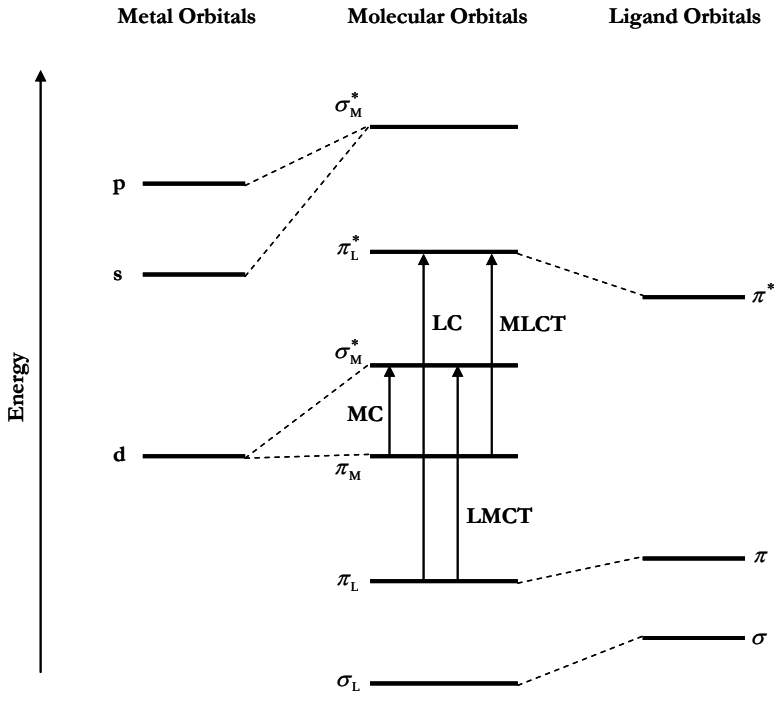

Figure 2. Schematic molecular orbital for a metal complex with octahedral geometry. The main electronic transitions involved in the absorption process are depicted.

In the Molecular Orbital (MO) theory, for an octahedral complex the *d* electron can be divided in two set, with π and $\sigma*$ character, corresponding to t_{2g} and e_g sets of the crystal field theory. In Figure 2 is show a typical MO diagram for a metal complex with octahedral geometry.

Although the electronic structure of a complex must be treated as a single entity, it is convenient to divide the electrons into two separate sets, one mainly localized on the metal centre and a second set mainly located on the ligand.

By using the Molecular Orbital (MO) theory, four types of electronic transitions are typically observed in an absorption process for octahedral metal complexes (Figure 2): 1) *metal-centered* (MC) transitions between MOs localized on the metal; 2) *ligand-centered* (LC) transitions, where the electron promotion considers only π MOs mainly involving to the ligands; 3) *ligand-to-metal charge transfer* (LMCT) transitions, where the absorbed photon causes a movement in electron density from a ligand centered MO to a metal centered MO; 4) *metal-to-ligand charge transfer* (MLCT) transitions, where the electron density moves from a mainly metal centered MO to a mainly ligand centered one. Singlet and triplet states labeled as MC, LC, LMCT and MLCT can be in principle found, however the nature of metal and ligands influences the relative energy ordering of these states and only some of them actively participate to the photophysical deactivation processes stimulated by a photon.

Among d^6 metal complexes, important differences are found in the electronic energy of the MC states, and in particular on the lowest lying one. This state is usually not emissive since it is strongly coupled to the ground state via non radiative decay and/or to ligand dissociation reactions. As already mentioned, for metal atoms lying on the first row of the periodic table, as Fe(II) (3*d* orbitals), the ligand field splitting Δ is so small that the lowest excited state for Fe(II)-polyimine complexes, as for instance $[Fe(bpy)_3]^{2+}$

where bpy is 2,2'-bipyridine, is mostly MC in character.[4,5] On the other hand, the analogous Ru(II) complexes are only partially deactivated, at room temperature, by the ^{3}MC state. Now, the lowest excited (and emitting) state is a ^{3}MLCT in nature and is thermally equilibrated with the ^{3}MC state, giving rise generally to poorly emissive complexes.[6] On the contrary, Re(I) and even more Ir(III) (5*d* orbitals) exhibit a very large Δ value and the ^{3}MC level are pushed so high in energy with respect to the emissive ^{3}MLCT and ^{3}LC levels, that usually do not affect the emission properties (Figure 3).

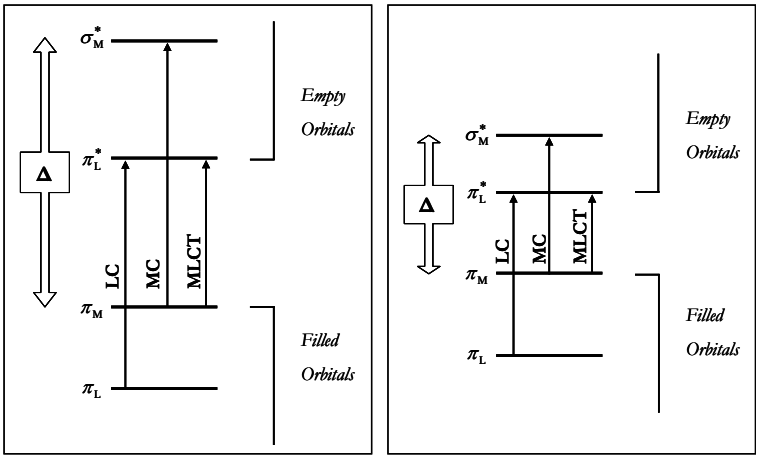

Ir(ppy)$_3$ **[Ru(bpy)$_3$]$^{2+}$**

Figure 3. Simplified molecular orbital diagram for two of the most important luminescent complexes, namely Ir(ppy)$_3$ and [Ru(bpy)$_3$]$^{2+}$, in octahedral symmetry showing the three main types of electronic transitions occurring at low energies. The ligand field splitting energy (Δ) is shown on the left side. For clarity, the LMCT transition is not shown.

Thus, a careful choice of the employed ligands is crucial in order to increase the Δ splitting and to avoid the parasitic radiationless deactivation channels involving the ^{3}MC level.

The amount of Δ splitting is also reflected in the emission quantum yields, which are usually higher for iridium than for ruthenium complexes for

the reasons above discussed. This behavior is in agreement with the so-called *energy gap law*, which indicates that the rate constant of non-radiative transitions (k_{nr}) increases with a decrease of the *energy gap* (ΔE) between the emissive state and the ground state (equation 6):

$$k_{nr} = \alpha \, exp^{-\beta \Delta E} \qquad \text{(eq. 6)}$$

where α and β are constant. In other words, due to the increase of the non-radiative rate constant, the lower is the energy of the emitted radiation the poorer is the emission quantum yield of the complex.

In the MO approximation, oxidation and reduction processes could be viewed as metal or ligand centred. For d^6 metal complexes with central atoms having small ionization potentials and "strong" ligands with easily available empty π^* orbitals, as for example $[Ru(bpy)_3]^{2+}$ or $Ir(ppy)_3$, the lowest excited state is normally assigned to a ^{3}MLCT transition. This transition can be *formally* viewed as oxidation of the metal ion and reduction of the ligand in the excited state. For the same case of metal complexes bearing "strong" ligands, the highest-occupied molecular orbital (HOMO) is most usually metal centered (in some cases, with the contribution of the ligand), while the lowest-unoccupied molecular orbital (LUMO) is ligand centered. Since the HOMO and LUMO orbitals are the ones involved in oxidation and reduction processes, the electrochemical properties result to be strictly related to the nature of the frontier orbitals.

2.2.1 Rhenium(I) complexes

Rhenium(I) complexes occupy a prominent position among luminescent transition metal complexes. The photochemistry and photophysics of carbonyl rhenium(I) complexes has been widely investigated, and Re(I) occupies a prominent position among luminescent transition metals. After the early preparative studies on photosubstitution of carbonyl species like $Re(CO)_5X$, seminal works on the preparation and characterization of luminescent mononuclear tricarbonyl rhenium complexes, of general formula *fac*-$Re(CO)_3(\alpha,\alpha'$-diimine)Cl, were reported by Wrighton and co-workers in the 70s.[7]

Most of the studied rhenium complexes contain, besides the three carbonyl ligands, a chromophoric diimine ligand (*N*-*N*) and a monodentate ancillary ligand (X). On varying the charge of the latter ligand, neutral or cationic complexes can be obtained, of general formula $[Re(CO)_3(N\text{-}N)X]$ and $[Re(CO)_3(N\text{-}N)X]^+$ respectively. The diimine ligands are either 2,2'-bipyridine or 1,10-phenanthroline, or one of their derivatives, although derivatives of 2,2'-bipyrimidine have also been reported.[8,9] In these complexes, the d orbital of the rhenium atom and the three carbonyls moieties contribute to the HOMO, for the cationic $[Re(N\text{-}N)(CO)_3(X)]^+$ species, while a further contribution from the anionic ancillary ligand X should be taken into account in the case of neutral complexes of general formula $[Re(N\text{-}N)(CO)_3(X)]$. On the contrary, the LUMO mainly consists of the π^* orbital of the diimine ligand in both cases.

Thus, the lowest lying optical transition is generally described as a metal-ligand-to-ligand charge transfer transition (MLLCT).[10]

However, it must be considered that the ^{1}MLCT absorption band, although occurring at lower energy with respect to the π-π^* diimine ligand centered transition (LC), often lies on the shoulder of it. Thus, a simultaneous population of both the ^{1}MLCT and ^{1}LC levels can occur. By varying the electronic properties of both the chromophoric and ancillary ligands, a modulation of the ^{3}MLCT and ^{3}LC energies as well as their relative energetic separation are possible, and consequently a change in the emission properties takes place. Thus, emission spectra are often found to drop in the 500 nm region with strong vibronic character consistent with a large ^{3}LC contribution. In other cases, the spectra show featureless emission around 600 nm which are assignable to a ^{3}MLCT state. However, a combination of ^{3}LC and ^{3}MLCT state is often taken into account for rationalizing the emission behavior, because the emission is red-shifted from that of the free ligand.

Indeed, by increasing the π-donor strength of an axial ligand the character of the lowest excited state changes from MLCT to LLCT. On the other hand, the presence of a covalently bound axial ligand in the coordination sphere introduces a $\sigma\pi^*$ lowest excited state that involves excitation of an electron from the metal–ligand σ-bonding orbital to the π^* orbital of the α-diimine. While the orbital parentage of the lowest excited state (MLCT, LLCT, $\sigma\pi^*$ or IL) is mostly determined by the axial ligand(s), its detailed properties (energy, lifetime, reactivity, decay mechanism) are dependent on both the

axial and diimine ligands. Depending on the molecular structure and the medium, the excited state behavior of these complexes ranges from a relatively strong, long-lived emission to a very fast photochemical homolysis of a metal–ligand bond.[11]

It is worth to note that rhenium possesses a lower Δ splitting as well as a weaker spin-orbit coupling respect to the later transition metal atoms. These features are reflected in generally poorer emission properties, both in terms of photoluminescence quantum yield and modulation of the emission color, with respect to iridium(III) and platinum(II) complexes. Indeed, neutral rhenium complexes showed Φ_{em} usually lower than 0.05, and emission wavelengths that did not go lower than 500 nm in fluid dearated solution, although some cationic complexes have shown better performances, with Φ_{em} up to 0.77.[12]

However, the interest toward the photochemical and photophysical properties of these complexes is far from being on a decline, due to their broad range of applications. These include photoredox chemistry,[13] chemi- or electrochemiluminescence,[14] chemical and biological sensing,[15,16] and bio-conjugation.[17] Recently, several papers have appeared dealing with their use as phosphorescent dopants for Organic Light Emitting Diodes (OLED),[18] and also as electroluminescent emitters in single-layer OLED devices.[19]

A possible way to overcome this limits is to enhance the spin-orbit coupling by linking two heavy metal atoms on the same ligand, whose orbitals are involved in the emission process. 1,2-diazines, such as pyridazine, are able to act as a bridge between two rhenium atoms, although few examples of

complexes containing 1,2-diazines are present in the literature, probably due to their steric requirements that seem to be unfavorable compared to the typical diimine ligands.

However, in my research group some dinuclear rhenium complexes some of which have shown really high photoluminescence quantum yields both in solution and solid state have been recently synthesized and characterized. These compounds, of general formula $[Re_2(\mu\text{-}X)_2(CO)_6(\mu\text{-}1,2\text{-diazine})]$ (Chart 1, X = hydrides[20] or halides[18a,21]), exhibit emission from triplet metal-to-ligand-charge transfer (^{3}MLCT) excited states.

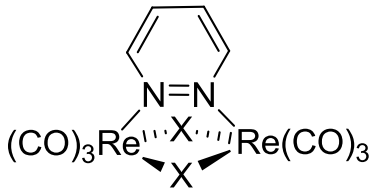

Chart 1.

Wavelengths, lifetimes and quantum yields of the emission dramatically vary on varying the diazine substituents and the ancillary ligands X.[18a,20,21] The presence of electron-donating groups, as alkyl chains, in the positions 4 and 5 of the diazine ligand increases the HOMO-LUMO gap. The derivatives with X = Cl and two alkyl groups in the β positions of the diazine give the highest photoluminescence quantum yields (PLQY), up to 0.53 in toluene solution at room temperature.[21] By contrast, the presence of substituents in the α positions nearly zeroes the emission, due to steric hindrance with the carbonyl ligands, which reduces the stiffness of the complex, promoting non-radiative deactivation pathways.[21] The replacement of chlorides by bulkier bromides and

iodides freezes the emission too (in solution at room temperature),[21] in agreement with the decreased rigidity of the coordination sphere on increasing the bulkiness of the bridging ligands.

(1) L. Moggi, A. Juris, M. T. Gandolfi, *Manuale del fotochimico*, Bonomia University Press, **2006**;

(2) M. Montalti, A. Credi, L. Prodi, M. T. Gandolfi, *Handbook of Photochemistry,* (*3rd Edition*, Taylor & Francis, **2006**;

(3) D. M. Roundhill, *Photochemistry and Photophysics of Metal Complexes*, Plenum Press, New York **1994**;

(4) C. Hamann, A. von Zelewsky, A. Neels, H. Stoeckli-Evans, *Dalton Trans.* **2004,** 402-406;

(5) P. S. Braterman, J. I. Song, R. D. Peacock, *Inorg. Chem.* **1992**, *31*, 555-559;

(6) A. Juris, V. Balzani, F. Barigelletti, S. Campagna, P. Belser, A. Von Zelewsky, *Coord. Chem. Rev.* **1988**, *84*, 85-277;

(7) M. Wrighton and D. L. Morse, *J. Am. Chem. Soc.*, **1974**, *96*, 998;

(8) L. Wallace and D. P. Rillema, *Inorg. Chem.* **1993**, *32*, 3836-3834;

(9) A. Juris, S. Campagna, I. Bidd, J.M. Lehn, and R. Ziessel, *Inorg. Chem.* **1988**, *27*, 4007-4011;

(10) S. R. Stoyanov, J. M. Villegas, A. J. Cruz, L. L. Lockyear, J. H. Reibenspies, D. P. Rillema *J. Chem. Theory Comput.* **2005**, *1*, 95;

(11) D. J. Stufkens, A. Vlček Jr, *Coord. Chem. Rev.* **1998**, *177*, 127-179;

(12) See for instance a) Villegas, J. M.; Stoyanov, S. R.; Huang, W.; Rillema, D. P. *Inorg. Chem*. **2005**, *44*, 2297-2309; b) Tseng, Y.-H.; Bhattacharya, D.; Lin, S.-H.; Thanasekaran, P.; Wu, J.-Y.; Lee, L.-W.; Sathiyendiran, M.; Ho, M.-L.; Chung, M.-W.; Hsu, K.-C.; Chou, P.-T.; Lu, K.-L. *Inorg. Chem.* **2010**, *49*, 6805-6807;

(13) See for instance: (a) Tsubaki, H.; Sekine, A.; Ohashi, Y.; Koike, K.; Takeda, H.; Ishitani, O. *J. Am. Chem. Soc.* **2005**, *127*, 15544–15555. (b) Gibson, D. H.; He, H. *Chem. Commun.* **2001**, 2082–2083, and refs therein. See also: (c) Kalyanasundaram, K. *J. Chem. Soc., Faraday Trans. 2* **1986**, *82*, 2401–2415;

(14) Richter, M. M. *Chem. Rev.* **2004**, *101*, 3003–3036;

(15) (a) Beck, D.; Brewer, J.; Lee, J.; McGraw, D.; DeGraff, B. A.; Demas, J. N. *Coord. Chem. Re*V. **2007**, *251*, 546–553. (b) Sathiyendiran, M.; Liao, R.-T.; Thanasekaran, P.; Luo, T.-T.; Venkataramama, N. S.; Lee, G.-H.; Peng, S.-M.; Lu, K.-L. *Inorg. Chem.* **2006**, *45*, 10052–10054. (c) Wong, K. M.-C.; Li, W.-P.; Cheung, K.-K.; Yam, V. W.-W. *New. J. Chem.* **2005**, *29*, 165–172. (d) Huynh, L.; Wang, Z.; Yang, J.; Stoeva, V.; Lough, A.; Manners, I.; Winnik, M. A. *Chem. Mater.* **2005**, *17*, 4765–4773. (e) Bare, W. D.; Mack, N. H.; Xu, W.; Demas, J. N. *Anal. Chem.* **2002**, *74*, 2198–2209. (f) Lee, S. J.; Lin, W. *J. Am. Chem. Soc.* **2002**, *124*, 4554–4555. (g) Uppadine, L. H.; Keene, F. R.; Beer, P. D. *J. Chem. Soc., Dalton Trans.* **2001**, 2188–2198. (h) Cooper, J. B.; Drew, M. G. B.; Beer, P. D. *J. Chem. Soc., Dalton Trans.* **2000**, 2721–2728. (i) Beer, P. D.; Tomoshenko, V.; Maestri, M.; Passaniti, P.; Balzani, V. *Chem. Commun* **1999**, 1755–1756;

(16) (a) Blanco-Rodriguez, A. N.; Busby, M.; Gradinaru, C.; Crane, B. R.; Di Bilio, A. J.; Matousek, P.; Towrie, M.; Leigh, B. S.; Richards, J. H.; Vlcˇek, A., Jr; Gray, H. B. *J. Am. Chem. Soc.* **2006**, *128*, 4365–4370. (b) Lo, K. K.-W.; Tsang, K. H.-K.; Sze, K.-S. *Inorg. Chem.* **2006**, *45*, 1714–1722. (c) Guo, X.-Q.; Castellano, F. N.; Lakowicz, J. R. *Anal. Chem.* **1988**, *70*, 632–637;

(17) For same recent papers, see: (a) James, S.; Maresca, K. P.; Babich, J. W.; Valliant, J. F.; Doering, L.; Zubieta, J. *Bioconjugate Chem.* **2006**,

17, 590–596. (b) Lo, K. K.-W.; Tsang, K. H.-K.; Zhu, N. *Organometallics* **2006**, *25*, 3220–3227. (c) Reece, S. J.; Seyedsayamdost, M. R.; Stubbe, J.; Nocera, D. G. *J. Am. Chem. Soc.* **2006**, *128*, 13654–13655. (d) Lo, K. K.-W.; Hui, W.-K.; Chung, C.-K.; Tsang, K. H.-K.; Lee, T. K.-M.; Li, C.-K.; Lau, J. S.-Y.; Ng, D. C.-M. *Coord. Chem. Re*V. **2006**, *250*, 1724–1736. (e) Lo, K. K.-W.; Hui, W.-K.; Chung, C.-K.; Tsang, K. H.-K.; Ng, D. C.-M.; Zhu, N.; Cheung, K.-K. *Coord. Chem. Re*V. **2005**, *249*, 1434–1450. (f) Lo, K. K.-W.; Tsang, K. H.-K.; Zhu, N. *Inorg. Chem.* **2005**, *44*, 6100–6110. (g) Wei, L.; Babich, J.; Eckelman, W. C.; Zubieta, J. *Inorg. Chem.* **2005**, *44*, 2198–2209. (h) Di Bilio, A. J.; Crane, B. R.; Wehbi, W. A.; Kiser, C. N.; Abu-Omar, M. M.; Carlos, R. M.; Richards, J. H.; Winkler, J. R.; Gray, H. B. *J. Am. Chem. Soc.* **2001**, *123*, 3181–3182;

(18) (a) Mauro, M.; Quartapelle Procopio, E.; Sun, Y.; Chien, C.H.; Donghi, D.; Panigati, M.; Mercandelli, P.; Mussini, P.; D'Alfonso, G.; De Cola, L. *Adv. Funct. Mater*. **2009**, *19*, 2607–2614. (b) Liu, C.; Li, J.; Li, B.; Hong, Z. R.; Zhao, F. F.; Liu, S. Y.; Li, W. L. *Chem. Phys. Lett.* **2007**, *435*, 54–58. (c) Liu, C.; Li, J.; Li, B.; Hong, Z.; Zhao, F.; Liu, S.; Li, W. *Appl. Phys. Lett.* **2006**, *89*, 243511. (d) Fu, C.; Li, M.; Su, Z.; Hong, Z.; Li, W.; Li, B. *Appl. Phys. Lett.* **2006**, *88*, 093507. (e) Lundin, N. J.; Blackman, A. G.; Gordon, K. C.; Officer, D. L. *Angew. Chem., Int. Ed.* **2006**, *45*, 2582–2584. (f) Duan, Y.; Li, J.; Zhao, Y.; Cheng, G.; Hou, J.; Liu, S. *Opt. Quant. Electron.* **2005**, *37*, 1121–1127. (g) Li, B.; Li,

M.; Hong, Z.; Li, W.; Yu, T.; Wei, H. *Appl. Phys. Lett.* **2004**, *85*, 4786–4788. (h) Wong, H. L.; Lam, L. S. M.; Cheng, K. W.; Man, K. Y. K.; Chan, W. K. *Appl. Phys. Lett.* **2004**, *84*, 2557–2559. (i) Li, F.; Zhang, M.; Cheng, G.; Feng, J.; Zhao, Y.; Ma, Y.; Liu, S.; Shen, J. *Appl. Phys. Lett.* **2004**, *84*, 148–150. (j) Li, F.; Cheng, G.; Zhao, Y.; Feng, J.; Liu, S.; Zhang, M.; Ma, Y.; Shen, J. *Appl. Phys. Lett.* **2003**, *83*, 4716–4718. (k) Li, F.; Zhang, M.; Feng, J.; Cheng, G.; Wu, Z.; Ma, Y.; Liu, S. *Appl. Phys. Lett.* **2003**, *83*, 365–367. (l) Ranjan, S.; Lin, S.-Y.; Hwang, K.-C.; Chi, Y.; Ching, W.-L.; Liu, C.-S.; Tao, Y.-T.; Chien, C.-H.; Peng, S.-M.; Lee, G.-H. *Inorg. Chem.* **2003**, *42*, 1248–1255. (m) Wang, K.; Huang, L.; Gao, L.; Jin, L.; Huang, C. *Inorg. Chem.* **2002**, *41*, 3353–3358. (n) Li, Y.; Liu, Y.; Guo, J.; Wu, F.; Tian, W.; Li, B.; Wang, Y. *Synth. Met.* **2001**, *118*, 175–179;

(19) (a) Yam, V. W.-W.; Li, B.; Yang, Y.; Chu, B. W.-K.; Wong, K. M.-C.; Cheung, K.-K. *Eur. J. Inorg. Chem.* **2003**, 4035–4042. (b) Chan, W. K.; Ng, P. K.; Gong, X.; Hou, S. *Appl. Phys. Lett.* **1999**, *75*, 3920–3922. (c) Gong, X.; Ng, K.; Chan, W. K. *Ad*V. *Mater.* **1998**, *10*, 1337–1340;

(20) Panigati, M.; Donghi, D.; D'Alfonso, G.; Mercandelli, P.; Sironi, A.; Mussini, P.; D'Alfonso, L. *Inorg. Chem.* **2006**, *45*, 10909-21;

(21) Donghi, D.; D'Alfonso, G.; Mauro, M.; Panigati, M.; Mercandelli, P.; Sironi, A.; Mussini, P.; D'Alfonso, L. *Inorg. Chem.* **2008**, *47*, 4243–4255;

Chapter 3

LUMINESCENT DIRHENIUM-PYRIDAZINE COMPLEXES CONTAINING BRIDGING OR OR SR ANIONS

New luminescent $[Re_2(\mu\text{-}X)_2(CO)_6(\mu\text{-pydz})]$ have been synthesized, in which the bridging ancillary ligands are OR^- or SR^- anions. Intriguing electrochemical properties have been evidenced, differentiating the OR derivatives from the SR one and the previously reported halide analogues. The bis(benzenethiolato) derivative exhibits a very small electrochemical energy gap and absence of photoluminescence. The best emitting properties, closely comparable to those of the dichloro complex, are shown by the bis(pentafluorophenolato) derivative (Φ = 5.5% in deaerated toluene).

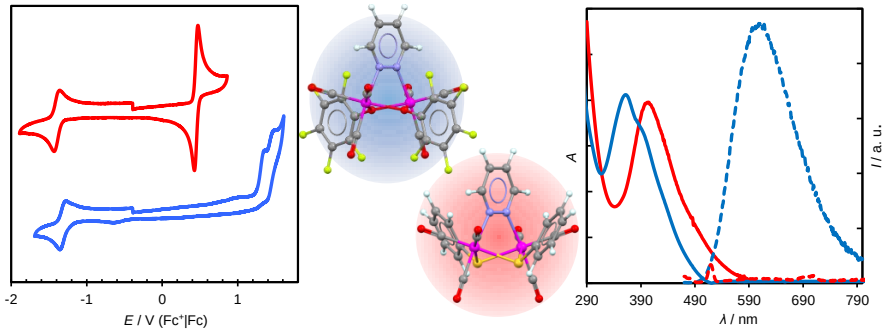

3.1 Introduction

We decided to investigate the photophysical properties of diazine complexes bearing polyatomic bridging ligands, with a twofold aim. Firstly we were interested in learning how to exploit the change of the ancillary ligands for controlling the HOMO-LUMO gap, and then modulating position and intensity of the emission. Moreover, the raising of the HOMO level could give low band gap complexes, of interest for efficient light harvesting in solar cells. Secondly, the replacement of chlorides by polyatomic ligands might also provide other sites, besides the diazine ring, for functionalizing the di-rhenium complexes, which might be useful for application as luminescent bio-probes, where the linking to suitable biomolecules is most often required.

We report here on the synthesis and on the electrochemical, computational and photophysical characterization of five new $[Re_2(\mu\text{-}ER)_2(CO)_6(\mu\text{-pydz})]$ complexes, containing pyridazine (pydz) as chromophoric ligand and ER^- groups as bridging ancillary ligands (E = S, R = C_6H_5, **2**; E = O, R = C_6F_5, **3**; C_6H_5, **4**; CH_3, **5**; H, **6**).

3.2 Results and discussion

3.2.1 Synthesis

The previously reported $[Re_2(\mu\text{-}Cl)_2(CO)_6(\mu\text{-pydz})]$ complex **1**, as well as all the others $[Re_2(\mu\text{-}X)_2(CO)_6(\mu\text{-1,2-diazine})]$ complexes (X = Cl, Br, I), were obtained by refluxing the proper $[Re(CO)_5X]$ starting material with the stoichiometric amount of 1,2-diazine. This method cannot be used for the preparation of the title derivatives, since $[Re(CO)_5(OR)]$ complexes are unstable and elusive species.[1] We therefore developed alternative routes, using different starting materials, as summarized in Scheme 1.

In a first approach, the $[Re(CO)_5(OTf)]$ complex,[2] containing the labile triflate $CF_3SO_3^-$ anion (OTf^-), was used. The complex was treated with the proper REH reagent (E = O or S) and stoichiometric pyridazine (pydz), in the presence of a base B, according to equation 1. Bis(dimethylamino)naphthalene (DMAN) was chosen as base, because it cannot compete with diazine for rhenium coordination.

$$2[Re(CO)_5(OTf)] + pydz + 2REH + 2B \rightarrow [Re_2(\mu\text{-}ER)_2(CO)_6(\mu\text{-pydz})] + 2BH^+OTf^- + 4CO \qquad \text{(eq. 1)}$$

This route worked satisfactorily with C_6H_5SH, in THF solution, and gave the bis(thiophenolato) derivative $[Re_2(\mu\text{-}SC_6H_5)_2(CO)_6(\mu\text{-pydz})]$ (**2**) in ca. 30% isolated yields. In the case of C_6H_5OH, reaction (1) worked as well, but gave cleanly $[Re_2(\mu\text{-}OC_6H_5)_2(CO)_6(\mu\text{-pydz})]$ (**4**) only using molten phenol as solvent.

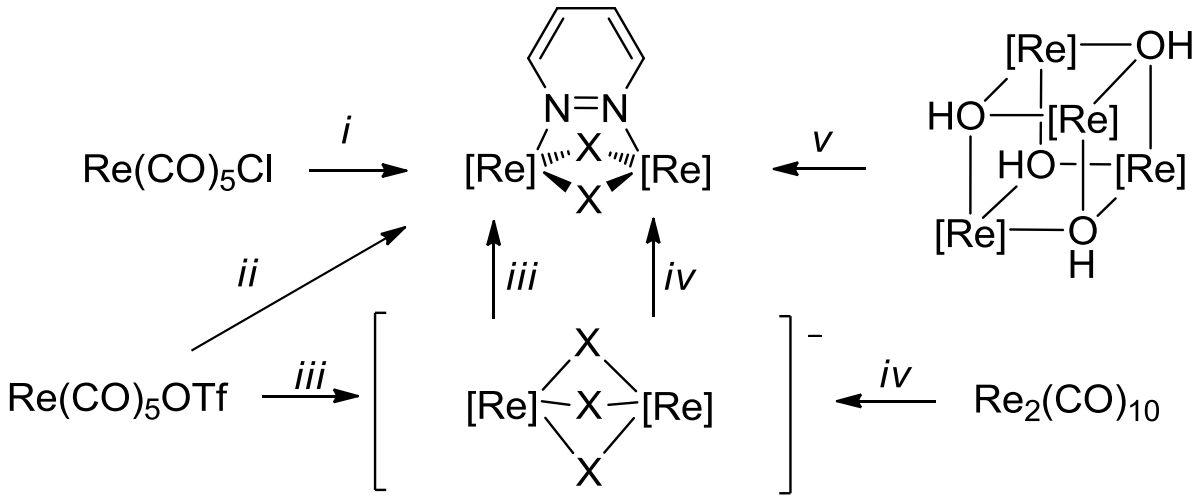

[Re] = $Re(CO)_3$; *i*: **1**; *ii*: **2**, **4**; *iii*: **3**; *iv*: **5**; *v*: **6**

X = Cl (**1**); = SC_6H_5 (**2**); = OC_6F_5 (**3**); = OC_6H_5 (**4**); = OCH_3 (**5**); = OH (**6**)

Scheme 1. The different synthetic routes *i-v* leading to complexes **1**–**6**

On the contrary, attempts to obtain the bis(pentafluorophenolato) derivative $[Re_2(\mu\text{-}OC_6F_5)_2(CO)_6(\mu\text{-pydz})]$ (**3**) with the same procedure afforded a mixture of products in which the expected derivative was present in relatively low concentration (less than 30% from ^1H NMR analysis). Then **3** was better obtained by a two steps procedure. At first the dinuclear anion $[Re_2(\mu\text{-}OC_6F_5)_3(CO)_6]^-$ was formed, by reacting $[Re(CO)_5(OTf)]$ with pentafluophenol in the presence of a base (B = DMAN, eq 2a), then the anion was treated with 1 equiv of pydz, resulting in the replacement of one phenolate by a diazine molecule (eq 2b).

$$2[Re(CO)_5(OTf)] + 3C_6F_5OH + 3B \rightarrow [Re_2(\mu\text{-}OC_6F_5)_3(CO)_6]^- + 4CO + 3HB^+ + 2OTf^- \quad \text{(eq. 2a)}$$

$$[Re_2(\mu\text{-}OC_6F_5)_3(CO)_6]^- + pydz \rightarrow [Re_2(\mu\text{-}OC_6F_5)_2(CO)_6(\mu\text{-pydz})] + C_6F_5O^- \quad \text{(eq. 2b)}$$

To prepare the $[Re_2(\mu\text{-}OCH_3)_2(CO)_6(\mu\text{-}pydz)]$ species (**5**) we used as starting material directly the dinuclear $[Re_2(\mu\text{-}OCH_3)_3(CO)_6]^-$ anion, which can be prepared in good yields, as NEt_4^+ salt, from the reaction of $[Re_2(CO)_{10}]$ with bases.[3] Differently from the bis(pentafluorophenolato) derivative, in this case the addition of one equivalent of triflic acid was necessary to promote the elimination of one of the bridging methoxo groups (equation 3). This agrees with the higher nucleophilicity and lower bulkiness of OCH_3^- with respect to $OC_6F_5^-$.

$$[Re_2(\mu\text{-}OCH_5)_3(CO)_6]^- + pydz + TfOH \rightarrow [Re_2(\mu\text{-}OCH_3)_2(CO)_6(\mu\text{-}pydz)] + CH_3OH + OTf^- \quad \text{(eq. 3)}$$

Finally, a still different method was developed for preparing the hydroxo $[Re_2(\mu\text{-}OH)_2(CO)_6(\mu\text{-}pydz)]$ derivative (**6**). The cubane-like $[Re_4(\mu_3\text{-}OH)_4(CO)_{12}]$ complex[4] (Scheme 1) was used as starting material, and it was reacted with 2 equivs of pydz, in water solution and under microwave activation, resulting in the clean formation of **6**, according to eq 4. This reaction resembles the previously reported fragmentation of the unsaturated tetranuclear cluster $[Re_4(\mu_3\text{-}H)_4(CO)_{12}]$ with 2 equivs of pydz,[5] even if in this case only the *[2+2]* fragmentation pathway was observed, affording quantitatively the dinuclear saturated derivative **6**.

$$[Re_4(\mu_3\text{-}OH)_4(CO)_{12}] + 2\ pydz \rightarrow 2[Re_2(\mu\text{-}OH)_2(CO)_6(\mu\text{-}pydz)] \quad \text{(eq. 4)}$$

The nature of the reaction products was unambiguously established by the spectroscopic and analytical characterization, and confirmed by the X-ray analysis of complexes **2**, **3**, and **4**. All the products exhibit in the ν(CO) regions of the IR spectra the four bands pattern typical of this class of compounds,[6] with a shift to low wavenumbers on increasing the donor power of the bridging ligand (this point will be better discussed below).

The ^{1}H NMR data agree with the expected structures. In particular the two resonances of the bridging pyridazine are down-field shifted by about 0.5-0.6 ppm with respect to the free ligand, as observed in related complexes.[6]

Variable temperature ^{19}F NMR spectra gave some information on the solution structure and dynamics of complex **3**. The low temperature (T < 221 K) spectra are consistent with the C_2 solid state structure (see below), with five different signals for the five fluorine atoms of the two (equivalent) pentafluorophenolato groups. The chemical shift difference between the two *ortho* resonances (> 5 ppm) is much higher than that between the two *meta* resonances (< 1 ppm), due to the shielding effect of the diazine π electrons on one of the *ortho* F atoms, as evidenced by the ^{1}H-^{19}F HOESY experiment shown in Figure 1. On increasing the temperature the *ortho* and *meta* signals broadened (Figure 2), indicating rotation of each C_6F_5 ring around the C-O axis, leading to equalization of the two *ortho* and two *meta* positions. Band shape analysis on the ^{19}F spectra provided the value of the activation energy for this process (42.4 kJ mol^{-1}).

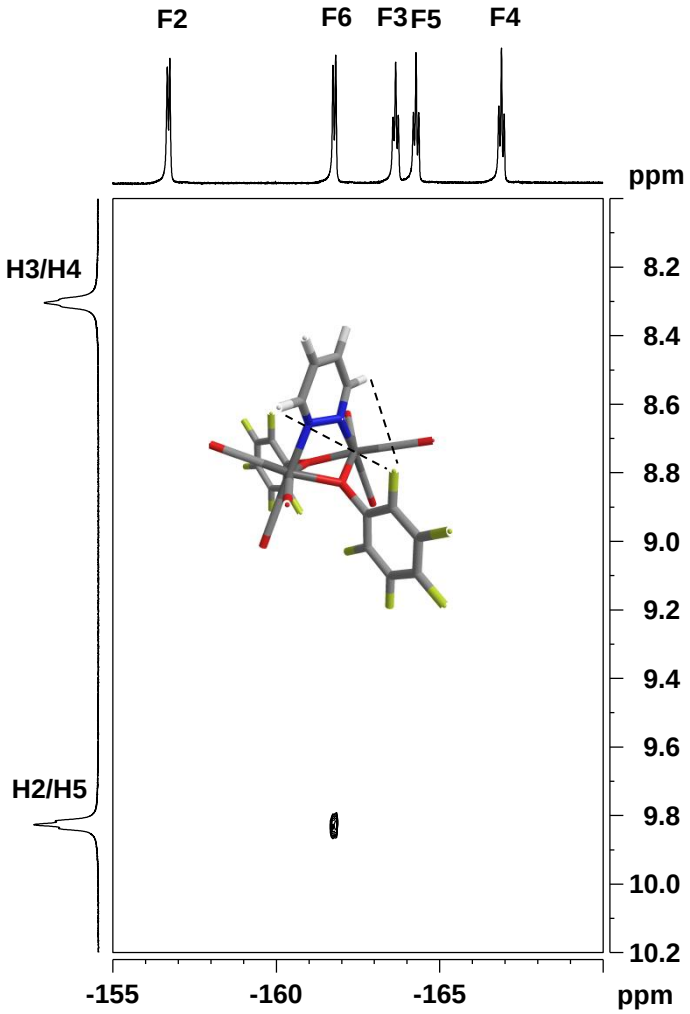

Figure 1. ^{19}F-^{1}H HOESY NMR experiment (CD_2Cl_2, 173 K) on a sample of **3**, showing that the upfield-shifted *ortho* ^{19}F signal is due to the F atoms of the two equivalent pentafluorophenolato groups closest to the pyridazine ligand, and then to its *ortho* hydrogen atoms.

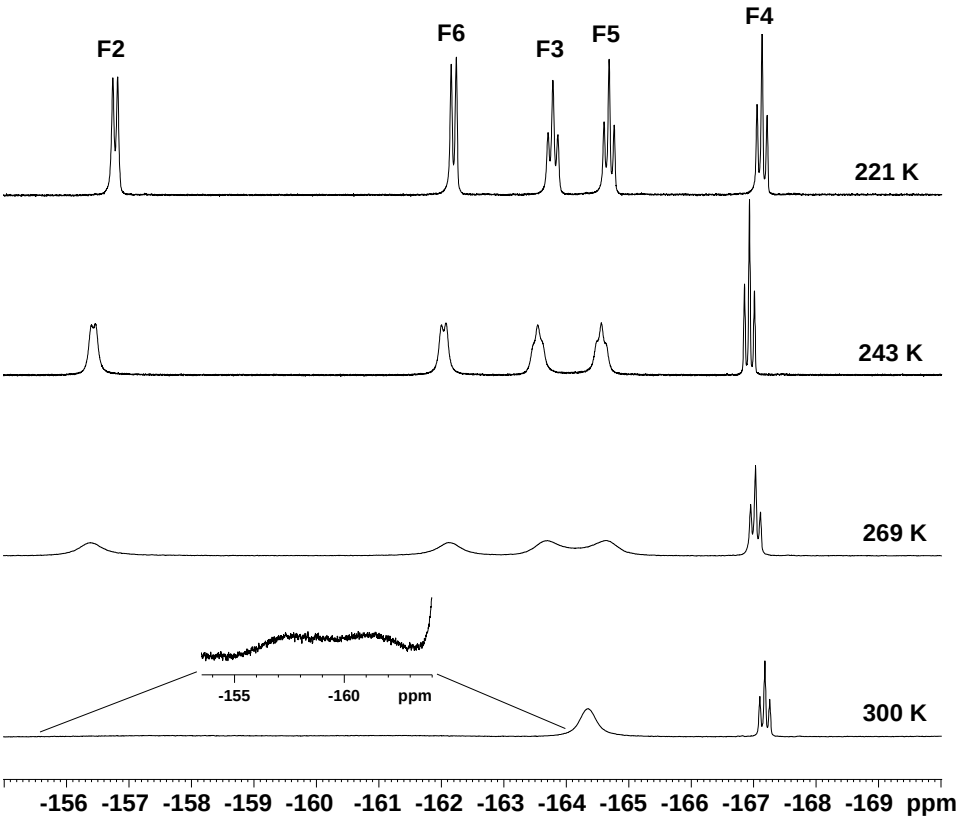

Figure 2. Variable temperature ^{19}F NMR spectra of **3** (CD_2Cl_2, 9.4 T).

In the case of the phenolato derivative **4** the ^{1}H NMR spectra did not show either splitting or broadening of the *ortho* and *meta* signals on lowering the temperature, indicating that the rotation of the C_6H_5 rings is faster than that of their C_6F_5 counterparts, due to the lower steric hindrance with the CO ligands.

3.2.2 Solid state structures

The crystal structures of the μ-benzenethiolato derivative (**2**) and of the two μ-phenolato derivatives (**3** and **4**) have been determined. Figure 3 shows frontal and lateral views of the complexes **2–4**.

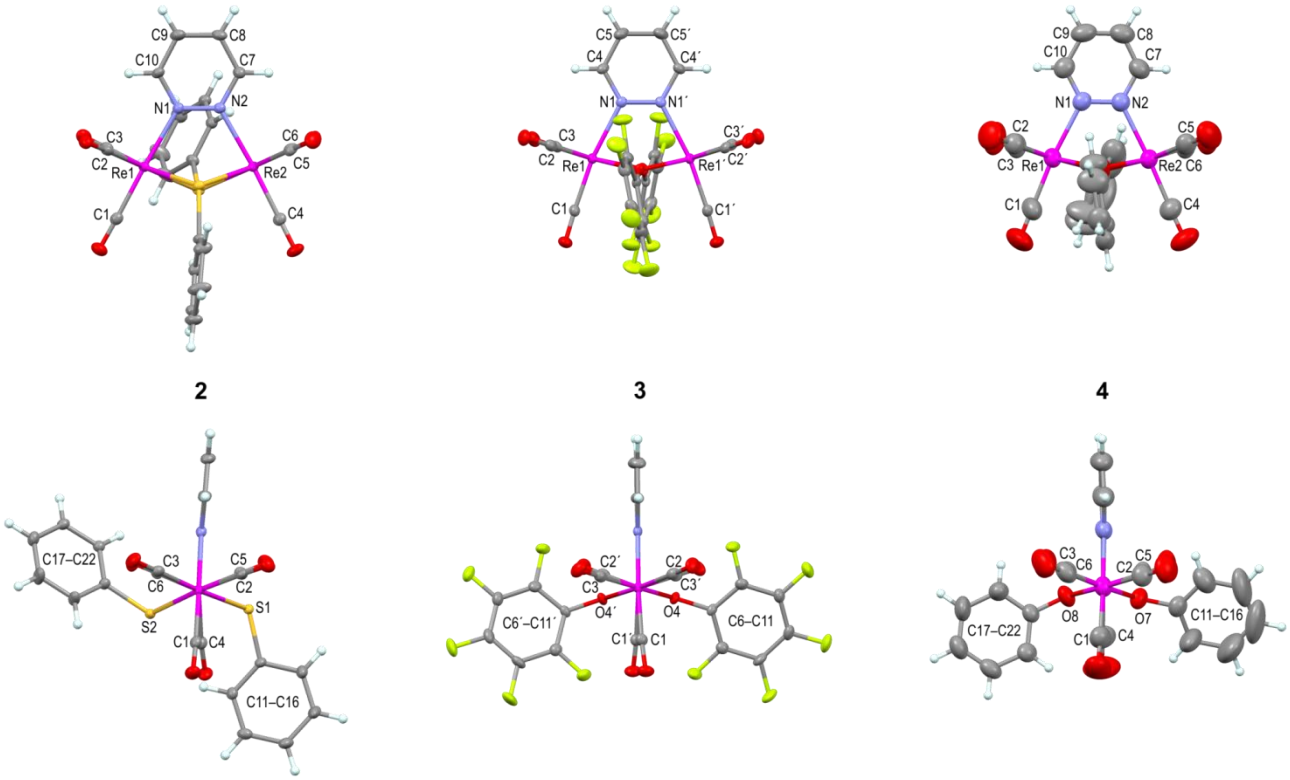

Figure 3. Crystal structures of $[Re_2(\mu\text{-}SC_6H_5)_2(CO)_6(\mu\text{-pydz})]$ **2**, $[Re_2(\mu\text{-}OC_6F_5)_2(CO)_6(\mu\text{-pydz})]$ **3,** and $[Re_2(\mu\text{-}OC_6H_5)_2(CO)_6(\mu\text{-pydz})]$ **4**: frontal and lateral views (upper line and lower line, respectively). Displacement ellipsoids are drawn at the 50% probability level. Color code: C, grey; H, white; F, lime; N, blue; O, red; Re, magenta; S, yellow.

In these dinuclear species, each rhenium atom attains a distorted octahedral coordination and bears three terminal carbonyl ligands in a facial arrangement, one of the nitrogen atoms of the bridging pyridazine ligand, and the sulfur (or oxygen) atoms of the two bridging benzenethiolato (or phenolato) ligands. The two μ-phenolato derivatives **3** and **4** possess an

idealized C_2 symmetry (although only **3** lies on a crystallographic twofold axis), while the thio-derivative **2** is asymmetrical, due to the different conformation adopted by the phenyl groups of the two bridging benzenethiolato ligands.

In spite of the smaller Re–S–Re bond angle in **2** (91.0°) with respect to the corresponding Re–O–Re angles in **3** and **4** (104.4 and 103.8°), the Re–Re distance is much longer in the sulfur-containing derivative (3.57 Å in **2** vs 3.39 and 3.35 Å in **3** and **4**) as a consequence of the larger covalent radius of sulfur compared to oxygen. The Re–S bond distance in **2** (2.50 Å) is indeed ca. 0.35 Å longer than the Re–O bond distances in **3** and **4** (2.15 and 2.13 Å).[7]

The coordination geometry of the oxygen atoms of the μ-phenolato ligands is almost exactly planar (sum of the bond angles: 359.9 and 358.8° in **3** and **4**), suggesting the presence of a partial double bond character in the Re–O bonds. On the contrary, the sulfur atoms of the μ-benzenethiolato ligands in **2** show a pyramidal geometry (sum of the bond angles: 314.6°). As a consequence, the phenyl substituents in the thio-derivative **2** are not constrained to lie in the plane defined by the Re–(μ-S)–Re atoms, leading to the possible existence of geometric isomers in which the phenyl groups are directed either towards or away from the μ-pyridazine ligand. Both the orientations can be observed in the molecular conformation adopted by the molecule in the solid state (see the lateral view of **2** in Figure 3). However, the presence in solution of other (more symmetrical) isomers can be foreseen.

3.2.3 Computational study

The new rhenium complexes **2**–**6** were studied by means of density functional and time-dependent density functional (TD-DFT) computations. The optimized structures of complexes **3**–**6** possess the highest possible symmetry for these species (C_{2v}), while the benzenethiolato derivative **2** belongs to the C_2 point group.[8] As already found for **1**,[6,9] LUMO and LUMO+1 are the two lowest-lying π^* orbitals of the coordinated pyridazine. The following four MO (from LUMO+2 to LUMO+5) are the e_g set of the two Re atoms, showing in addition a large C≡O π^* character.

For species **5** and **6** the six HOMOs are the t_{2g} set of the two Re atoms in a pseudo-octahedral environment. In particular, the three highest lying orbitals show a strong Re–(μ-O) π^* character, in close analogy with the halogenated derivatives previously described.[6] For species **2**–**4** ten HOMOs have to be taken into account, since the energy of the t_{2g} orbitals of the Re atoms are similar to those of the four highest lying π orbitals of the two phenyl groups of the phenolato (or pentafluorophenolato) bridging ligands. For species **2**, in addition, a partial mixing of these two kinds of MO is observed and some of the t_{2g} orbitals are partially delocalized over the phenyl moieties. Molecular orbital energies are listed in Table 1, while partial orbital diagrams are depicted in Figure 4 and views of the isodensity surface plots of the HOMOs of **1**, **2**, **4**, and **6** are reported in Figure 5.

		1	**2**	**3**	**4**	**5**	**6**
e_g	LUMO + 5	– 0.65	– 0.53	– 0.79	– 0.38	– 0.25	– 0.23
	LUMO + 4	– 1.00	– 0.74	– 1.00	– 0.75	– 0.59	– 0.62
	LUMO + 3	– 1.04	– 1.06	– 1.13	– 0.77	– 0.75	– 0.86
	LUMO + 2	– 1.39	– 1.08	– 1.57	– 0.99	– 0.96	– 1.09
π^* pydz	LUMO + 1	– 2.67	– 2.42	– 2.68	– 2.52	– 2.44	– 2.46
	LUMO	– 3.52	– 3.25	– 3.54	– 3.36	– 3.27	– 3.29
t_{2g} (+ π_{Ph})	HOMO	– 6.84	– 6.34	– 6.82	– 6.31	– 6.15	– 6.28
	HOMO – 1	– 6.87	– 6.48	– 6.86	*– 6.42*	– 6.30	– 6.53
	HOMO – 2	– 7.01	– 6.54	*– 7.05*	– 6.44	– 6.63	– 6.63
	HOMO – 3	– 7.40	– 6.83	*– 7.08*	*– 6.48*	– 6.98	– 7.03
	HOMO – 4	– 7.42	*– 6.99*	*– 7.28*	– 6.81	– 7.01	– 7.06
	HOMO – 5	– 7.45	– 7.08	*– 7.28*	*– 7.00*	– 7.05	– 7.08
	HOMO – 6		– 7.19	– 7.31	*– 7.02*		
	HOMO – 7		*– 7.36*	– 7.45	– 7.11		
	HOMO – 8		*– 7.37*	– 7.49	– 7.16		
	HOMO – 9		*– 7.40*	– 7.52	– 7.20		

Table 1. A list of Computed Molecular Orbital Energies [eV] for the complexes **1-6**

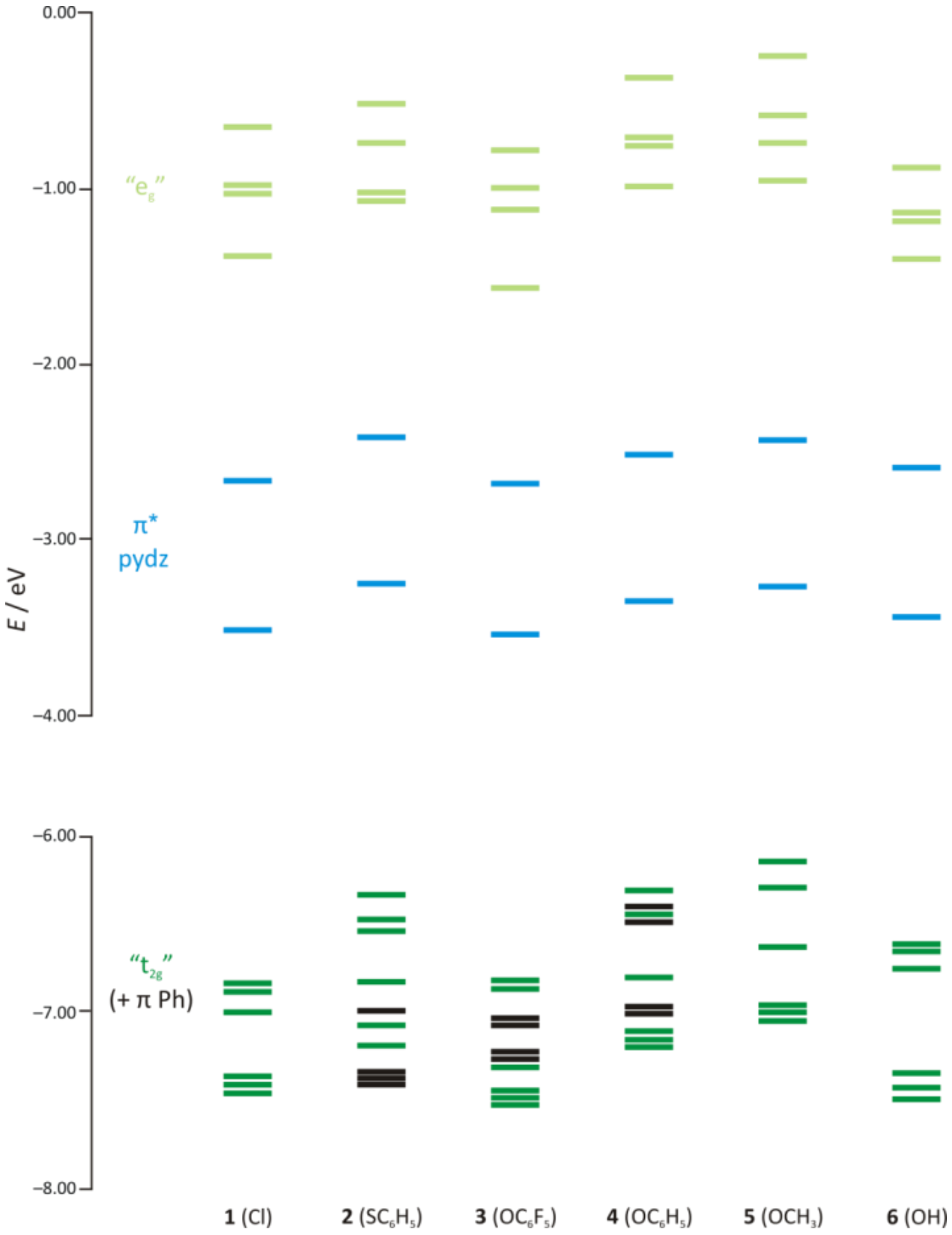

Figure 4. Partial molecular orbital diagram for the complexes $[Re_2(\mu\text{-}X)_2(CO)_6(\mu\text{-pydz})]$, X = Cl (**1**), SC_6H_5 (**2**), OC_6F_5 (**3**), OC_6H_5 (**4**), OCH_3 (**5**), and OH (**6**). The black lines are referred to the π orbitals of the phenyl groups in complexes **2–4**.

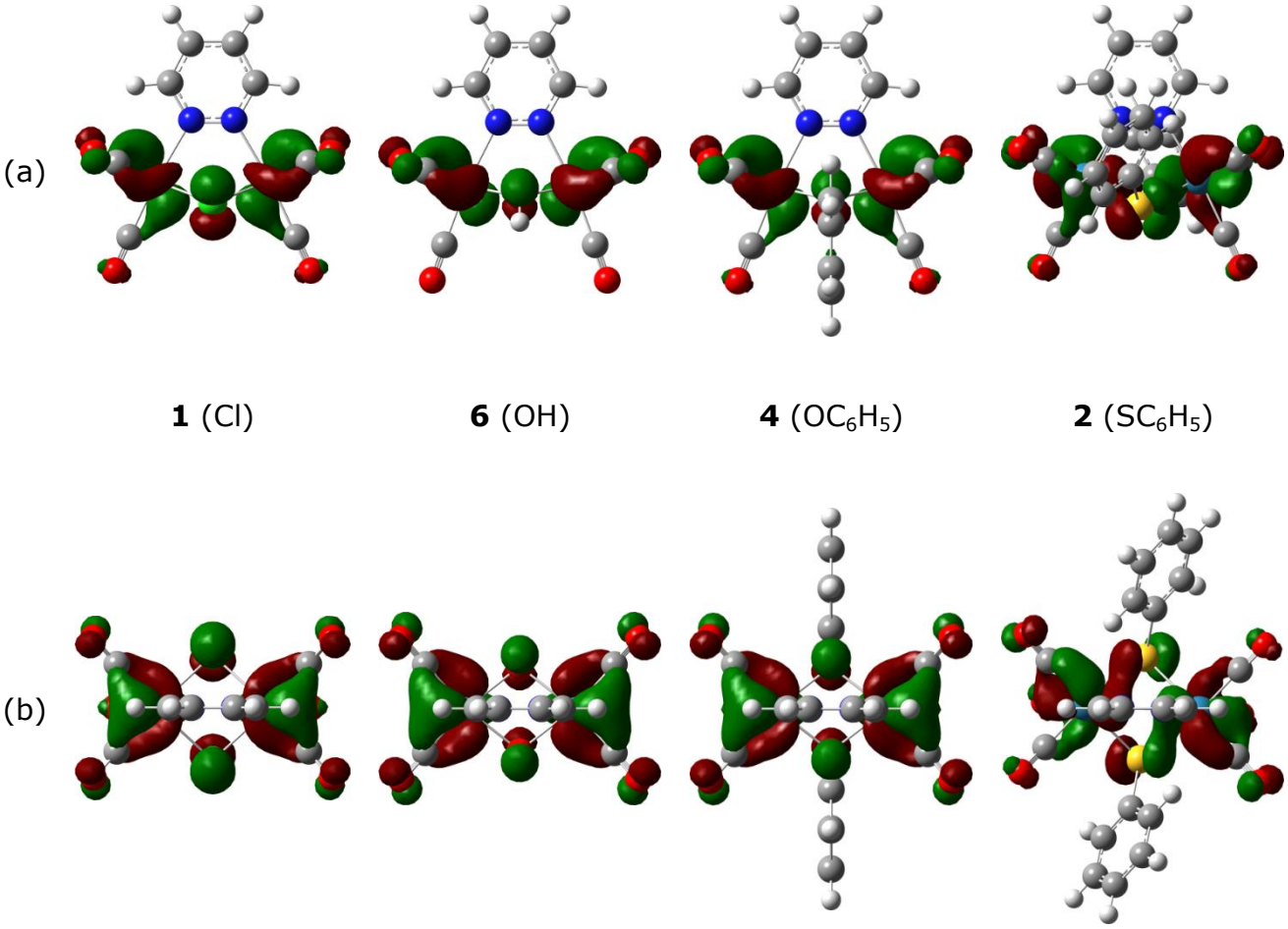

Figure 5. Frontal (a) and top (b) views of the isodensity surface plots of the highest occupied molecular orbital (HOMO) of some relevant [$Re_2(\mu\text{-}X)_2(CO)_6(\mu\text{-pydz})$] complexes. The HOMO of the three C_{2v} species **1** (Cl), **6** (OH), and **4** (OC_6H_5) is totalsymmetric (a_1), while the HOMO of the C_2 benzenethiolato derivative **2** (SC_6H_5) shows a reduced symmetry (b). However, the HOMO of all the species can be qualitatively described as an antibonding combination of the rhenium atoms' d orbitals and the bridging atoms' p orbitals, with minor contributions from the π * orbitals of the carbonyl ligands (mainly the equatorial ones).

In all the species but **2** the HOMO is a totalsymmetric orbital analogous to those previously found in the halogenated derivatives.[6] The HOMO of **2** has a very similar composition, however it is antisymmetric with respect to the C_2 axis. The absorption spectrum of all the complexes down to 230 nm was simulated by computing the lowest 50 singlet excitation energies. Selected

transitions are reported in Table 2. The results will be discussed in the paragraph devoted to the photophysical characterization.

	1	**2**	**3**	**4**	**5**	**6**
Gas-phase values						
λ_{d-d} (*f*)	258, 4.80 (0.06)	261, 4.75 (0.02)	255, 4.86 (0.03)	256, 4.84 (0.02)	257, 4.82 (0.07)	257, 4.82 (0.03)
λ_{MLCT} (*f*)	370, 3.35 (0.04)	370, 3.35 (0.05)	373, 3.32 (0.05)	387, 3.20 (0.13)	401, 3.09 (0.16)	385, 3.22 (0.08)
	385, 3.22 (0.14)	414, 2.99 (0.07)	381, 3.26 (0.10)	409, 3.03 (0.03)	415, 2.99 (0.00)	397, 3.12 (0.10)
	484, 2.56 (0.07)	517, 2.40 (0.03)	493, 2.52 (0.07)	544, 2.28 (0.06)	564, 2.20 (0.05)	509, 2.43 (0.07)
Toluene solution values (CPCM) [b]						
λ_{MLCT} (*f*)	342, 3.63 (0.02)	353, 3.52 (0.05)	363, 3.41 (0.13)	363, 3.41 (0.07)	381, 3.25 (0.01)	361, 3.44 (0.03)
	370, 3.35 (0.21)	396, 3.13 (0.09)	371, 3.34 (0.06)	380, 3.26 (0.14)	386, 3.22 (0.20)	382, 3.25 (0.20)
	446, 2.78 (0.10)	479, 2.59 (0.05)	458, 2.71 (0.09)	494, 2.51 (0.08)	515, 2.40 (0.06)	475, 2.61 (0.09)

Table 2. Computed Excitation Energies [nm, eV] and Oscillator Strengths (*f*, in parenthesis) for the complexes **1-6**. [a] λ_{d-d} and λ_{MLCT} refer to the higher and lower energy bands, respectively. Data for **1** are taken from our previous works[6,9]. [b] The higher energy band λ_{d-d} is almost unaffected by solvation. As a consequence, only the CPCM λ_{MLCT} values are reported.

3.2.4 Electrochemical characterization

Figure 6 shows the results of cyclic voltammetry (CV) analyses of complexes **2**–**6** in acetonitrile solution, including, for comparison, the previously published data concerning the dichloro complex **1** and the analogous dibromo and diiodo derivatives, that hereafter will be indicated as **1'** and **1"**, respectively.[6] The most significant CV features are reported in Table 3, while a more extensive selection of the CV data is provided in Table 4; in Figure 7 are also reported the voltammograms recorded in CH_2Cl_2.

Comp	X	*F*	*R*	$E_{pmax,red}$ (V)	$E_{pmax,Iox}$ (V)	$E_{pmax,IIox}$ (V)	LUMO (eV)	HOMO (eV)	E_g (eV)
1 [6]	Cl	0.42	-0.19	-1.345	1.315		-3.46	-6.12	2.66
1' [6]	Br	0.45	-0.22	-1.365	1.163		-3.44	-5.96	2.53
1'' [6]	I	0.42	-0.24	-1.378	0.944		-3.42	-5.74	2.32
2	SC_6H_5	0.30	-0.23	-1.431	0.473		-3.37	-5.27	1.90
3	OC_6F_5	n.a.	n.a.	-1.352	1.345	1.463	-3.45	-6.15	2.70
4	OC_6H_5	0.37	-0.40	-1.416	1.100	1.254	-3.38	-5.90	2.52
5	OCH_3	0.29	-0.56	-1.475	0.911	1.114	-3.33	-5.71	2.39
6	OH	0.33	-0.70	-1.527	0.854	1.070	-3.27	-5.65	2.38

Table 3. Selected CV features for the $[Re_2(\mu\text{-}X)_2(CO)_6(\mu\text{-pydz})]$ complexes investigated here and in a previous work.[6] Values of the Swain-Lupton parameters *F* and *R* are also provided for each X group. [a] Peak potentials E_p (0.2 V s^{-1} scan rate); electrochemical HOMO and LUMO energy levels and gaps calculated along the peak maxima. Potentials are referred to the $Fc^+|Fc$ couple in the operating media (MeCN + 0.1 M $TBAPF_6$).

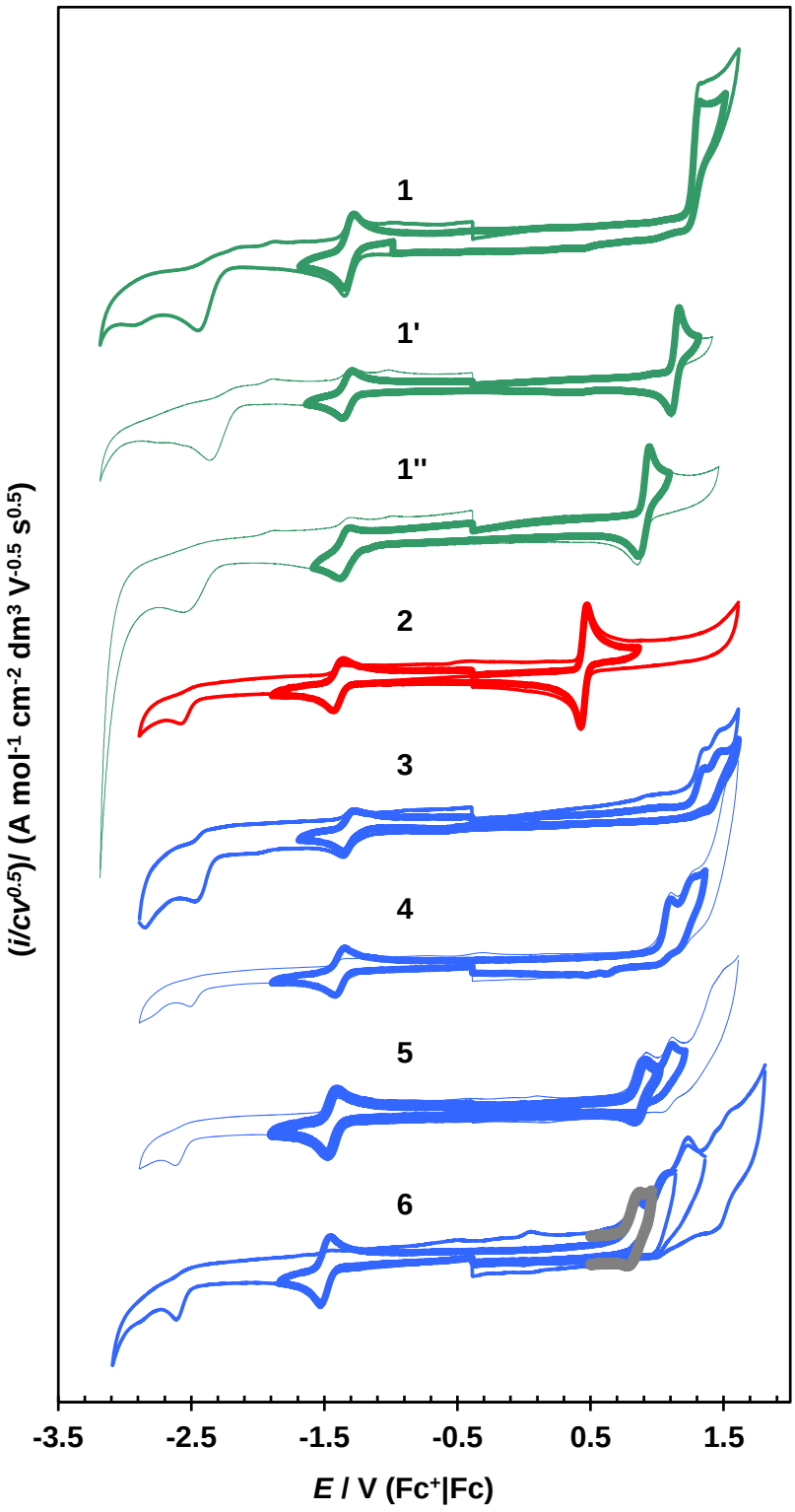

Figure 6. Normalized CV features for the complexes investigated in this work and the three complexes with halide ligands previously investigated **1**, **1'**, **1''** (green lines),[6] recorded on GC electrode at 0.2 V s^{-1} in acetonitrile solution. The gray line for **6** refers to a scan at 2 V s^{-1}.

					First reduction peak					First oxidation peak					Second oxidation peak	Electrochemical energy gaps	
#	X	*F*	*R*	Solvent	$E_{p,max}$	$E_{p,onset}$	$E_p - E_{p/2}$	$dE_p/d\log v$	$i_{L,conv}/c$	$E_{p,max}$	$E_{p,onset}$	$E_p - E_{p/2}$	$dE_p/d\log v$	$i_{L,conv}/c$	$E_{p\,IL,max}$	$E_{g,EC\,max}$	$E_{g,EC\,onset}$
free ligands																	
	Pydz			MeCN	**-2.600**	-2.474	0.063	0.029	1.35								
	C_6H_5OH			MeCN						**1.274**	1.020	0.127	0.056	0.71			
	C_6F_5OH			MeCN						**1.203**	0.957	0.123	0.084	0.29			
complexes																	
1	**Cl** [ECI]	0.42	-0.19	MeCN	**-1.345**	-1.231	0.057	0.002	0.48	**1.315**	1.241	0.037	0.006→0.035	0.66		**2.66**	**2.47**
1'	**Br**[ECI]	0.45	-0.22	MeCN	**-1.365**	-1.253	0.056	0.002	0.32	**1.163**	1.103	0.030	0.002→0.032	0.62		**2.53**	**2.36**
1''	**I**[ECI]	0.42	-0.24	MeCN	**-1.378**	-1.232	0.073	0.001	0.29	**0.944**	0.870	0.037	0.009→0.027	0.50		**2.32**	**2.10**
2	**SC_6H_5**	0.30	-0.23	MeCN	**-1.431**	-1.315	0.058	0	0.31	**0.473**	0.407	0.033	0	0.61		**1.90**	**1.72**
				CH_2Cl_2	**-1.616**	-1.452	0.082	0	0.14	**0.421**	0.311	0.055	0	0.34		**2.04**	**1.76**
3	**OC_6F_5**	n.a.	n.a.	MeCN	**-1.352**	-1.224	0.064	0.002	0.11	**1.345**	1.255	0.045	0.12	0.12	**1.463**	**2.70**	**2.48**
4	**OC_6H_5**	0.37	-0.40	MeCN	**-1.416**	-1.298	0.059	0.008	0.33	**1.100**	1.008	0.046	0.023	0.29	**1.254**	**2.52**	**2.31**
				CH_2Cl_2	**-1.588**	-1.440	0.074	0.004	0.34	**0.961**	0.867	0.047	0.026	0.22	**1.196**	**2.55**	**2.31**
5	**OCH_3**	0.29	-0.56	MeCN	**-1.475**	-1.353	0.061	0.002	0.39	**0.911**	0.837	0.037	-0.002	0.37	**1.114**	**2.39**	**2.19**
				CH_2Cl_2	**-1.663**	-1.511	0.076	0.004	0.39	**0.714**	0.630	0.042	0.004	0.60	**1.114**	**2.38**	**2.14**
6	**OH**	0.33	-0.70	MeCN	**-1.527**	-1.413	0.057	0.005	0.45	**0.854**	0.736	0.059	0.013	0.37	**1.070**	**2.38**	**2.15**

[a] Peak potentials E_p, half-peak widths ($E_p - E_{p/2}$), and onset potentials, $E_{p,onset}$ (0.2 V s^{-1} scan rate); slopes of the linear E_p \ log*v* characteristics (dE_p /dlog*v*); normalized limiting currents after convolution ($i_{L,conv}/c$), electrochemical energy gap calculated along the peak maxima and the peak onset criteria ($E_{g\,EC\,max}$ and $E_{g\,EC,onset}$, respectively). Potentials are referred t the $Fc^+|Fc$ couple in the operating media (MeCN + 0.1 M $TBAPF_6$ or CH_2Cl_2 + 0.1 M $TBAPF_6$).

Table 4. Selected CV features for the complexes investigated in this work and for some of the ligands.[a] Values of the Swain-Lupton parameters *F* and *R* are also provided for each X group

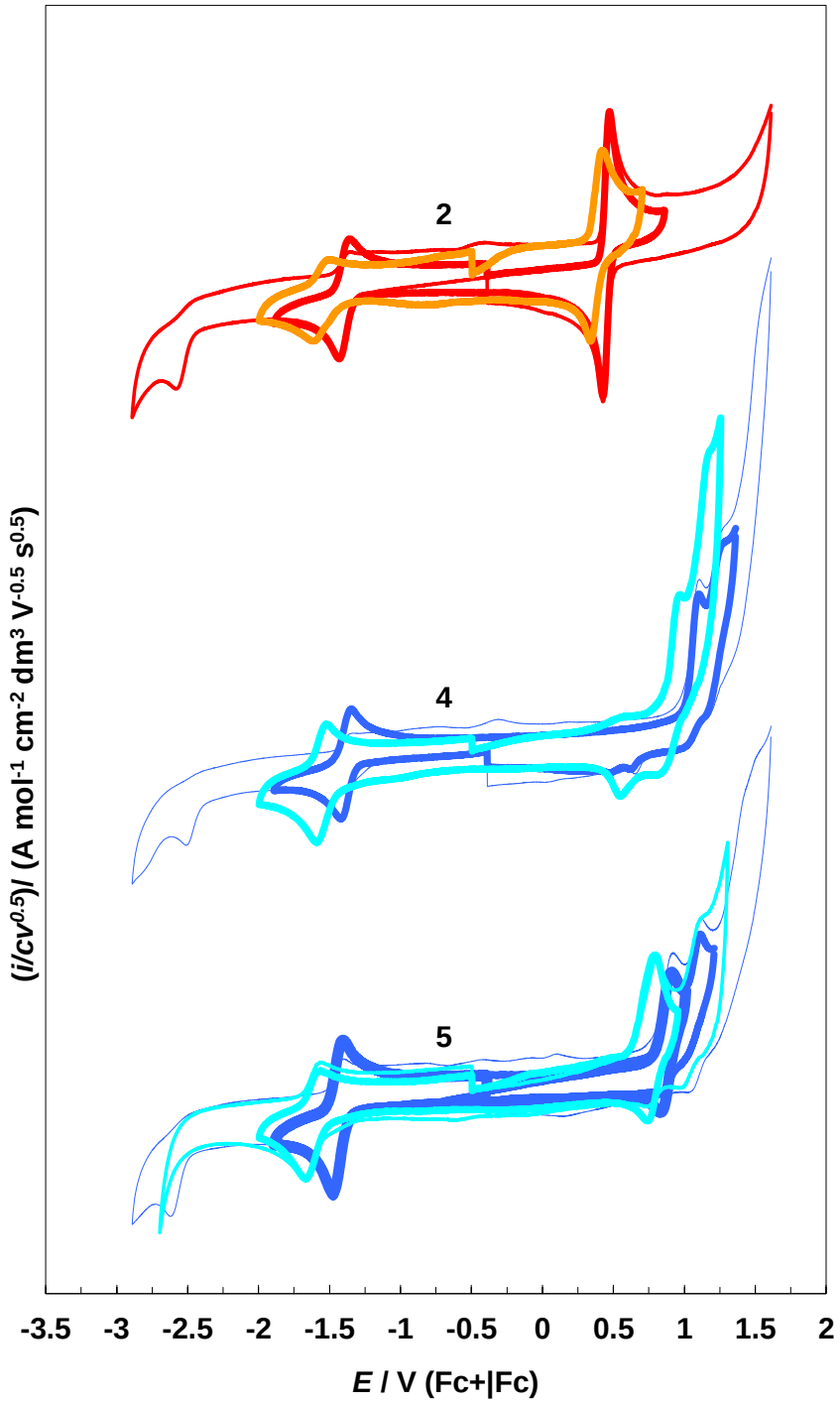

Figure 7. Normalized CV features (GC electrode, 0.2 V s^{-1}) in CH_2Cl_2 solution (orange for **2**, clear blue for **4** and **5**), compared with the traces recorded in acetonitrile solution (red for **2**, blue for **4** and **5**).

First Reduction Peaks. The first reduction peaks must be localized for all complexes on their common pyridazine ligand, consistently with our previous work.[6] Accordingly, such peaks are quite similar for all complexes, both in shape and potential, while they strongly differ from the free ligand one. In fact the first reduction peak of pyridazine, located at a quite negative potential (-2.6 V), is chemically irreversible and accounts for an uptake of two electrons,[6] while the first reduction peaks of the complexes are much more positive (by 1.05 ÷ 1.25 V), implying that the coordination makes the diazine ligand much electron-poorer. Moreover, the reduction of all complexes is monoelectronic and reversible, both from the chemical point of view (symmetrical return peaks, stable product) and the electrochemical one (facile transfer of a single electron, accounted by the ≈ 57 mV half-peak widths together with the nearly zero E_p versus logν slopes), thus accounting for very fast formation of a stable radical anion (Table 4). The normalized convoluted peak currents (see Experimental) regularly decrease with increasing bulkiness of the X ligands, in agreement with the regular decrease of the diffusion coefficients of the investigated complexes.

The radical anion formation appears to be significantly favored by the more polar CH_3CN solvent with respect to CH_2Cl_2, in both thermodynamic and kinetic terms, since the normalized reduction potentials are significantly less negative, and the electrochemical reversibility criterion (E_p - $E_{p/2}$ ≈ 0.057) much more strictly met (Table 4).

First Oxidation Peaks. In our former study on dirhenium-diazine complexes with halide ancillary ligands[6] the first oxidation site was found to be localized on the metal core, and the corresponding oxidation peak to be chemically and electrochemically reversible and bielectronic, pointing to simultaneous two-electron loss from the dinuclear metal core. On the contrary, in the series of the OR derivatives **3**–**6** here reported, a close sequence of two monoelectronic peaks is observed (the number of exchanged electrons being confirmed by comparison of the oxidation limiting currents with the reduction ones, see Table 4). The first peak tends to chemical irreversibility at low scan rates (no return peak, half-peak widths lower than in the reversible case, consistently with an EC mechanism), while chemical reversibility improves with increasing scan rate, at least in the OCH_3 and OH complexes **5** and **6** (see for instance the grey curve in the OH case in Figure 3, corresponding to 2 V s^{-1}).

The much more pronounced reversibility for the OCH_3 derivative **5**, qualitatively recognizable in Figure 6, has been confirmed by the quantitative estimate of the pseudo first-order rate constants *k*' for the chemical reaction of the product of the first monoelectronic oxidation step (see Experimental and Figure 8). On the contrary, the two phenolato derivatives **3** and **4** show a combination of an irreversible first peak followed by a reversible second peak, in the whole scan rate range explored. These features resemble the usual oxidative CV patterns of alkyl-aryl ethers,[10] although it could be only a coincidence.

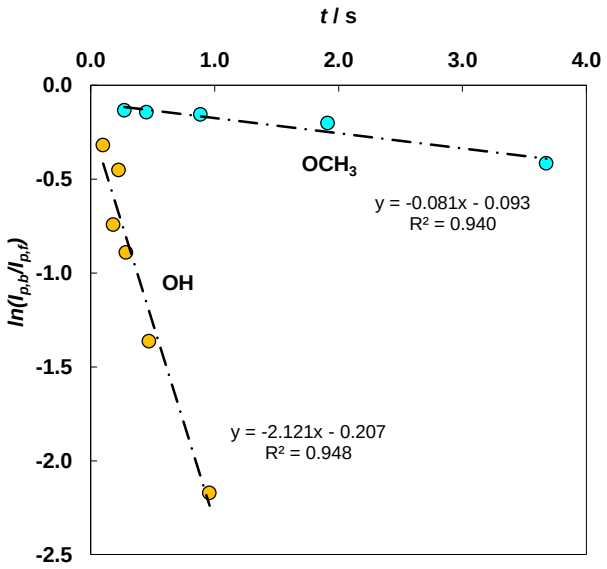

Figure 8. Estimation of pseudo first-order rate constant for the chemical reaction step following the first oxidation one, for the complexes with OCH_3 (**5**) and OH (**6**) bridging ligands. The plot evidences the much higher reactivity of the product of the first oxidation step in the case of the OH ligand (k' = 2.12 s^{-1}) compared to the OCH_3 one (k' = 0.08 s^{-1}), corresponding to halving times of 0.33 s and 8.6 s, respectively.

The picture here described appears strictly connected with the presence of bridging oxygen atoms. Indeed the SC_5H_6 derivative **2** shows (in both the investigated solvents) the reversible, bielectronic oxidation peak already observed in the halide cases. Another surprising feature of **2** is the value of its oxidation potential (0.47 V), much lower than that of the phenolato derivative **4** (1.1 V), in spite of the close similarity of their HOMO energies (Figure 4, Table 1).

Figure 9a shows a plot of the E_p values (for compounds **2**–**6** and the related halide derivatives **1**, **1'**, and **1"**)[6] vs. the energies computed for the HOMO in vacuo. Two trends can be clearly recognized (a part the aberrant behavior of the μ-hydroxo species **6**, attributable to the presence of specific hydrogen bond interactions with the solvent that are not described by the

calculation). The sulphur derivative **2** perfectly fits with the trend of the complexes bearing halide ancillary ligands, whilst the phenolato **4** agrees with the trend of the OR derivatives.

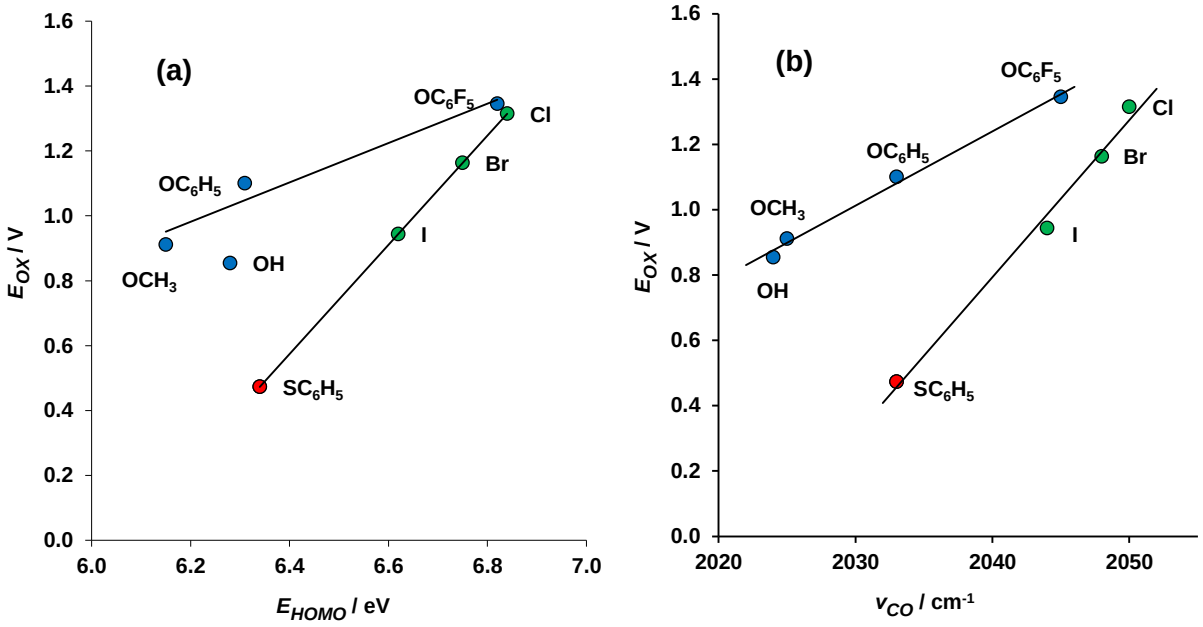

Figure 9. Plot of the first oxidation E_p values (measured in acetonitrile solution) vs. (a) the vacuum computed HOMO energies, and (b) the wavenumbers of the highest energy (totalsymmetric) ν(CO) band (acetonitrile solution).

An impressively similar two-trend plot (Figure 9b) is obtained by correlating the measured oxidation potentials with the ν(CO) values of the stretching modes, which are reliable indicators of the electron density on the metal atom. In this second correlation both the plotted quantities have been measured in solution and then in this case also the OH derivatives **6** fits the trend of the other OR species.

A similar correlation (Figure 10) is obtained also by evaluating the variation of the oxidation potentials *vs.* one (*R*) of the two descriptors of the substituents effects in organic reactions, developed by Swain and Lupton for

factoring the Hammett's σ constants into its inductive and resonance components (the *F* and *R* parameters, respectively).[11]

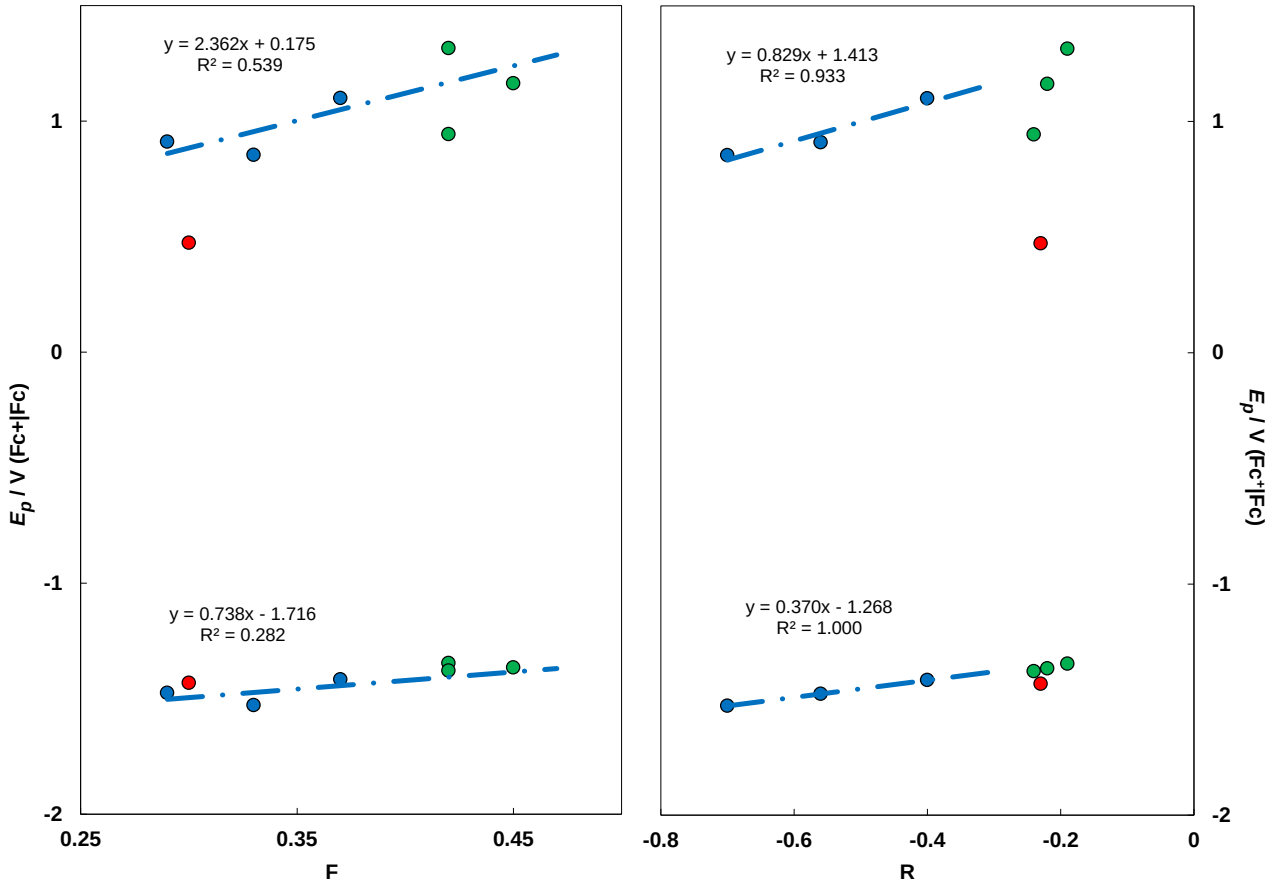

Figure 10. Correlations between first oxidation and reduction peak potentials of the investigated complexes and the Swain-Lupton's *F* and *R* parameters: *F* accounts for field effects (increasing with increasing net charge localization on the substituent), and *R* accounts for electron attracting/donating effects arising from resonance (including hyperconjugation for aliphatic groups). Unfortunately no *F* and *R* parameters appear to be available in the literature for the OC_6F_5 case. Blue circles: OR bridging ligands; green circles: halide bridging ligands; red circle: SR bridging ligand. Both the *F* and *R* plots evidence the much stronger effects of the substituents on the oxidation process with respect to the reduction one, confirming that the reduction is localized on the pyridazine ring, whereas the oxidation involves the Re_2X_2 core. Focusing on the substituent effects in the OR series alone, the *R* parameter appears to be a more efficient descriptor than the *F* one, but the trend for the halides and thiolate substituents is completely different with respect to the OR series, in line with an oxidation process taking place along different mechanisms in the two cases.

These findings fully support the view that the oxidation process is markedly different in the case of the oxygen-bridged derivatives (which show two monoelectronic oxidation steps) with respect to the other four complexes, which exhibit a single bielectronic oxidation step. This might be related the closer $Re(\mu\text{-}X)_2Re$ scaffold and to the harder nature of the bridging ligands in the case of the OR derivatives, which could result in a less efficient stabilization of the cationic products with respect to the softer anions. A detailed mechanistic electrochemical investigation will be necessary to throw light into this point.

The last column of Table 3 shows the electrochemical HOMO-LUMO gap. The energy gap for the SR derivative **2** is by far the smallest in the series (lower than 2 eV, both along the maxima and the onset criteria, see Table 4 for the latter value), while the highest energy gap is obtained, as expected, with the OC_6F_5 ligand, approximately corresponding to the chloride case in the halide series. Actually the effects of Cl and OC_6F_5 ligands appear to be nearly equivalent from a thermodynamic point of view (nearly equal HOMO and LUMO levels and first oxidation and reduction potentials, albeit the oxidative reaction mechanism is different).

3.2.5 Photophysical characterization

At room temperature, in dichloromethane solution, all the complexes show spectra dominated by two main absorption features in the UV-Vis region (see Figure 11, and Figure 12 for complex **3** in different solvents).

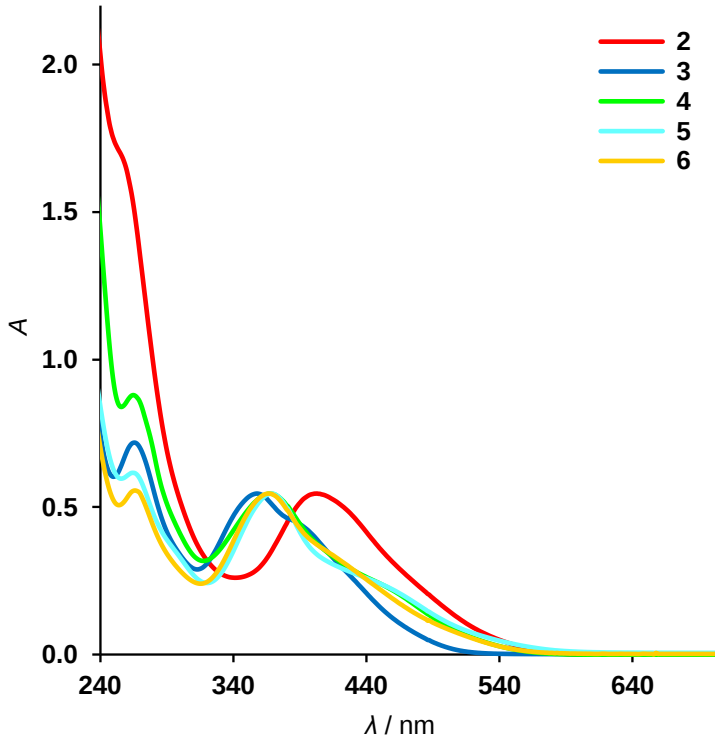

Figure 11. UV-Vis absorption spectra of complexes **2**-**6** in CH_2Cl_2 solution.

On the basis of the TD-DFT computations, the bands at higher energy, whose position (ca. 270 nm) is independent of the polarity of the solvent, can be attributed to the superposition of many singlet *d*-*d* excitations from the t_{2g} set to the e_g set of the two Re atoms. Some π–π* excitations of the pyridazine ligand fall in the same range of energy (230–300 nm), however their transition probabilities are significantly lower than those of the *d*–*d* ones (at least for the transitions lying in the energetic range considered in the computational study).

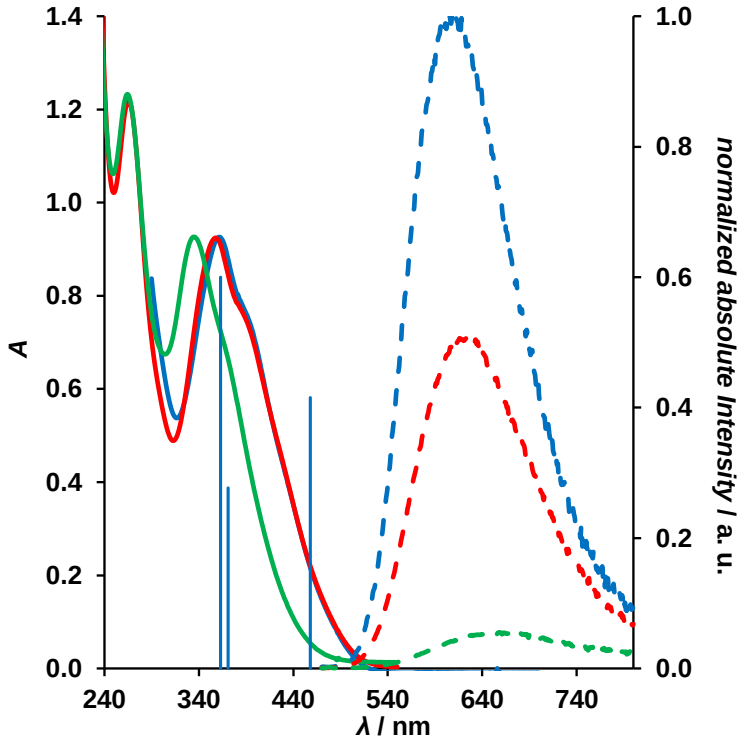

Figure 12. Solvent effect on the absorption (—) and emission (- - -) spectra of [Re_2(μ-OC_6F_5)$_2$(CO)$_6$(μ-pydz)] **3**. A comparison with excitation energies and oscillator strengths (vertical blue lines) computed in toluene is reported. Blue: toluene; red: dichloromethane; green: acetonitrile.

In Table 2 only the most intense transition of *A1* (or *A*) symmetry is reported. CPCM calculations confirm that these transitions are almost unaffected by the solvent.

The lower energy absorption bands, which have a slightly lower intensity, can be assigned to metal-ligand-to-ligand charge transfer (MLLCT) transitions, taking into account the significant contribution of the bridging ancillary ligands to the metal-centered HOMO set. These bands arise from the convolution of multiple transitions, as testified by the more or less pronounced shoulders observed at lower frequencies. In particular, the three transitions (from HOMO-*n* to LUMO or LUMO+1 orbitals) already described for the halogenated

derivatives[6] can be identified also for the new species **2**–**6**, and are listed in Table 2. The computed wavelengths are in fair agreement with the experimental absorption maxima measured in toluene solution. The mean absolute deviation between the experimental λ_{max} and the wavelength for the more intense totalsymmetric excitation computed in the gas phase is 24 nm. The agreement strongly improves (the mean absolute deviation reduces to 9 nm) including the toluene solvent in the calculation by means of the conductor-like polarizable continuum model (CPCM).

The charge-transfer character of such transitions is supported by their strong solvent dependence:[12] indeed, as already reported for the related Re_2(μ-diazine) complexes,[5,6,9] a blue shift is observed upon increasing solvent polarity (for instance from 363 nm in toluene to 335 nm in MeCN for **3**, see Figure 12). Upon excitation at 450 nm (for **2**–**4**) or 480 nm (for **5**, **6**), at room temperature in diluted deoxygenated toluene solutions, all the complexes with bridging OR groups show broad, featureless emission in the red region of the visible spectrum (range 608 ÷ 708 nm). The photoluminescence spectra for complexes **3**-**6** are shown in Figure 13 and the data are summarized in Table 5.

Compl.	X	λ_{abs} ($\varepsilon \times 10^{-3}$) [nm, $M^{-1}cm^{-1}$]	λ_{em} (nm)	$\Phi_{em} \times 10^2$	τ (ns)	$k_r \times 10^{-5}$ [s^{-1}]	$k_{nr} \times 10^{-5}$ [s^{-1}]
1 [6]	Cl	379 (8.1)	603	7.0	800	0.88	11.6
2	SC_6H_5	403 (7.0)	-	-	-	-	-
3	OC_6F_5	362 (7.6)	608	5.5	550	1.0	17.2
4	OC_6H_5	374 (6.9)	680	0.55	37	1.5	270
5	OCH_3	372 (8.7)	708	0.07	8.6	0.81	1160
6	OH	369 (8.0)	702	0.09	9.2	0.98	1090

Table 5. Absorption and emission data in toluene solution of complexes **1-6**

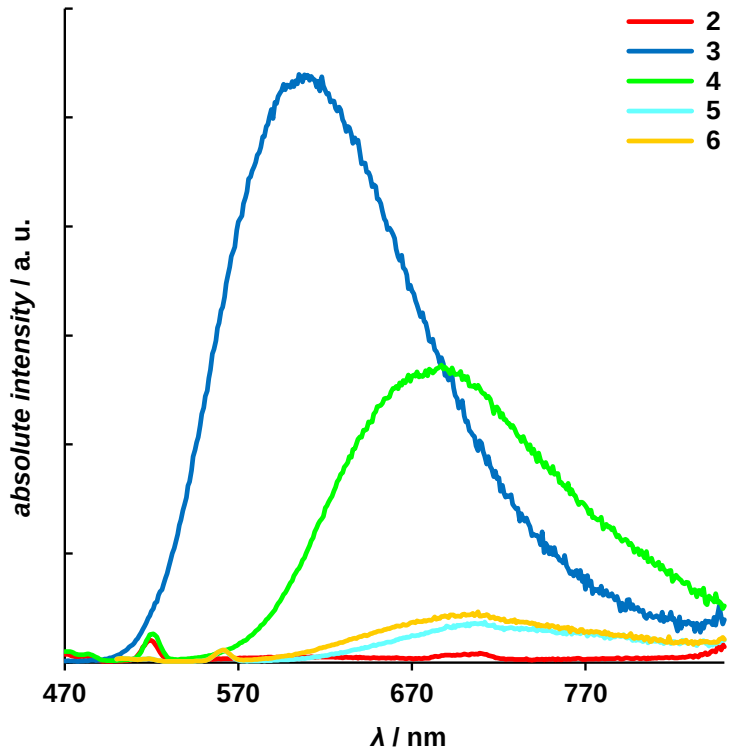

Figure 13. Effect of the ancillary OR or SR ligands on the emission spectra, recorded at room temperature in deoxygenated toluene solution, upon excitation at 450 nm (for **2**–**4**) or 480 nm (for **5**, **6**). The emission intensity of the OC_6F_5 derivative **3** has been decreased 5 times with respect to the other complexes.

It has been checked that the emission is independent of the excitation wavelength and that all the complexes are photostable. On the basis of previous results on related systems, the emission can be confidently described as arising from triplet metal-to-ligand charge transfer (^{3}MLCT) states, as supported by the red shift (for **3**: γ_{em} = 608 nm in toluene, 620 nm in dichloromethane, 650 nm in acetonitrile) and the strong decrease of the emission intensity observed on increasing the solvent polarity (see Figure 12 for complex **3**).

The photophysical properties of the pentafluorophenolato derivative **3** are closely comparable to those of the parent dichloro-derivative **1** (see Table

5), in agreement with the close similarity of their HOMO and LUMO levels, and then of their reduction and oxidation potentials. The position of the emission of the four complexes **3**-**6** is strongly affected by the nature of the OR groups and red shifts on increasing the donor power of the ligand, following the trend of the electrochemical HOMO-LUMO gaps. The photoluminescence quantum yields decrease in the same order (Table 5, Figure 13), according to the Energy Gap law (EGL), and the k_{nr} values roughly lie on the same line as the previously reported dichloro derivatives containing pydz, and mono and di-alkylpyridazines (Figure 14).

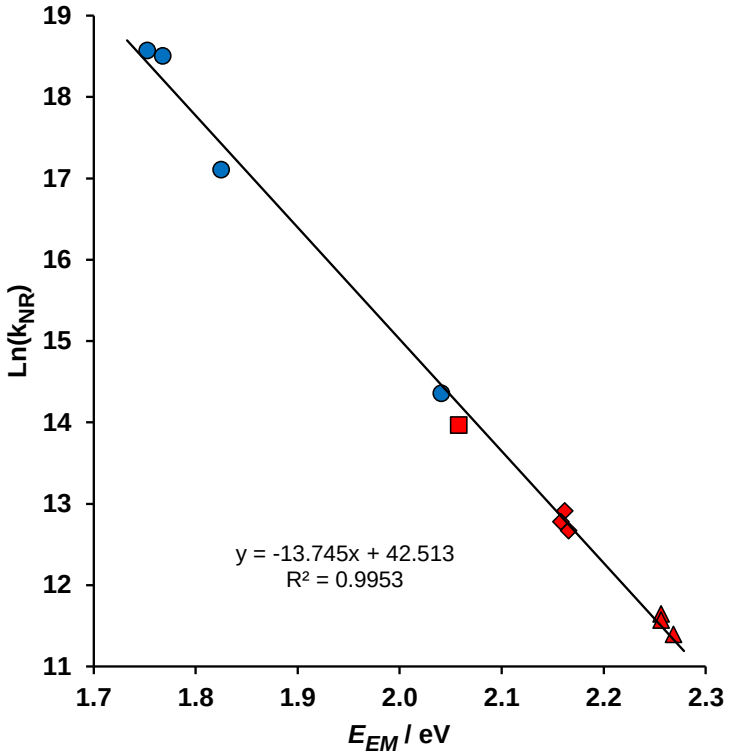

Figure 14. EGL plot concerning the novel $[Re_2(\mu\text{-}OR)_2(CO)_6(\mu\text{-pydz})]$ complexes **3**-**6** (blue circles) and a series of previously characterized $[Re_2(\mu\text{-}Cl)_2(CO)_6(\mu\text{-1,2-diazine})]$ complexes: red square, diazine = pydz (**1**), red diamonds, diazine = 4-alkyl-pydz,; red triangles, diazine = 4,5-dialkyl-pydz (the red data are from refs. 7-9).

This indicates that the nature of the excited states and the pathways responsible for their non-radiative deactivation are little affected by the nature of the bridging ancillary ligands X, provided that these ones do not perturb the stiffness of the $Re_2(\mu\text{-}X)_2(\mu\text{-diazine})$ core (as it occurs with the bulky Br derivative, whose k_{nr} falls well above the EGL line).

It is worth mentioning that complexes containing analogous $Re_2(\mu\text{-}ER)_2(CO)_6$ fragments (E = O, S), joined by 4,4'-bipyridil ligands in $[Re_2(\mu\text{-}ER)_2(CO)_6(4,4'\text{-bpy})_2]_2$ molecular rectangles, had been previously reported,[13] and also in these cases (very weak) emission in solution was observed only from some of the OR derivatives (highest PLQY 0.039% in acetonitrile solution).[13d]

3.3 Conclusions

The synthesis of a series of neutral dinuclear rhenium complexes of general formula $[Re_2(\mu\text{-}ER)_2(CO)_6(\mu\text{-pydz})]$ (E = O or S) has been performed. Several new synthetic routes have been developed, all of which are more complex than those used for the related di-halogen $[Re_2(\mu\text{-}X)_2(CO)_6(\mu\text{-1,2-diazine})]$ complexes, due to the unavailability of $[Re(CO)_5X]$ starting materials when X = ER.

The substitution of halides by OR groups does not modify significantly the nature of the frontier orbitals and of the absorption/emission processes, which maintain the previously described metal-ligand-to-ligand charge transfer character. The bridging OR groups are deeply involved in the HOMO set, whose energy progressively rises on increasing the OR donor power (a part the deviant behavior of the OH derivative), with consequent easier oxidation of the complex and reduced band gap. Accordingly a progressively red shifted and weakened emission is observed on going from OC_6F_5 to OC_6H_5 to OCH_3 (and OH).

These results confirm that it is possible to modulate the photophysical properties of the Re_2-diazine complexes in a two-fold manner: the variation of the substituents on the chromophoric moiety (the diazine ring) affects the LUMO level, while the variation of the ancillary ligands modifies the HOMO level.

The behavior of the bis-pentafluorophenolato complex **3** is comparable to that of the dichloro complex **1**, and therefore improvement in the

photoluminescence quantum yields is expected on raising the LUMO levels, by replacing pyridazine with the 4,5-dialkyl-pyridazine ligands, as previously observed in the series of dichloro derivatives.[9]

However, a perfluorophenolate unit is of limited interest for bioconjugation. Therefore, the low emission properties of the complexes bearing OR groups different from OC_6F_5, together with the not straightforward synthesis of this family of $[Re_2(\mu\text{-}OR)_2(CO)_6(\mu\text{-}pydz)]$ complexes, indicate that this approach might not be ideal for conjugating a luminescent Re_2-diazine group to biomolecules bearing ROH moieties. Different routes will be investigated, involving *inter alia* mixed $[Re_2(\mu\text{-}Cl)(\mu\text{-}OR)(CO)_6(\mu\text{-}diazine)]$ derivatives, which are expected to exhibit higher PLQYs than the corresponding bis-(OR) derivatives. Moreover, the strong enhancement of the luminescence on going from organic to aqueous solution, exhibited by some $[Re_2(\mu\text{-}OR)_2(CO)_6(4,4'\text{-}bpy)_2]_2$ rectangles bearing long alkyl chains,[13d] suggests that analogous self-aggregation phenomena might positively perturb the emissive behavior of our systems when bonded to large biomolecules.

As far as the benzenethiolate derivative **2** is concerned, in spite of its lack of luminescent properties, it appears of interest from a different point of view. Its low energy band gap and its perfectly reversible oxidation and reduction processes might find application for current generation by light harvesting. We are currently investigating the modulation of the electrochemical and light absorption properties of similar $[Re_2(\mu\text{-}SR)_2(CO)_6(\mu\text{-}1,2\text{-}diazine)]$ complexes on varying the nature of the SR groups and of the diazine substituents.

(1) See Lucenti, E.; D'Alfonso, G.; Macchi, P.; Maranesi, M.; Roberto, D.; Sironi, A.; Ugo, R. *J. Am. Chem. Soc.* **2006**, *128*, 12054–12055, and refs therein;

(2 Schmidt, S. P.; Nitschke, J.; Trogler, W. C. *Inorg. Synth.*, **1989**, *26*, 113–117;

(3) a) Ciani, G.; D'Alfonso, G.; Freni, M.; Romiti, P.; Sironi, A. *J. Organomet. Chem.* **1978**, *152*, 85–94; b) Jiang, C.; Wen, Y.-S.; Liu, L.-K.; Hor, T. S. A.; Yan, Y. K. *Organometallics* **1998**, *17*, 173–181;

(4) Herberhold, M.; Süss, G.; Ellermann, J.; Gäbelein, H. *Chem. Ber*. **1978**, *111*, 2931–2941;

(5) Panigati, M.; Donghi, D.; D'Alfonso, G.; Mercandelli, P.; Sironi, A.; Mussini, P.; D'Alfonso, L. *Inorg. Chem.* **2006**, *45*, 10909–10921;

(6) Donghi, D.; D'Alfonso, G.; Mauro, M.; Panigati, M.; Mercandelli, P.; Sironi, A.; Mussini, P.; D'Alfonso, L. *Inorg. Chem.* **2008**, *47*, 4243–4255;

(7) Geometric parameters found in **2**–**4** are unexceptional and similar to those reported for analogous species containing a Re–(μ-OR)–Re or a Re–(μ-SR)–Re fragment (Cambridge Structural Database 5.32). Bond distances and angles reported in the text are average values; the largest standard uncertainty on bond distances and angles are 0.012 Å and 0.5°, respectively;

(8) The *C*2*v* geometry of **2** possesses two imaginary frequencies (34*i* e 31*i*). This conformation lays 4.6 kJ mol–1 higher than the *C*2 minimum. In addition, starting the optimization from the solid-state geometry an asymmetric minimum was found, whose energy is only negligibly different from those of the *C*2 minimum. Since MO energies and excitations are almost identical for the *C*2 and the *C*1 conformers, only the values computed for the symmetric species will be reported and discussed;

(9) Mauro, M.; Quartapelle Procopio, E.; Sun, Y.; Chien, C.H.; Donghi, D.; Panigati, M.; Mercandelli, P.; Mussini, P.; D'Alfonso, G.; De Cola, L. *Adv. Funct. Mater*. **2009**, *19*, 2607–2614;

(10) a) Wendt, H.; Bitterlich, S. *Electrochimica Acta* **1992**, *37*, 1951–1958; b) Said, A. H.; Mhalla, F. M.; Amatore, C.; Verpeaux, J. N. *J. Electroanal. Chem.* **1999**, *464*, 85–92; b) Said, A. H.; Mhalla, F. M.; Amatore, C.; Thouin, L.; Pebay, C.; Verpeaux, J. N. *J. Electroan. Chem.* **2002**, *537*, 39–46;

(11) a) Swain, C. G.; Lupton, E. C. Jr. *J. Am. Chem. Soc.* **1968**, *90*, 4328–4337; b) Hansch, C.; Leo, A.; Taft, R. W. *Chem. Rev*. **1991**, *91*, 165–195;

(12) Giordano, P. J.; Wrighton, M. S. *J. Am. Chem. Soc.* **1979**, *101*, 2888–2897;

(13) a) Benkstein, K. D.; Hupp, J. T.; Stern, C. L., *Inorg. Chem.* **1998**, *37*, 5404-5405; b) Woessner, K. D.; Helms, J. B.; Shen, Y.; Sullivan, B. P., *Inorg. Chem*, **1998**, *37*, 5406-5407; c) Marimaran, B.; Rajendran, T.; Lu, Y. L.; Lee, G. H.; Peng, S. M.; Lu, K. L., *J. Chem. Soc, Dalton Trans.* **2001**, 515-517; d) Marimaran, B.; Thanasekaran, P.; Rajendran, T.; Lin, R. J.; Chang, I. J.; Lee, G. H.; Peng, S. M.; Rajagopal, S.; Lu, K. L., *Inorg. Chem.* **2002**, *42*, 5323-5325.

Chapter 4

DINUCLEAR RHENIUM(I) COMPLEXES CONTAINING TRIAZOLE AND TETRAZOLE LIGANDS

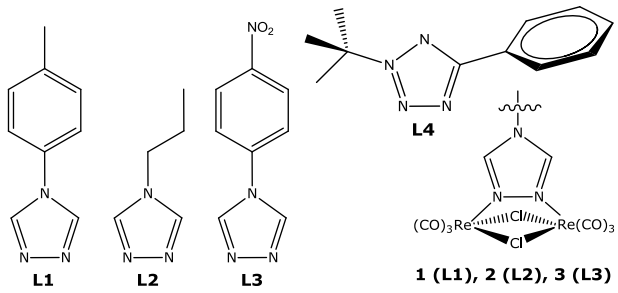

A new series of neutral dinuclear complexes of rhenium containing bridging 1,2,4-triazole ligands (**L1**-**L3**) has been synthesized. The complexes were designed to obtain a blue shift of the emission compared to the corresponding diazine complexes. The absorption spectra and the electrochemical data show that the rising of the HOMO-LUMO gap has actually occurred, but the intensity of the emission is too weak to have any applicative interest. Experiments trying to obtain complexes in which triazolate ligands coexist with a diazine chromophore are also described. The possible synthesis of analogous derivatives containing 5-aryl tetrazoles (**L4**) is also under investigation. In both the triazole and tetrazole cases, the new species are examples of a very limited family of molecular complexes in which such ligands are bound to metals in low oxidation state.

4.1 Introduction

Triazoles and tetrazoles are pentatomic aromatic heterocycles, as depicted in Scheme 1. Generally, triazoles are good donor ligands, very often used in inorganic chemistry due to their propensity to link metal ions leading to the formation of coordination polymers, hybrid organic/inorganic structures with the metal centers connected through organic ligand in mono-, bi- or tridimensional structures.[1]

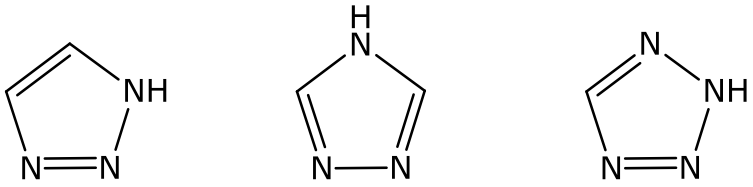

1,2,3-triazole 1,2,4-triazole tetrazole

Scheme 1.

The use of N-donor linkers in these Metal Organic Frameworks (MOFs) is increasingly reported,[2,3] most likely because they allow the preparation of inorganic/organic materials, like the Zeolitic Imidazolate Frameworks (ZIFs),[4] with exceptional chemical and thermal stability.

The two families of triazoles – the 1,2,3-triazoles and the 1,2,4-triazoles – show different properties and reactivity: in this work we have considered 1,2,4 triazoles substituted in position 4 with aryl and alkyl groups. The choice of 4-substituted 1,2,4-triazoles prevents the formation of triazolate anion, maintaining the ligand neutral; moreover, in this way we can obtain dinuclear neutral complexes without substituents in the 3 and 5 positions of the bridging ligand, which could affect the stiffness of the scaffold, due to steric hindrance

with the carbonyls. Finally, the use of these ligands could promote a blue-shift of the emission maxima of the corresponding rhenium(I) complexes: in fact DFT preliminary calculations have indicated, strong destabilization of the LUMO level in the corresponding complexes, with respect to the analogous diazine compounds.

Despite these systems are generally considered electron-poor, due to the mesomeric effect of the nitrogen on the aromatic ring, we can write five resonance structures (Scheme 2) in which the positive charge is always localized on the apical nitrogen, whilst the negative charge is localized on the carbon atoms or on the nitrogen atoms in 1 and 2 position, whose electron pairs are not involved in the aromaticity of the ring.

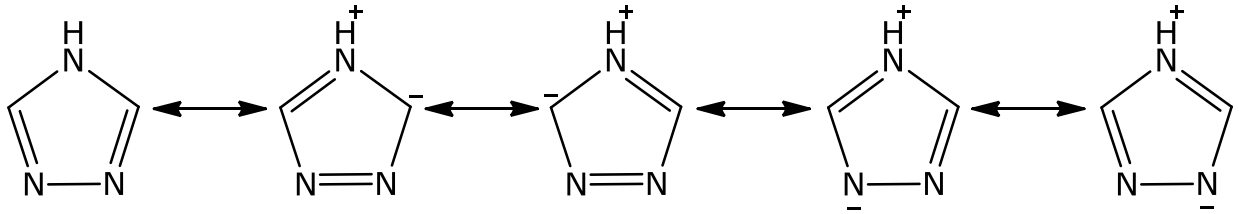

Scheme 2. Resonance structures of 1,2,4-triazole.

This suggests that, whilst the heteroatom 4 is particularly electron-poor, the two carbon atoms and the two adjacent nitrogen atoms are electron-rich. This excess of negative charge contribute to destabilize the π^* orbital of the ring, with a subsequent enhancement of the LUMO level of the corresponding complexes.

The possibility to obtain dinuclear complexes, similar to those formed by 1,2-diazines, by using five membered heterocycles had been previously verified in our research group, using 2,5-diphenyl-1,3,4-oxadiazole.[5] It is also

well known the propensity of tetrazole and triazole rings to act as bridging ligands between two metal centres, leading to the formation of dinuclear complexes of type [M-N-N-M']. In order to assess the influence of the substituent in the 4-position on the photophysical properties of the complexes, we have synthesized triazoles containing either electron-donor or electron-withdrawing substituents (Scheme 3).

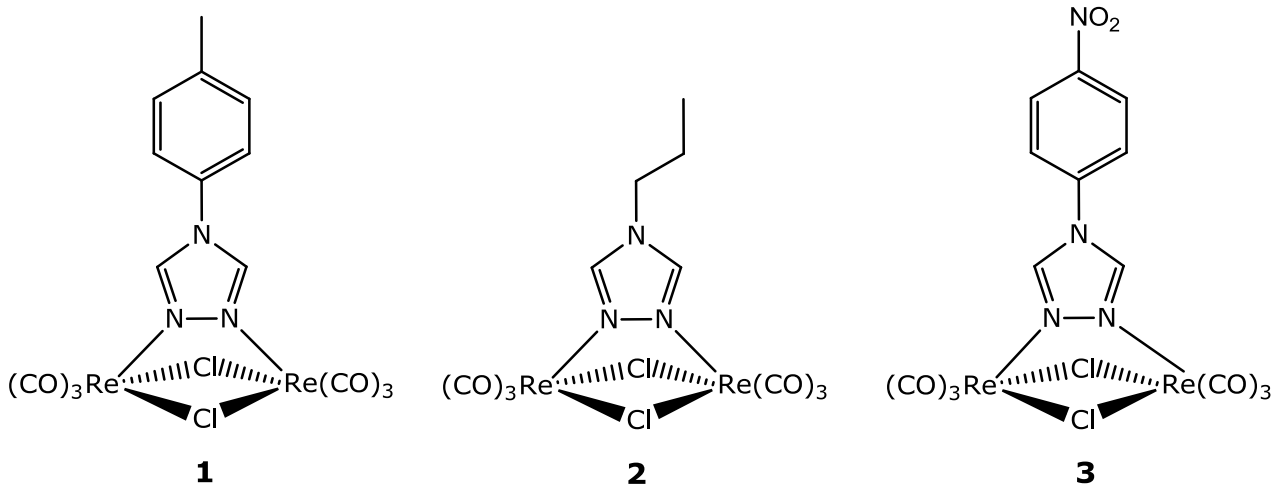

1 **2** **3**

Scheme 3. The synthesized complexes **1**-**3**.

Also the synthesis of neutral dinuclear rhenium complexes containing as chromophore a bridging 1,2-diazine and as ancillary ligands one or two unsubstituted 1,2,4-triazolates has been attempted. The aim was to obtain luminescent complexes, thanks to the presence of the pyridazine chromophore, that might be inserted within a mono or bidimensional coordination polymers, by exploiting the third coordination position of the triazole ligands.

A few experiments with an alkyl-tetrazole ligand, selected in order to obtain neutral complexes, have also been performed. The ligand (2-(*t*-butyl)-5-phenyl-2*H*-tetrazole) (**L4**) was provided by Dr. S. Stagni of the Inorganic and Physical Chemistry Department of the University of Bologna.

4.2 Results and discussion

4.2.1 Synthesis

The method used for the synthesis of the triazole ligands involves the condensation-dehydration reaction between N,N'-diformyl-hydrazine, obtained by N-formyl-hydrazine and triethyl orthoformate (TEOF) in methanol, and the appropriate primary amine (Scheme 4).

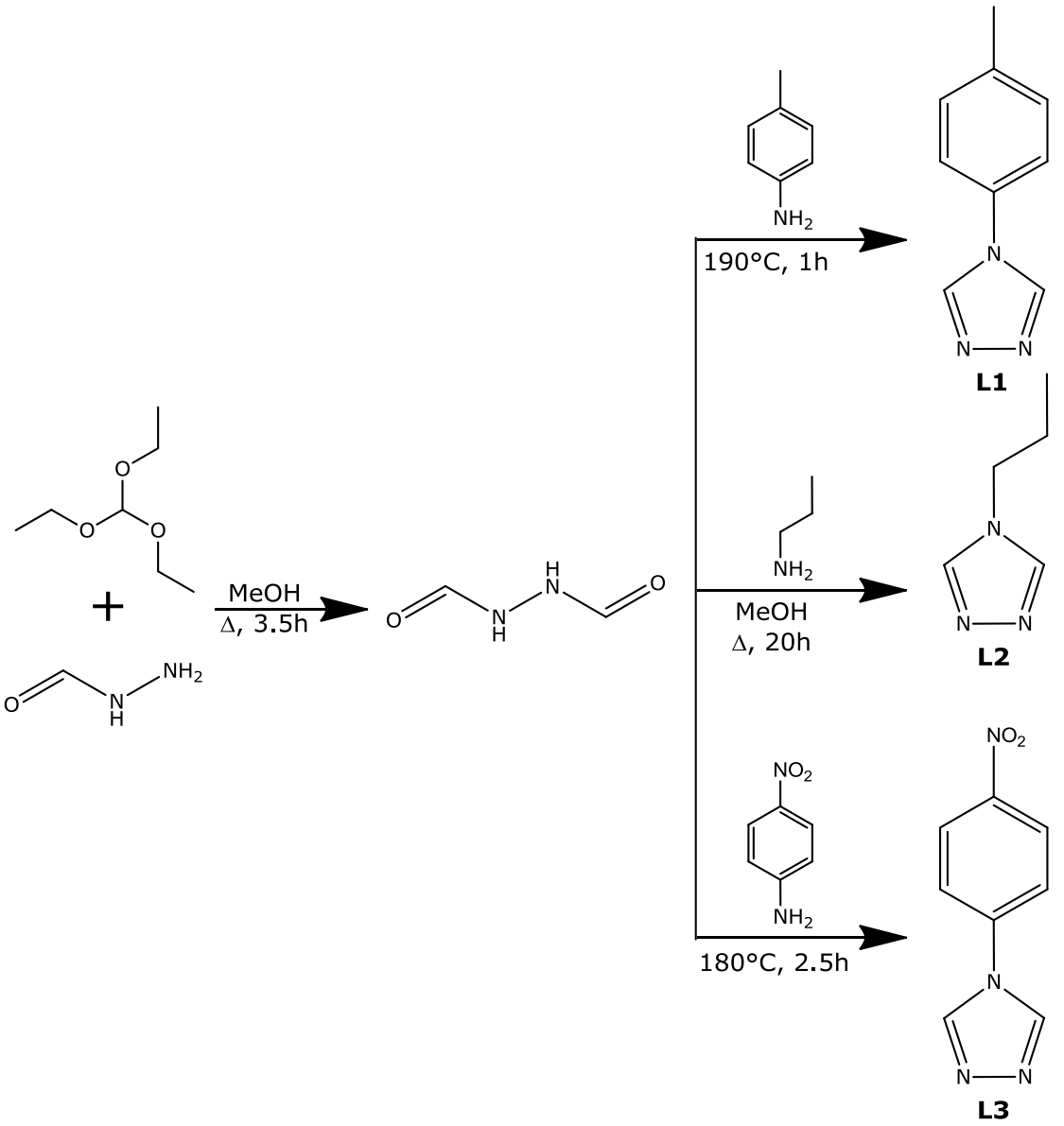

Scheme 4. Synthesis of ligands **L1**-**L3**.

^{1}H-NMR data of the synthesized ligand are reported in Table 1. It is worth to note in the two aryl triazoles the strong effect of the substituents in the 4 position (methyl or nitro)- on the chemical shift of the triazole signal.

Ligand	**^{1}H NMR** (δ ppm, $(CD_3)_2CO$, 300K)	
	Triazole	***Substituent***
4-(*p*-tolyl)-4*H*-1,2,4-triazole	8.50 (s, 2H)	2.45 (s, 3H) 7.31 (d, 2H) 7.35 (d, 2H)
4-(*n*-propyl)-4*H*-1,2,4-triazole	8.40 (s, 2H)	0.99 (t, 3H) 1.88 (m, 2H) 4.07 (t, 2H)
4-(4'-nitrophenyl)-4*H*-1,2,4-triazole	9.08 (s, 2H)	8.08 (d, 2H) 8.47 (d, 2H)

Table 1. ^{1}H NMR data of triazole ligands.

The complexes were obtained in acceptable yields (40-60%) by following the same methodology used for the diazinic ligands, i.e. by refluxing the appropriate triazole and two equivalent of $[Re(CO)_5Cl]$ for 2 h in toluene solution. Scheme 5 shows the synthesized complexes: : $[Re_2(\mu\text{-}Cl)_2(CO)_6$(μ-4-(p-tolyl)-4*H*-1,2,4-triazole)] (**1**), $[Re_2(\mu\text{-}Cl)_2(CO)_6$(μ-4-(n-propyl)-4*H*-1,2,4-triazole)] (**2**), and $[Re_2(\mu\text{-}Cl)_2(CO)_6$(μ-4-(4'-nitrophenyl)-4*H*-1,2,4-triazole)] (**3**).

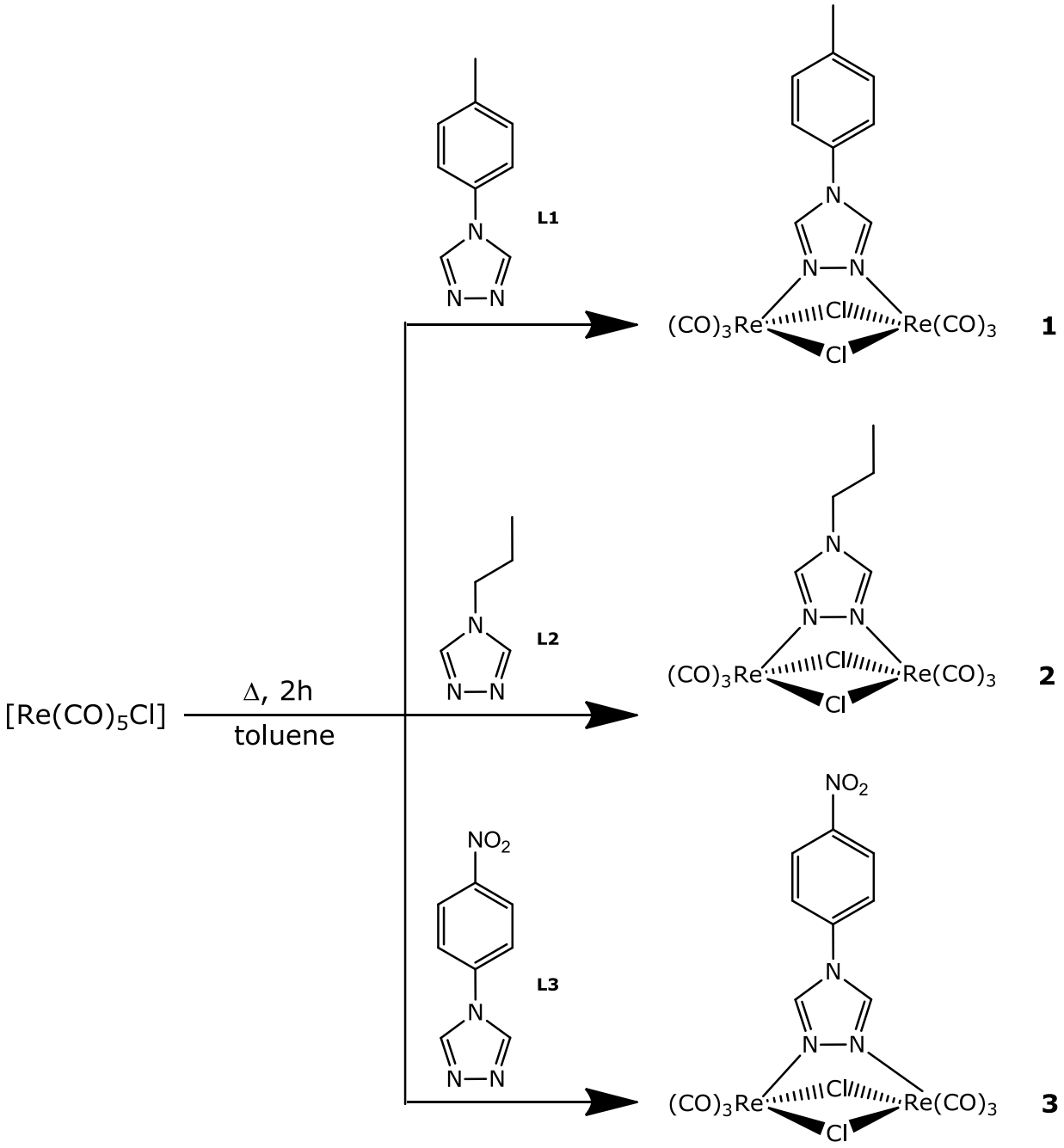

Scheme 5. Synthesis of complexes **1**-**3**.

The ν(CO) IR values and the ^{1}H NMR data of complexes **1-3** are reported in Table 2.

Complex	**IR** ν(CO) cm^{-1} (CH_2Cl_2)	**^{1}H NMR** (δ ppm, $(CD_3)_2CO$, 300K)	
		Triazole	***Substituent***
1	2049m, 2033s 1940s, 1914s	10.38 (s, 2H)	2.48 (s, 3H) 7.55 (d, 2H) 7.94 (d, 2H)
2	2049m, 2033s 1940s, 1914s	9.93 (s, 2H)	1.11 (t, 3H) 2.21 (m, 2H) 4.56 (t, 2H)
3	2050m, 2035s 1944s, 1917s	10.63 (s, 2H)	8.46 (d, 2H) 8.61 (d, 2H)

Table 2. IR and ^{1}H NMR data of complexes **1**-**3**.

The IR spectra showed, in the carbonyl stretching region, the presence of four bands, a common feature of this kind of $Re_2(CO)_6$ complexes. The bands shift at higher frequencies for complex **3**, due to the presence on the triazole ring of an electron withdrawing substituent, causing a lower donor capability of the ligand, i.e. lower electron-density on the metal centers. Also the ^{1}H NMR data are consistent with the proposed structure: because of the coordination on the metal centre, the resonance of the aromatic protons of the triazole ring is shifted to high fields by about 1.5 ÷ 1.9 ppm with respect to the free ligand, as also observed for diazine complexes.[6]

The stability of the synthesized complexes in the presence of other mono or bidentate σ-donor ligands has been investigated, using complex **1** as example of this class of compounds. In the presence of coordinating solvents, such as acetonitrile or of other nitrogen ligands, such as pyridazine, no substitution of the 1,2,4-triazole ligand was observed, at variance with what observed for the complex with the oxadiazole ligand.[5] Instead the slow formation of two mononuclear species, in a 1:1 ratio, has been observed. The two species have been formulated as $[Re(CO)_3ClL_2]$ and $[Re(CO)_3Cl(triaz)L]$ (L = CH_3CN, pydz), on the basis of the IR and NMR data. Likely the reaction runs through an intermediate, in which both triazole and L are terminally bound on the two Re atoms of the binuclear complex (as depicted in Scheme 6 for L = pydz).

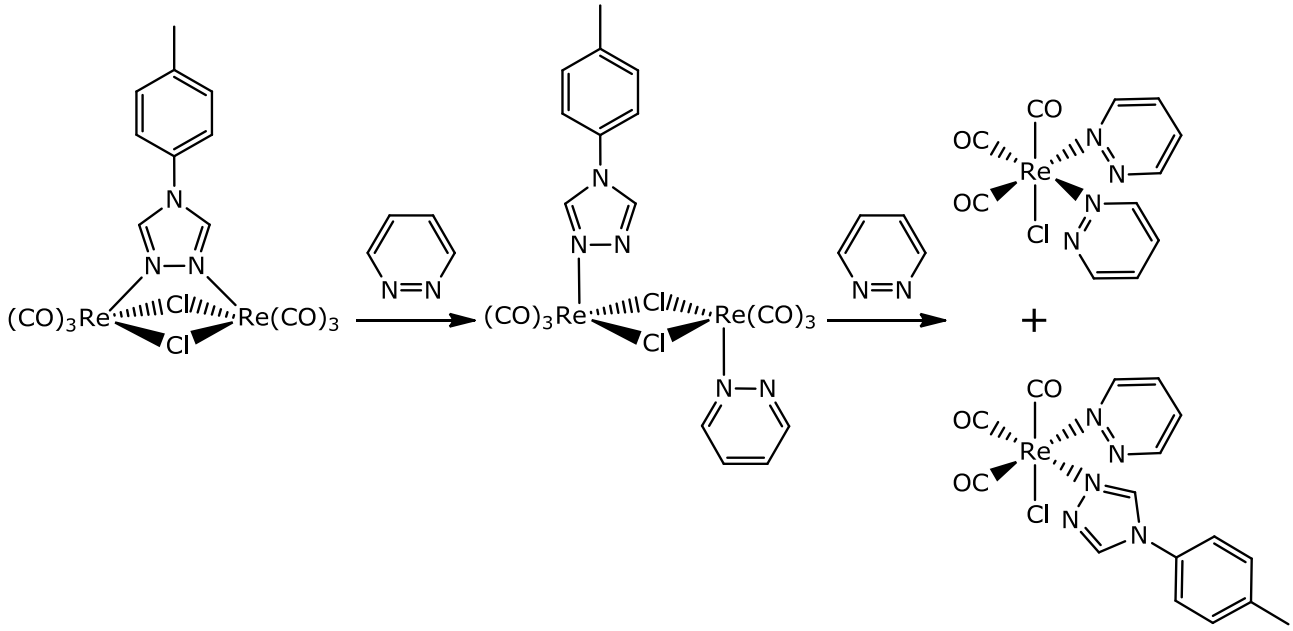

Scheme 6. Stability of complex 1 in presence of pyridazine.

The stability of this intermediate, characterized in solution for L = pydz, would explain the failure of the substitution of triazole by the pyridazine,

differently from what previously observed for the derivative containing a bridging diaryl-oxadiazole, which is a good leaving group due to its steric congestion. Increasing the pyridazine/complex ratio and heating the solution led to the opening of the chloride bridges with the formation of the two above mentioned mononuclear complexes.

In the case of the 4-alkyl tetrazole ligand **L4** the reaction with $[Re(CO)_5Cl]$ was performed in the same conditions described before, but in this case a mixture of at least three species (**4**-**6**) was obtained, no one of which was the expected product (Scheme 7).

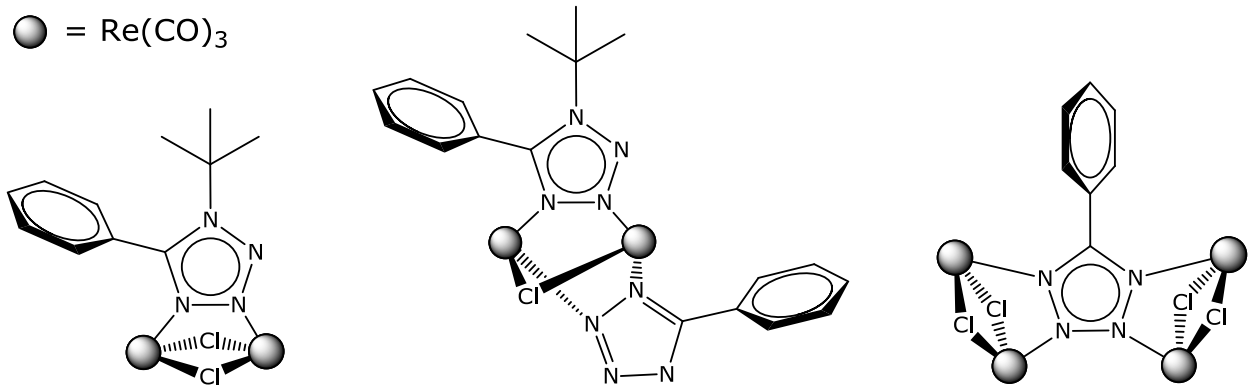

Scheme 7. Complexes **4**-**6** obtained by reaction of **L4** with $[Re(CO)_5Cl]$.

The first complex **4**, isolated and characterized through X-ray diffraction analysis (Figure 1) on a single crystal, is a structural isomer of the expected derivative, since the *t*-butyl group is bound to nitrogen N-1, in β position with respect to the N-3 and N-4 nitrogen atoms involved in the metal coordination. This migration likely leads to the formation of a sterically less hindered and then more stable complex.

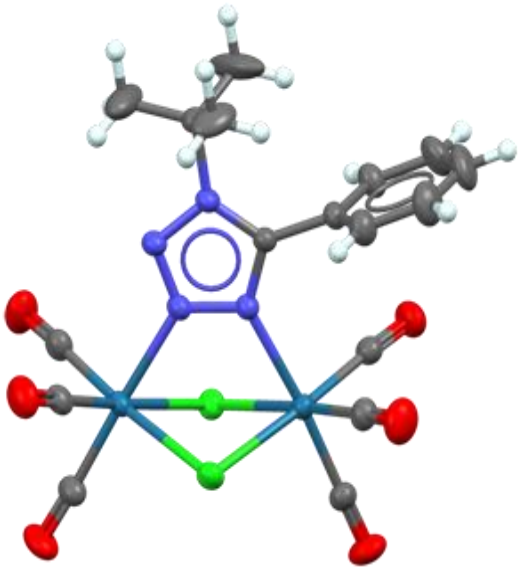

Figure 1. ORTEP view of complex **4**.

The main reaction product (70%) is a poorly soluble species, which has been formulated, on the basis of NMR data, as the dinuclear complex [Re_2(μ-Cl)$(CO)_6$(μ-5-phenyl-tetrazolate)(μ-1-(*t*-butyl)-5-phenyl-2*H*-tetrazole)] (**5**), containing a bridging neutral tetrazole and a bridging tetrazolate anion.

In the aromatic region (7.80 ÷ 7.75 ppm) of ^{1}H NMR spectrum of complex **5** are present four signals in the ratio 1:2:1:1, ascribed to the protons of the phenyl ring in the 5 position of the tetrazole.

^{1}H COSY experiment (Figure 2) allows to identity two partially overlying aromatic system. The integrated signals of the aromatic systems accounts exactly twice for the *t*-butyl signal at 1.82 ppm. The presence of the same NMR signals, in the same integration ratios, even after different purification processes (such as chromatographic column and recrystallization) supports the view that the observed signal are due to a single species rather than to a mixture.

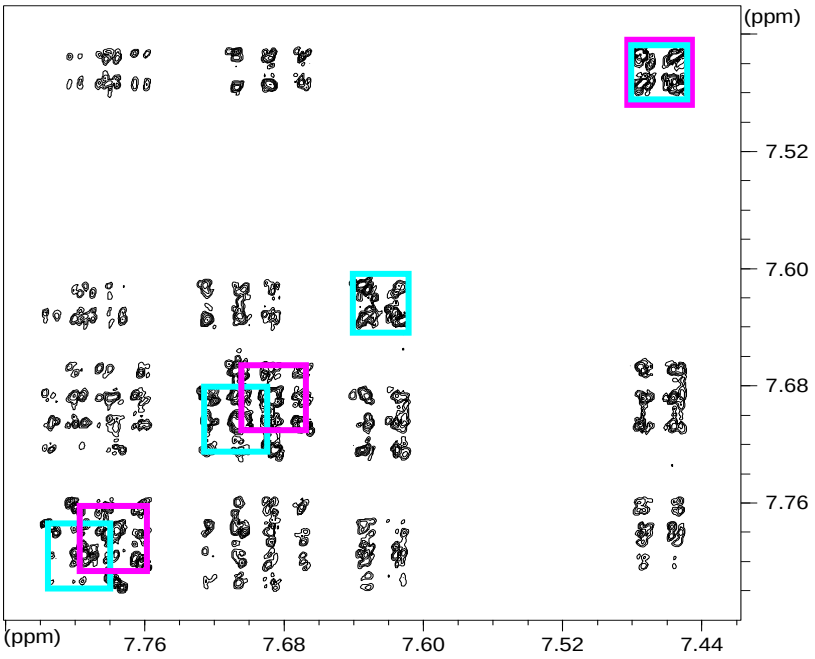

Figure 2. ^{1}H COSY of complex **5** (CD_2Cl_2, 298 K).

The dissociation of the *t*-butyl group, affording the tetrazolate anion, is responsible also of the formation of the third product (**6**). It is an anionic tetra-nuclear species in which a single tetrazolate anion acts as a bridging ligand towards two Re(μ-Cl)$_2$Re units using all its four nitrogen atoms. This coordination, revealed by the single crystal X-ray structure analysis (Figure 3) is a rather unusual, at least for rhenium complexes, although in the literature some examples of tetrazolate anions acting as tetradentate ligands are known.[7]

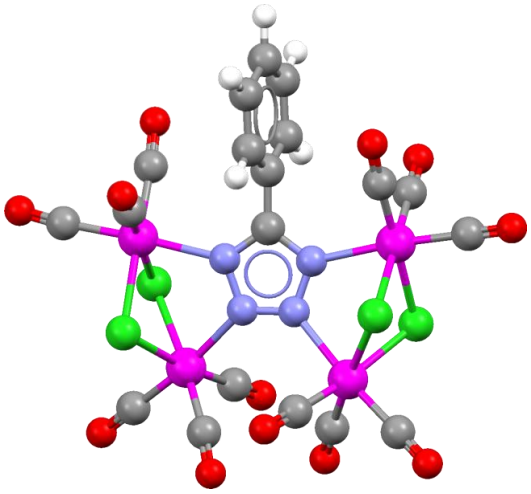

Figure 3. ORTEP view of complex **6.**

A second section of this chapter is devoted to the synthesis of neutral dinuclear rhenium complexes containing as bridging ligands both one 1,2-diazine and one or two triazolate anions. These complexes are expected to be luminescent, thanks to the presence of the pyridazine chromophore, and also to be able to make mono or bidimensional coordination polymers, due to the third coordination position of the triazole ligands. We designed two synthetic routes to these complexes, starting from different dinuclear complexes (Scheme 7).

The first one concerns the use as starting compounds of $[Re_2(\mu\text{-triazolate})_2(\mu\text{-OH})(CO)_6]^-$ anions, obtained through the reaction of $[Re_2(\mu\text{-OH})_3(CO)_6]^-$ in molten triazole). The substitution of one of the anionic ligands with pyridazine, promoted by the addition of a strong not coordinating acid (HBF_4), is shown in the top of Scheme 7. However, NMR and IR evidence suggests that the protonation occurred on one of the N-4 nitrogen atoms, rather than on one of the atoms involved in the coordination to the metal, giving rise to the new stable neutral dinuclear species $[Re_2(\mu\text{-triazolate})(\mu\text{-}$

OH)$(CO)_6$(μ-triazole)(] and [Re_2(μ-triazolate)$_2$$(CO)_6$(μ-triazole)], both of which contain a neutral triazole ligand.

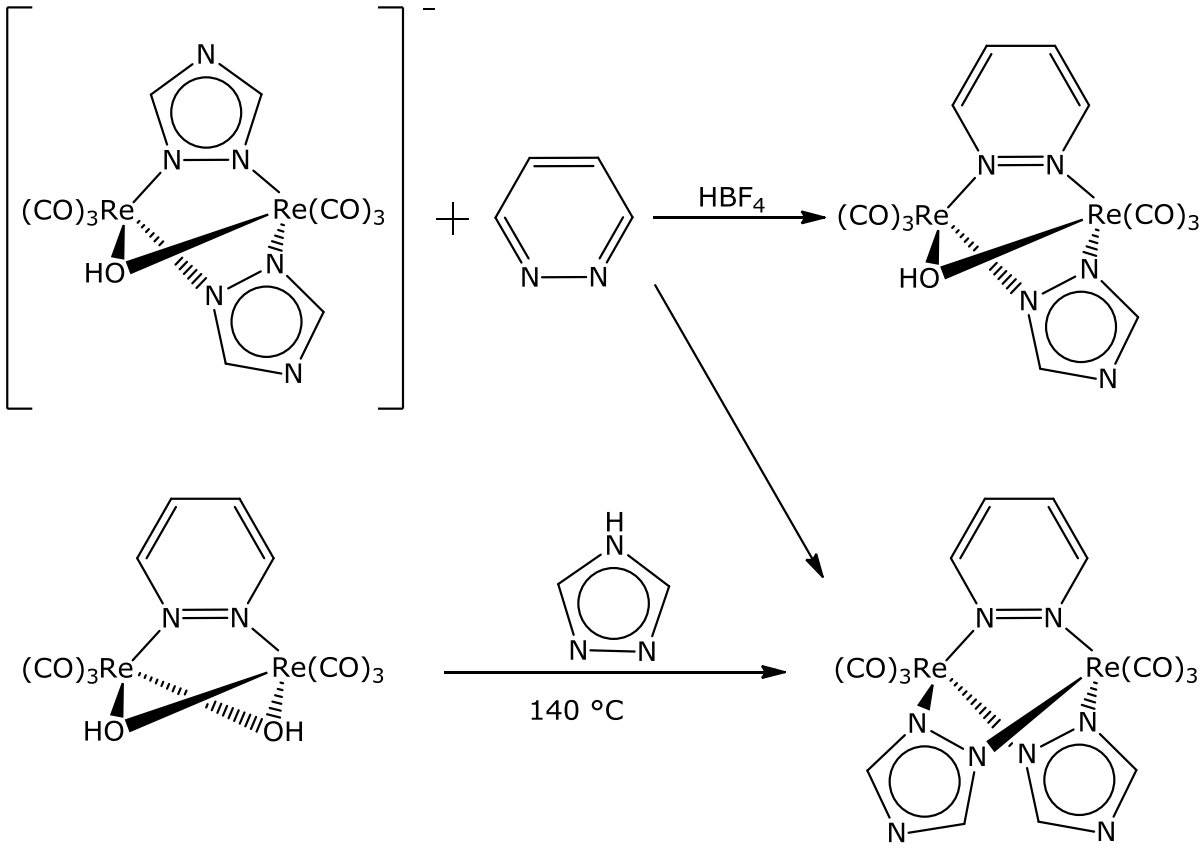

Scheme 7. Scheme of two different designed synthesis routes.

The second synthetic approach that has been explored concerns the substitution reaction of one or two hydroxy ligands of the neutral dinuclear complex [Re_2(μ-OH)$_2$$(CO)_6$(μ-pydz)], by triazolate anions. In this case the triazole itself should act as the protonating agent. The substitution of OH groups by a triazolate anion in molten triazole is largely documented.[8] Preliminary experiments suggest that the formation of the desired complex is actually feasible, but requires the optimization of a purification procedure from the many (albeit in low concentration) by-products.

Particularly noteworthy is the obtainment of the new tris-triazolate anion $[Re_2(\mu\text{-}1,2,4\text{-triazolate})_3(CO)_6]^-$ (**7**) starting from $[Re_2(\mu\text{-}OH)_3(CO)_6]^-$ in molten 1,2,4-triazole (Scheme 8).

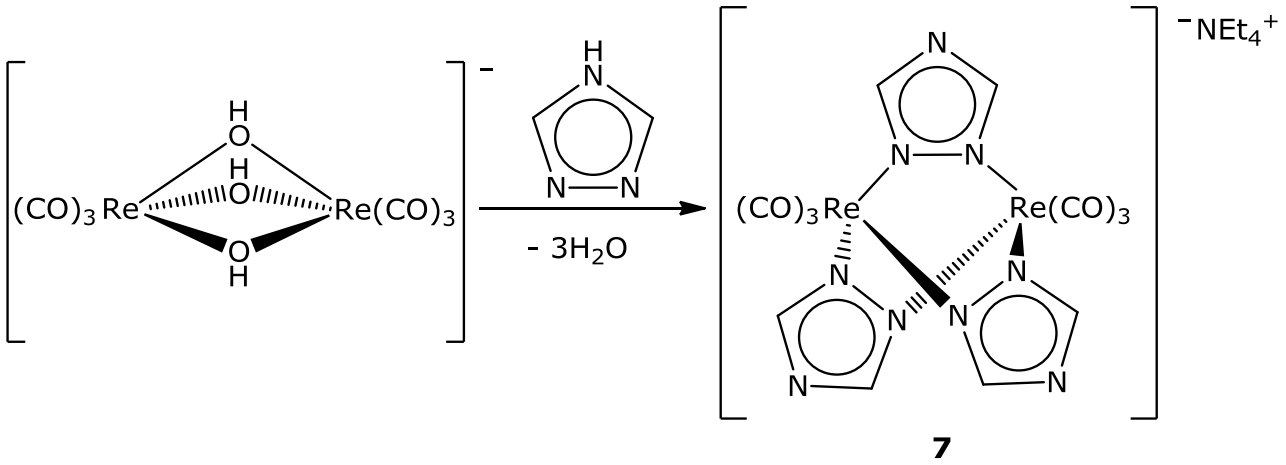

7

Scheme 8.

In a previous work the complexes $[Re_2(\mu\text{-triazolate})_3(\mu\text{-}OH)_2(CO)_6]^-$ and the analogous $[Re_2(\mu\text{-triazolate})_3(\mu\text{-}OMe)_2(CO)_6]^-$ had been obtained treating the respective parental anion in molten triazole under milder condition.[8] The anion **7** was isolate as NEt_4^+ salt after sublimation of the excess of triazole and washing with water. The ν(CO) IR values and the ^1H NMR data of complexes **7** are reported in Table 3.

Complex	**IR** ν(CO) cm^{-1} (CH_2Cl_2)	**^{1}H-NMR** (δ ppm, $(CD_3)_2CO$, 300K)	**Elemental analysis**	
			Calculated	***Found***
7	2016s 1908s	8,25 (s, 6H) 3,46 (q, 8H) 1,41 (tt, 12H)	%C (27,46) %H (2,995) %N (16,01)	%C 27,0 %H 2,98 %N 17,18

Table 3. IR and ^1H NMR data of complexes **7**.

The formation of dinuclear complexes in which two metal centres are linked by three bridging triazolates is rare and was never reported before for complexes of metals in low oxidation states.[1]

4.2.2 Computational study

DFT calculation, performed by dr. Pierluigi Mercandelli of the Department of Structural Chemistry and Inorganic Stereochemistry of Università degli Studi di Milano allowed to understand the nature of the frontier orbitals of complexes **1-3** (Figure 5). As for the complexes with diazine ligands, the HOMO orbital set is essentially constituted by phase and antiphase combination of t_{2g} orbitals of the two metal centres, with a contribution, in the higher energy levels, of the *p* orbitals of the ancillary ligands. Phenyl and triazole ring π^* orbitals form the set of the LUMO orbitals, stabilized by the presence of electron-withdrawing substituents on the aromatic ring. Ongoing from the free ligand to the complex, the LUMO is stabilized, because the coordination to the metal centre reduces the electron density on the ligand, according to the electrochemical data.

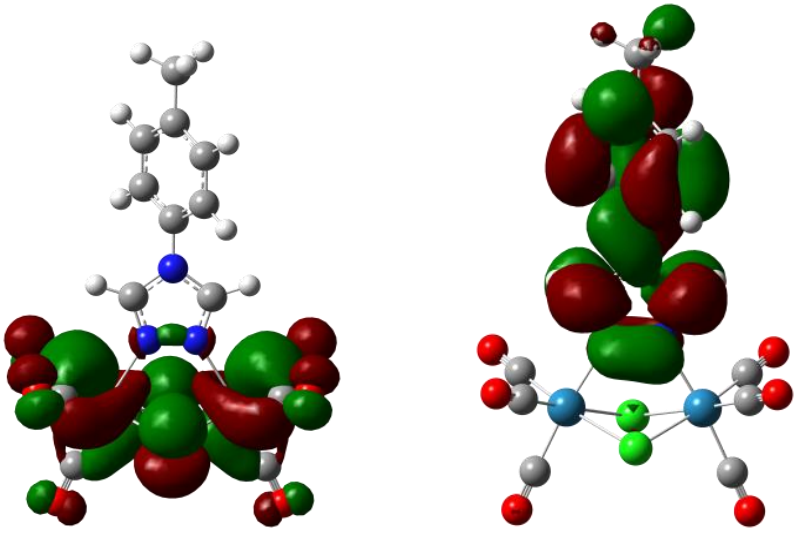

Figure 5. Views of the isodensity surface plots of the HOMO (left) and LUMO (right) of **1.**

4.2.3 Electrochemical characterization

Cyclic voltammetric analysis of complexes **1**-**3** has been performed in collaboration with Prof. P. Mussini. The cyclovoltammograms are reported in Figure 4, while the most significant CV features are reported in Table 4.

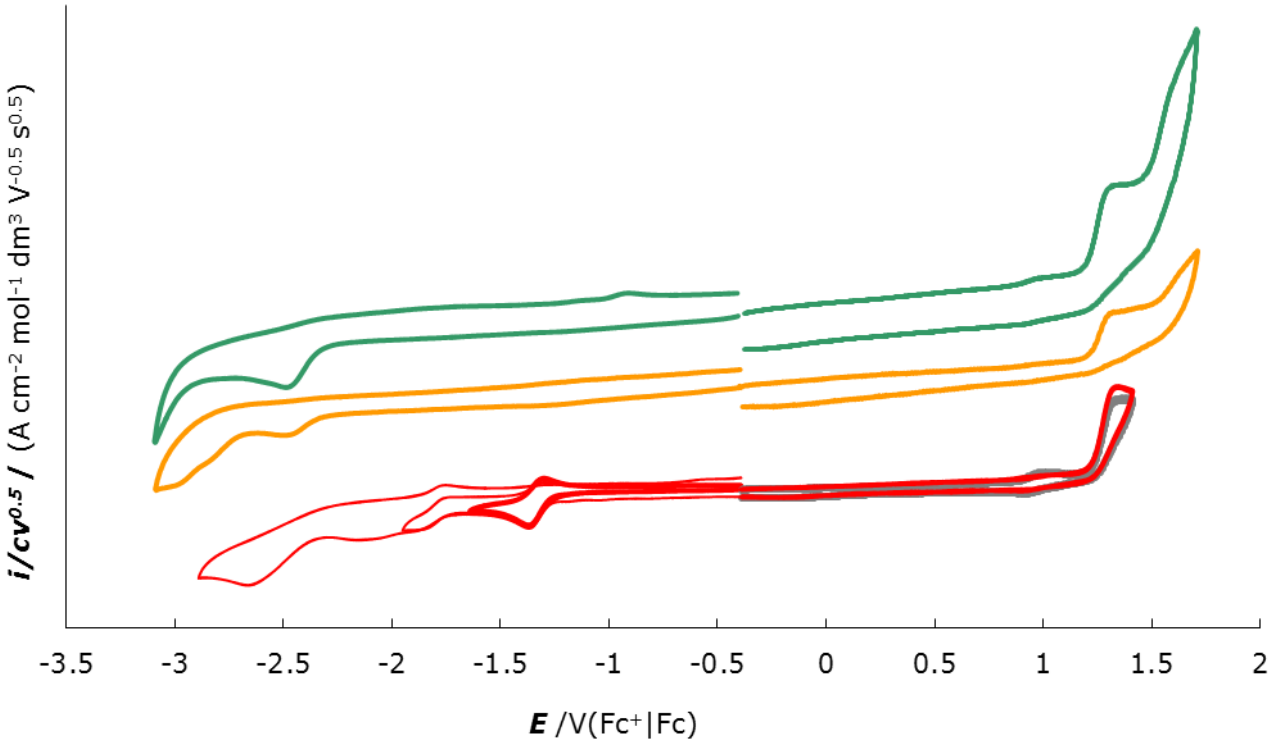

Figure 4. Cyclovoltammetric analysis of complexes **1** (yellow line), **2** (green line) and **3** (red line) recorded in MeCN solution at room temperature. The gray superimposed curve in complex **3** refers to apparent solvolysis process.

The first reduction peak centered on the triazole fragment is observed around -2.5 V (vs. $Fc^+|Fc$), indicating a much easier reduction than the free ligand (coordination stabilizes LUMO). In the case of the free 4-(*p*-tolyl)-4*H*-1,2,4-triazole ligand no reduction peak is observed at potentials as low as -3 V. This indicates that the coordination stabilizes the LUMO by about 1 eV, more than what observed in case of corresponding oxadiazole complex.[5]

All complexes show a bi-electronic oxidation peak at ca. +1.3 V (vs. $Fc^+|Fc$), similar to the ones observed in the corresponding diazine[9,10] or oxadiazole complexes.[5], practically unaffected by the substituent on the triazole unit, in spite of its radical change from electron donating to strongly electron withdrawing. This behavior clearly indicates that the oxidation is metal centered. The presence of a more electron-withdrawing ligand (the triazole) makes the oxidation more difficult with respect to the complex with 1,2-diazines. As in the case of the oxadiazole derivative,[5] both the oxidation and the reduction processes are chemically and electrochemically irreversible.

Complex	$E_{pmax,red}$ (V)	$E_{pmax,ox}$ (V)	**LUMO** (eV)	**HOMO** (eV)	E_g (eV)
1	-2.47	1.31	-2.33	-6.11	3.78
2	-2.49	1.31	-2.32	-6.11	3.80
3	-1.37	1.33	-3.43	-6.13	2.70

Table 4. Selected CV features for complexes **1**-**3**. Peak potentials E_p (0.2 V s^{-1} scan rate); electrochemical HOMO and LUMO energy levels and gaps calculated along the peak maxima. Potentials are referred to the $Fc^+|Fc$ couple in the operating media (MeCN + 0.1 M $TBAPF_6$).

Introducing a nitro group in *para* position on the phenyl substituent on the triazole unit results in a much more stabilized LUMO, localized on the same nitro group. It gives rise to two monoelectronic reduction peaks,[11] the first of which happens at a remarkably less negative potential (-1.37 V). It is electrochemically reversible and chemically quasi reversible at 0.2 V/s (actually the follow-up reaction has a rate constant perceivable in the operating 0.05 ÷

2 V/s scan rate, the process appearing entirely reversible at 2 V/s). As a consequence, the electrochemical HOMO-LUMO gap is much narrower.

On the other hand, the strongly withdrawing character of the nitro group can be perceived in complex **3** apparently undergoing slow solvolysis by the acetonitrile solvent (gray superimposed curve recorded after about half an hour), possibly yielding a single rhenium complex species, as in our formerly studied 3,6-dichloro-diazine case.[9] In other words, inserting strong electron attractor groups on the diazine or triazole ligand decreases the electron donating ability of the two nitrogen atoms bridging the two Rhenium atoms, and therefore destabilizes the complex, especially in a solvent like acetonitrile, highly competitive in cation coordination. Actually the observed solvolysis rate constant could be considered an indicator of bridging strength from the heteroaromatic ring.

4.2.4 Photophysical characterization

The free ligands 4-(p-tolyl)-4*H*-1,2,4-triazole and 4-(4'-nitrophenyl)-4*H*-1,2,4-triazole show two bands in the UV region (Figure 6).

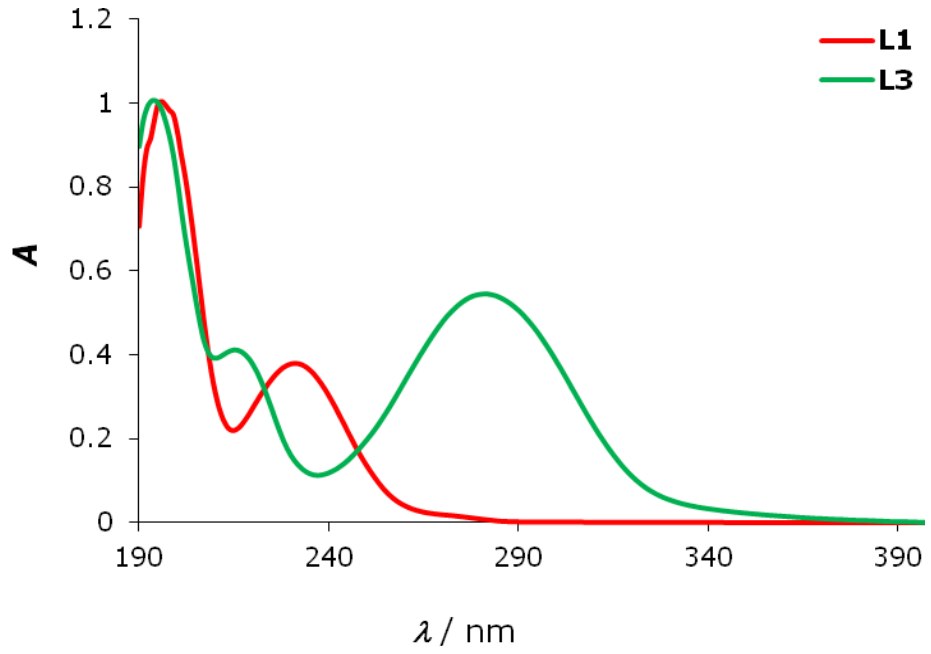

Figure 6. Absorption spectra of free ligands 4-(p-tolyl) (**L1**) and 4-(4'-nitrophenyl)-4*H*-1,2,4-triazole (**L2**) in MeCN solution at room temperature.

The lower energy band is attributable to a n-π* transition, with a contribution of the π-π* transition of the phenyl group in 4-position, as confirmed by the shift of the relative band from 232 to 282 nm on going from to 4-(*p*-tolyl) to 4-(4'-nitrophenyl)-4*H*-1,2,4-triazole as confirmed by DFT calculations. The electron-withdrawing character of the nitro group is responsible for the decrease of the π* level, which lowers the energy of the transition. Moreover, for both the ligands, the position of the band is slightly solvent-dependent, in accord with the weak charge transfer character of n-π* transitions. The band at higher energy (~ 190 nm) is ascribed to a π-π*

transition, although DFT calculations indicate a weak contribution of n-π* transitions. A third weak band (~ 217 nm) is also present for 4-(4'-nitrophenyl)-4*H*-1,2,4-triazole, due to transitions involving the nitro group .

All the complexes show an absorption band at 195 nm (Figure 7) attributed to π-π* transitions of both aromatic and heterocyclic rings.

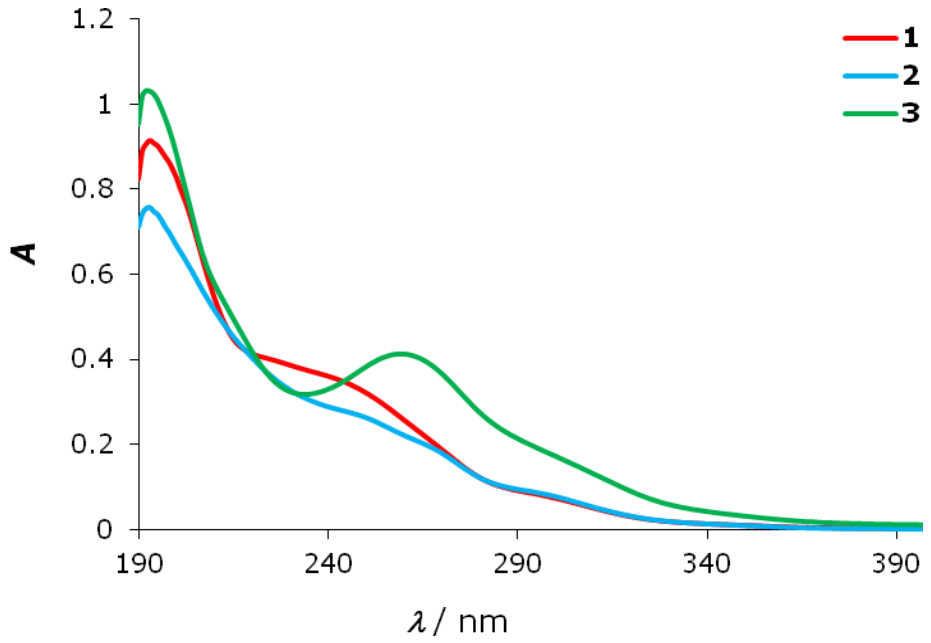

Figure 7. UV-Vis absorption spectra of complexes **1**-**3** in MeCN solution at room temperature.

Moreover all the complexes show at least two very broad absorption bands at lower energy, ranging from 240 and 300 nm. On the basis of DFT calculations, these latter bands have been assigned to ^{1}MLCT transitions, with a small contribution of π-π* transitions for the higher energy absorptions. In this case, the ^{1}MLCT bands undergo a hypsochromic shift of about 50 nm with respect to the corresponding diazine complexes, in line with the raising of the LUMO levels and the higher HOMO-LUMO gap (about 3.8 eV for **1** and **2** vs. 2.66 for the dichloro-pydz derivative[9]). As far as the substituent effect is

concerned, the MLCT bands of complex **3** are shifted to lower energy as expected for the presence of the electron-withdrawing nitro group.

Table 5 summarizes the most meaningful photophysical data for all the investigated compounds.

Compound	**λ_{abs} (ε x 10^{-3})** [nm, M^{-1} cm^{-1}] π- π^*	**λ_{abs} (ε x 10^{-3})** [nm, M^{-1} cm^{-1}] MLCT mix d-d
4-(*p*-tolyl)-4*H*-1,2,4-triazole	196 (32,9) 231 (12,5)	-
4-(4'-nitrophenyl)-4*H*-1,2,4-triazole	194 (26,9) 215 (11,1) 281 (14,6)	-
1	193 (46,5)	ca. 240 (17,7) ca. 300 (3,6)
2	193 (36,1)	ca. 250 (12,8) ca. 300 (3,7)
3	192 (49,3)	259 (19,8) ca. 300 (7,7)

Table 5. Absorption spectral data of 4-(p-tolyl) and 4-(4'-nitrophenyl)-4*H*-1,2,4-triazole and for complexes **1**-**3** in MeCN solution at room temperature.

The emitting properties of the complexes were studied at RT in CH_2Cl_2 solution. All the complexes resulted to be bad emitters, as the analogous oxadiazole derivative: very weak emission bands in the range 350-450 nm are observed after excitation at 300 nm (Figure 8). In the case of the oxadiazole derivatives, the lack of emission was attributed to the poor stiffness of the complex, due to the lower basicity of the oxadiazole nitrogen atoms and to the

significant steric hindrance determined by the presence of two phenyl substituents in ortho position. This should not be the case for the complexes here presented since the lack of substituents in ortho position and the better σ-donor properties of the ligand should improve the stiffness of the complexes. Therefore, their photophysical behaviour should be attributed to photoinstability or to LUMO destabilization, which allows the overlap between the potential energy surfaces of MLCT triplet states, populated by ISC from the ^{1}MLCT state, and those of d^{π}-$d^{\sigma*}$ states, whose decay to the ground state is spin forbidden.

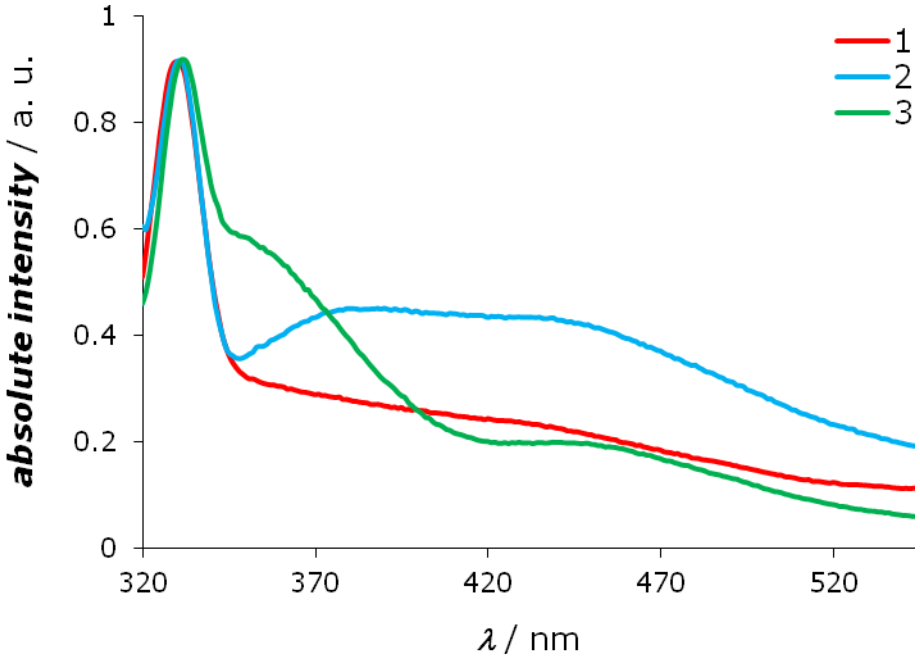

Figure 8. Emission spectra of complexes **1**-**3** in CH_2Cl_2 solution at room temperature. The signals at ca. 335 nm arise from the Raman emission of the solvent.

Attempts to evaluate the photostability of the complexes were hampered by the lack of emissive properties of the triazole fragment eventually obtained from the photodegradation of the complexes.

4.3 Conclusions

New dinuclear luminescent tricarbonyl Re(I) complexes containing multi-nitrogen heterocyclic ligand have been studied. Different 4-substituted 1,2,4-triazoles have been synthesized in order to investigate how the change of the substituents in the 4 position affects the properties of the corresponding Re(I) complexes. In literature very few cases of molecular complexes containing 1,2,4-triazole are reported, especially with metal in low oxidation states.

The first family of compounds employed triazoles as potential chromophore. In such complexes a raising of the LUMO (and then a possible blue-shift of the emission) is expected with respect to the analogous compounds containing 1,2-diazines. The corresponding neutral dinuclear dichloro species have been synthesized; the complexes are stable, and the absorption bands are significantly blue-shifted, in agreement with the expected rise of the LUMO level. The intensity of the emission however is very low: more detailed photophysical and computational investigation is necessary to explain this point.

The reaction of 2-(*t*-butyl)-5-phenyl-2*H*-tetrazole with $[Re(CO)_5Cl]$ allows to obtain, in mixture with other species, a very unusual tetranuclear complex in which a single tetrazolate anion acts as a bridging ligand towards two $Re(\mu\text{-}Cl)_2Re$ units using all its four nitrogen atoms. The electrochemical and photophysical characterization of such system is currently under investigation.

A second class of compounds has been obtained using triazolate anions as ancillary ligands in complexes bearing 1,2-diazine as chromophoric moiety.

Some species have been isolated and characterized, starting from different rhenium precursors, although the synthesis and the isolation of such complexes is difficult due to the presence of many byproducts. The photophysical characterization is still in progress, and will allow to better understand the role of the ancillary ligand in the modulation of the emission properties of such complexes. Moreover, it would be possible a further modulation of the photophysical properties of the complexes through the coordination of another metal centre to the free nitrogen atom in the 4-position.

(1) Aromí, G.; Barrios, L. A.; Roubeau, O.; Gamez, P. *Coord. Chem. Rev*. **2011**, *255*, 485-546;

(2) Venna, S. R.; Carreon, M. A. *J. Am. Chem. Soc.* **2010**, *132*, 76-78;

(3) Phan, A.; Doonan, C. J.; Uribe-Romo, F. J.; Knobler, C. B.; O'Keeffe, M.; Yaghi, O. M. *Acc. Chem. Res.* **2010**, *43*, 58-67;

(4) Lu, Z.; Knobler, C. B.; Furukawa, H.; Wang, B.; Liu, G. N.; Yaghi, O. M. *J. Am. Chem. Soc.* **2009**, *131*, 12532-12533;

(5) Mauro, M.; Panigati, M.; Donghi, D.; Mercandelli, P.; Mussini, P.; Sironi, A.; D'Alfonso, G. *Inorg. Chem.* **2008**, *47*, 11154-11165;

(6) Raimondi, A.; Panigati, M.; Maggioni, D.; D'Alfonso, L.; Mercandelli, P.; Mussini, P.; D'Alfonso, G. *Inorg. Chem.* **2011***, submitted article;*

(7) Zhao, H.; Qu, Z.-R.; Ye, H.-Y.; Xiong, R.-G. *Chem. Soc. Rev.* **2008**, *37*, 84-100;

(8) Barea, E.; Rodriguez-Diéguez, A.; Navarro, J.A.R.; Sironi, A.; D'Alfonso, G. *Dalton Trans.* **2008**, 1825-1827;

(9) Donghi, D.; D'Alfonso, G.; Mauro, M.; Panigati, M.; Mercandelli, P.; Sironi, A.; Mussini, P.; D'Alfonso, L. *Inorg. Chem.* **2008**, *47*, 4243-4255:

(10) Mauro, M.; Quartapelle Procopio, E.; Sun, Y.; Chien, C.-H.; Donghi, D.; Panigati, M.; Mercandelli, P.; Mussini, P.; D'Alfonso, G.; De Cola, L. *Adv. Funct. Mater.* **2009**, *19*, 2607-2614.

(11) a) H. Lund, O Hammerich, Organic Electrochemistry, 4th ed., Dekker, New York, 2001; b) Smith, W. H.; Bard, A. J. *J. Am. Chem. Soc.* **1975**, *97*, 5203-5210.

Chapter 5

LUMINESCENT HYDRIDO-CARBONYL CLUSTERS OF RHENIUM(I) WITH SQUARE GEOMETRY

The reactions of the unsaturated tetranuclear cluster of formula $[Re_4(\mu_3\text{-}H)_4(CO)_{12}]$ (**1**) with diazines bearing substituents in 4 and 5 positions (**L1**, **L2**) and with 1,8-naphthyridine (**L3**) have been performed. The reaction pathways and the influence of the substituents on the fragmentation reactions have been investigated. The photophysical properties of the main reaction products have been preliminary determined.

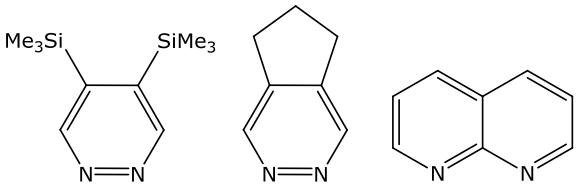

5.1 Introduction

A large number of electronically unsaturated hydrido-carbonyl clusters of rhenium have been synthesized and characterized in the past,[1,2] much larger than for any other transition metal. In a previous work of my group[3] the reactivity of the unsaturated tetranuclear complex $[Re_4(\mu_3\text{-}H)_4(CO)_{12}]$ (**1**) towards pyridazine and phthalazine was deeply investigated. Different reaction paths have been identified, as summarized in Scheme 1.

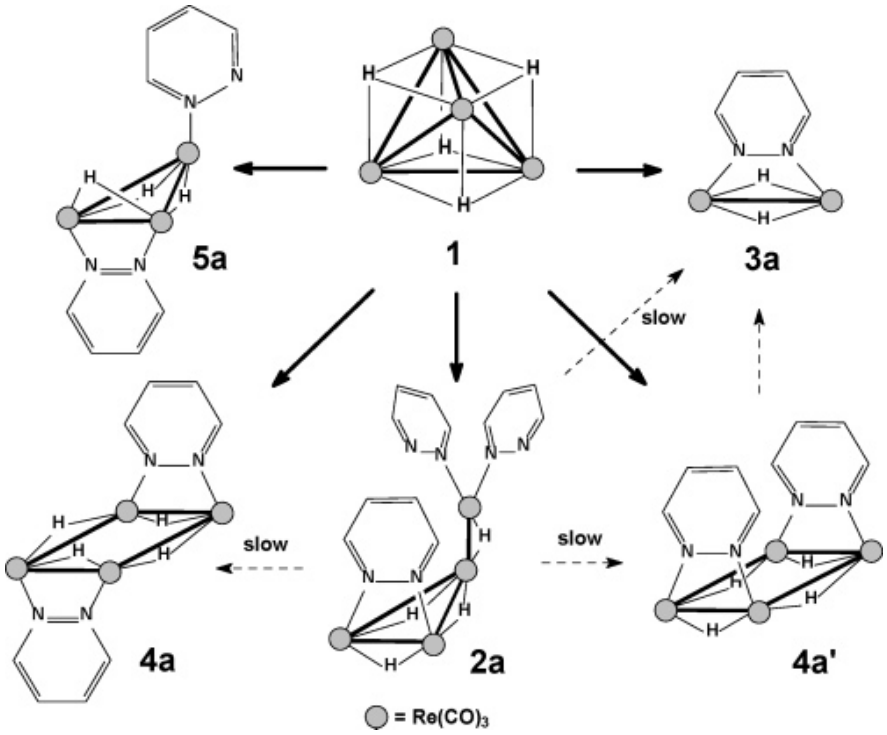

Scheme 1. Reaction paths of $[Re_4(\mu_3\text{-}H)_4(CO)_{12}]$ (**1**) in presence of pyridazine.

In the case of the reaction with pyridazine, the main reaction products are the dinuclear unsaturated clusters (32 v.e.s.) of formula $[Re_2(\mu\text{-}H)_2(CO)_6(\mu\text{-pydz})]$ (**3a**) and the tetranuclear square cluster $[Re_4(\mu\text{-}$

$H)_4(CO)_{12}(\mu\text{-pydz})_2]$ (**4a**), electronically saturated, in which the two pyridazine ligands are disposed in a *trans* configuration with respect to the plane of clusters. The reaction mechanism leading to the formation of the above mentioned species is rather complicated, and two different and competitive reaction pathways have been found. The first process involves a [2 + 2] fragmentation of the parent cluster **1**, leading to the formation of the dimeric species **3a** (equation 1), while an unusual direct rearrangement process of **1**, without the formation of detectable intermediates, leads to the formation of the *trans*-square species **4a**, accompanied by its *cis* isomer **4a'**, in minor concentration (equation 2).

$$[Re_4(\mu_3\text{-}H)_4(CO)_{12}] + 2pydz \rightarrow 2[Re_2(\mu\text{-}H)_2(CO)_6(\mu\text{-}pydz)] \qquad \text{(eq. 1)}$$

$$[Re_4(\mu_3\text{-}H)_4(CO)_{12}] + 2pydz \rightarrow [Re_4(\mu\text{-}H)_4(CO)_{12}(\mu\text{-}pydz)_2] \qquad \text{(eq. 2)}$$

A third reaction pathway involves the addition of three molecules of pyridazine, leading to the formation of the 64 valence electron cluster $[Re_4(\mu\text{-}H)_4(CO)_{12}(\mu\text{-}pydz)(pydz)_2]$ (**2a**), with a typical spiked triangular geometry: such species contains three ligands only, since one of them acts as four-electron donor, by bridging the cluster edge opposite to the vertex bearing the spike and from the same side of the triangle plane as the spike.

Complex **2a** is unstable in solution and slowly decomposes to give **3a** and **4a**.

Since the very beginning of the reaction, the NMR spectra revealed the presence of other minor byproducts. Among these, the most important was the species **5a** (~ 10%), identified as the triangular cluster $[Re_3(\mu\text{-}H)_3(\mu\text{-}pydz)(pydz)(CO)_9]$.

When the reaction was performed using diazines bearing substituents in the α positions the reaction path was completely different and only the formation of the dinuclear species $[Re_2(\mu\text{-}H)_2(CO)_6(\mu\text{-}1,2\text{-diazine})]$ was observed. No evidence of formation of the spiked triangle species, as well as the tetranuclear square species was observed. This is probably due to the steric hindrance of the α-substituents of the diazine ligands, which prevents the formation of some key intermediates.

The photophysical properties of the main products obtained in the reactions with pyridazine and phthalazine have been determined, showing emission from a ^{3}MLCT states ($d\pi(M) \rightarrow \pi^*(L)$), with PLQYs relatively small (the highest value being about 0.02 for **4a**).

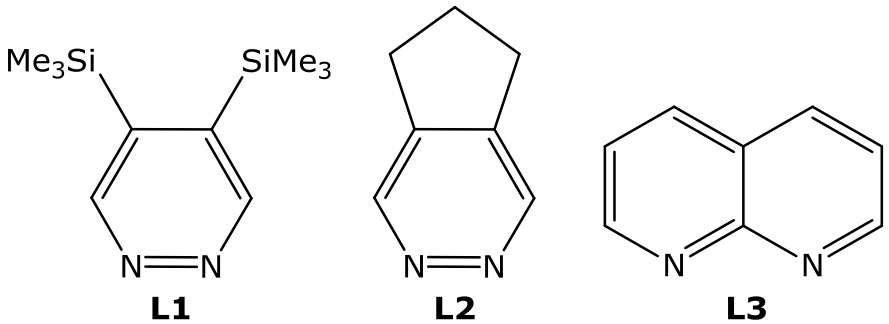

Chart 1.

We were interested in understanding how the photophysical properties of the hydrido products can be modified using different β-substituted 1,2-

diazines. We chose 4,5-bis(trimethylsilyl)pyridazine (**L1**) and 6,7-dihydro-5*H*-cyclopentapyridazine (**L2**) (Chart 1) because their corresponding dichloro complexes show very high PLQYs, in solid (**L1**) or in solution (**L2**).[4,5] Moreover, the presence of bulky substituents in the 4 and 5 positions could influence the fragmentation path of the parent clusters **1**.

Finally also the reaction of **1** with 1,8-naphthyridine (**L3**) has been investigated, in order to understand how a different steric hindrance and the capability to act both as bridging and chelating ligand could influence the reaction pathways as well as the photophysical properties of the reaction products.

5.2 Results and discussion

5.2.1 Synthesis

The synthesis of the ligands **L1** and **L2** involved a [4 + 2] Diels–Alder cycloaddition between 1,2,4,5-tetrazine and the proper dienofile (substituted alkyne or cyclopentene enamine, see Scheme 2).[6]

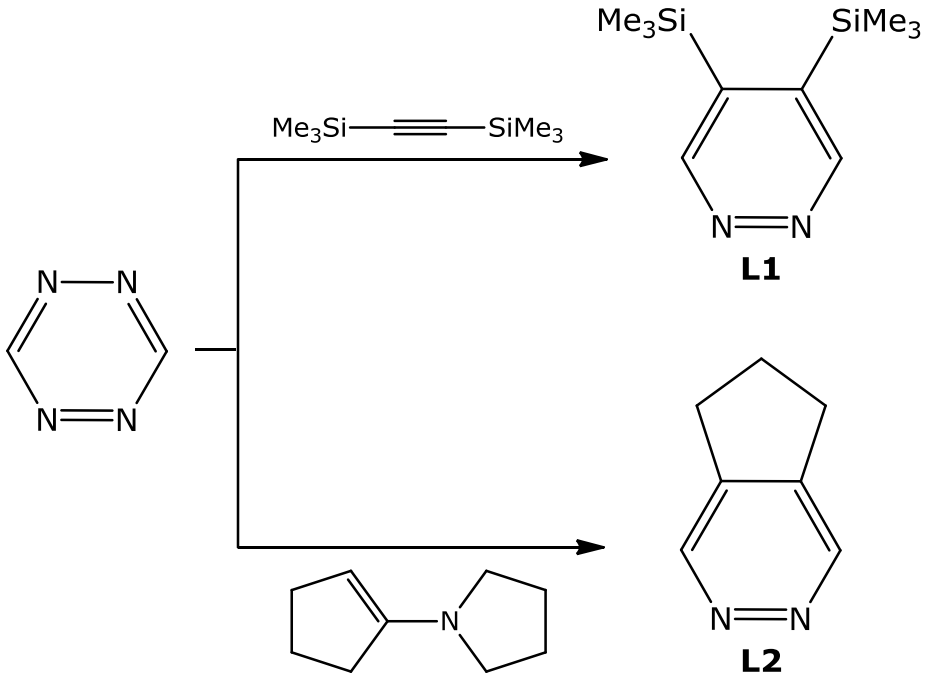

Scheme 2. Synthesis of the diazine ligands **L1** and **L2**.

5.2.1.1 Reaction of **1** with **L1**

The reaction of **1** with **L1** has been monitored by ^{1}H NMR spectroscopy (Figure 1, these species are noted by letter b). As in the case of pyridazine, the intensity of the signals in the hydride region of the spectrum (from 0 to -20 ppm) has been exploited to investigate the course of the reaction and to evaluate the amount of the different species. After 2 h the reaction is almost complete and does not further evolves.

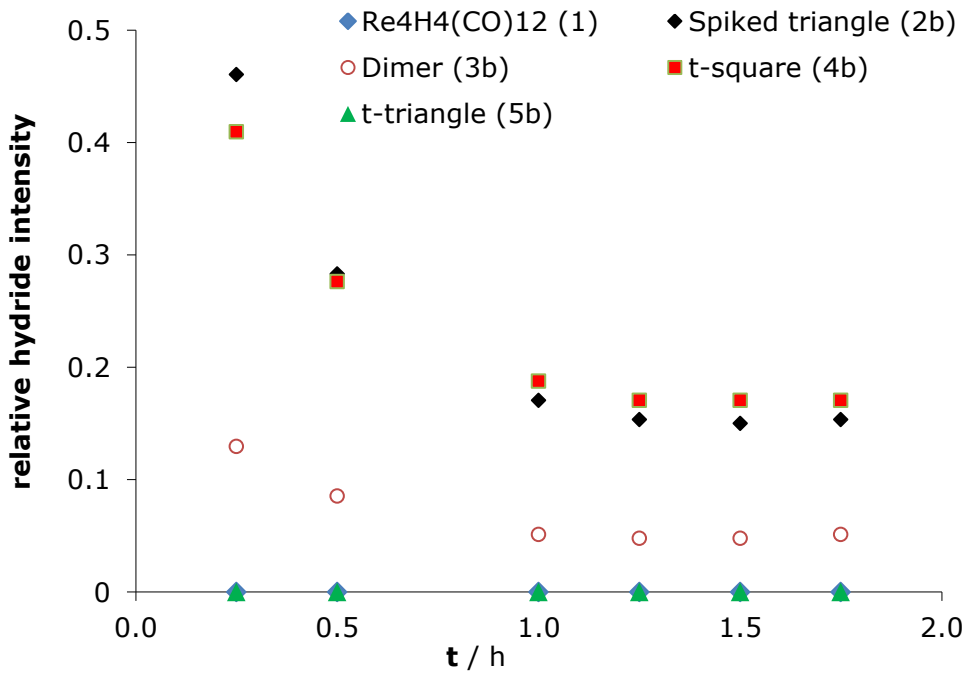

Figure 1. ^{1}H NMR monitoring of the course of the reaction of **1** with 2 equivalents of **L1** (CD_2Cl_2, 298 K). In the ordinate, the fraction of the overall hydride intensity for each species is reported.

The species initially present in the highest concentration is the complex $[Re_4(\mu\text{-}H)_4(\mu\text{-}\mathbf{L1})(\mathbf{L1})_2(CO)_{12}]$ (**2b**), with a tetranuclear spiked triangular metallic skeleton, accounting for about 50% of the overall intensity in the hydride region of the NMR spectra. Such species rapidly converts mainly into

the dimer **3b** (that is only partially soluble) and in the *trans*-square **4b** (that precipitate as an orange microcrystalline solid). Differently from the case of pyridazine, in the case of $(SiMe_3)_2$pydz (**L1**) the spike triangle species **2b** is more stable and it is present also at the end of the monitoring.

Noteworthy, the *cis*-square **4b'** is not formed, due to the steric hindrance of the $SiMe_3$ groups on the pyridazine ring. Also the amount of triangular specie **5b** is negligible. The *trans*-square species **4b** is more soluble in CD_2Cl_2 then the corresponding species with pyridazine, due to the presence of the $SiMe_3$ groups. In Table 1 are summarized the NMR data of all the species.

Complex	**4,5-$(SiMe_3)_2$pydz**		**Hydrides**
	H_3, H_6	**$SiMe_3$**	
2b	9.27 (dt, 2H)$_t$, 9.08 (t, 2H)$_b$, 9.06 (dt, 2H)$_t$,	0.45 (m, 18H)$_t$, 0.47 (m, 18H)$_t$, 0.43 (t, 18H)$_b$	-10.60 (d, 2H) -11.22 (s, 1H) -12.25 (t, 1H)
3b	8.99 (s, 2H)	0.53 (s, 18H)	-3.95 (s, 2H)
4b	9.16 (t, 4H)	0.49 (s, 36H)	-9.94 (t, 2H) -12.64 (t, 2H)
5b	9.47 (dd, 1H)$_t$, 9.09(t, 2H)$_b$, 9.00 (dd, 1H)$_t$	n.a. n.a.	-8.55 (s, 2H) -11.12 (m, 1H)

Table 1. ^{1}H NMR data of the novel complexes (δ, CD_2Cl_2, 298 K). For compounds **2b** and **5b**, the subscripts b and t indicate protons belonging to the bridging and terminal diazine ligands, respectively.

5.2.1.2 Reaction of **1** with **L2**

The reaction of **1** with **L2** showed a similar trend to the previous one (Figure 2, these species are noted by letter c), although the experiment was affected by a sub-stoichiometric amount of diazine **L2**, resulting in ~ 15% of unreacted **1**.

At the beginning of the reaction the spiked triangle derivative **2c** was present in high concentration, but rapidly it disappeared, probably also due to the defect of diazine (the cluster **2c** contains a higher diazine / Re ratio than products **3c** and **4c**). The dimeric specie **3c** was the main product at the end of the reaction.

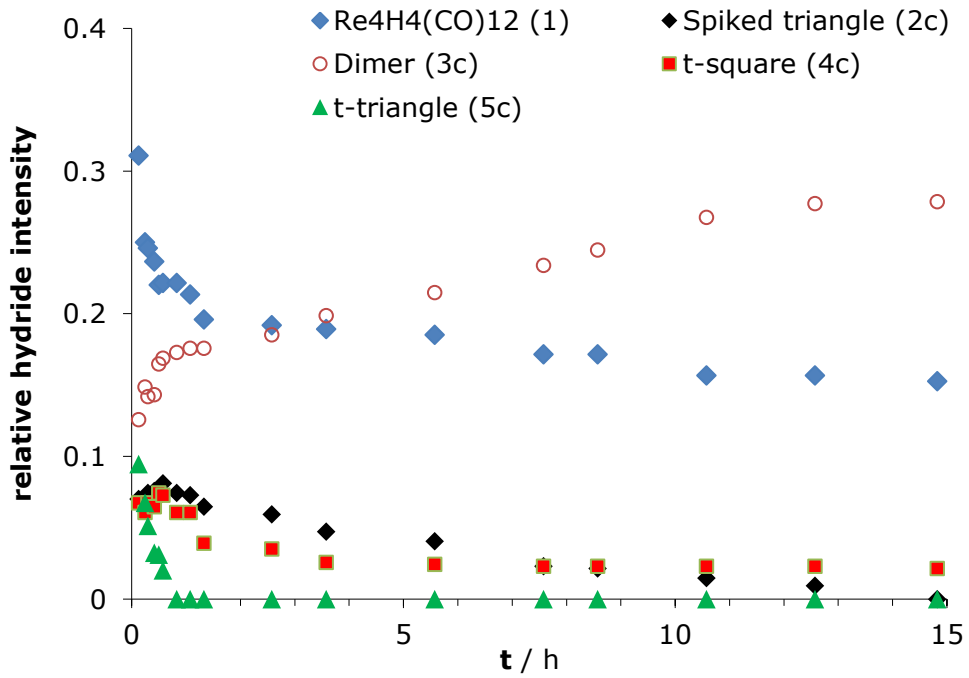

Figure 2. ^{1}H NMR monitoring of the course of the reaction of **1** with 1.7 equivalents of **L2** (CD_2Cl_2, 298 K). In the ordinate, the fraction of the overall hydride intensity for each species is reported.

The *trans*-triangle species **5c** has also been observed at the initial reaction stages, although in low concentration. Its amount then rapidly went to zero, together with a slow decrease of the parent cluster **1** and the spiked triangle **2c**, accompanied by a slow progressive increase of the dimeric species **3c**. This unusual behavior suggests that the species **5c** and **2c** can act as diazine reservoir for the parent cluster **1**, leading to a [2 + 2] fragmentation according e.g. to equation 3.

$$[Re_4(\mu_3\text{-}H)_4(CO)_{12}] + 4[Re_3(\mu\text{-}H)_3(CO)_9(\mu\text{-}\mathbf{L2})_2(\mathbf{L2})] \rightarrow 8[Re_2(\mu\text{-}H)_2(CO)_6(\mu\text{-}\mathbf{L2})] \qquad \text{(eq. 3)}$$

Differently from the analogous complex with pyridazine, the *cis*-square species **4c'** has been observed only in the precipitate, due to its poor solubility in dichloromethane.

After the addition of the residue 15% of **L2** the parent cluster **1** disappeared, and at the end of the reaction the only species present in solution was the dimeric complex **3c**.

In Table 2 are summarized the NMR data of all the species.

Complex	cyclopentapydz		Hydrides
	H_3, H_6	H_{cp}	
2c	9.51 (s, 2H)$_t$, 8.96 (m, 2H)$_b$, 8.83 (m, 2H)$_t$,	n.a.	-10.67 (d, 2H) -11.00 (s, 1H) -11.66 (t, 1H)
3c	9.08 (s, 2H)	3.05 (t, 4H) 2.35 (m, 2H)	-3.93 (s, 2H)
4c	9.33 (s, 4H)	3.32-3.10 (m, 8H) 2.36-2.27 (m, 4H)	-9.69 (m, 2H) -11.04 (m, 2H)
4c`	9.16 (t, 4H)	n.a.	-10.27 (m, 2H) -11.04 (m, 2H)
5c	9.20 (m, 1H)$_t$, 8.95 (s, 2H)$_b$, 8.87 (m, 1H)$_t$	n.a.	-9.89 (s, 2H) -11.30 (s, 1H)

Table 2. ^{1}H NMR data of the novel complexes (δ, CD_2Cl_2, 298 K). For compounds **2c** and **5c**, the subscripts b and t indicate protons belonging to the bridging and terminal diazine ligands, respectively.

5.2.1.3 Reaction of **1** with **L3**

In the case of the reaction of **1** with 1,8-naphthyridine (**L3**), at the end of the reaction only one hydride resonance was present at δ = -3.39 ppm (s, 2H), a chemical shift typical of the family on unsaturated dinuclear species **3**. This suggests the presence of the dimeric species $[Re_2(\mu\text{-}H)_2(CO)_6(\mu\text{-}\eta^2\text{-}\mathbf{L3})]$ (**3d**) as the only hydride-containing complex (Chart 2).

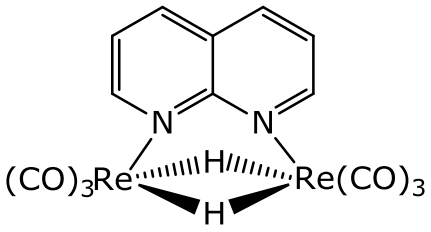

Chart 2. The dimeric species **3d**.

The presence in the aromatic region of the ^1H NMR spectrum of three resonances at 10.14 ppm (dd, 2H), 8.71 ppm (dd, 2H) and 7.76 ppm (dd, 2H) in 1:1:1 ratio with respect to the hydride intensity confirms this hypothesis. A second aromatic set is also present (Chart 3), attributed to the monomeric species $[Re(CO)_3Cl\mathbf{L3}]$, already known in literature[7], in which the naphthyridine acts as chelate ligand. The formation of the chloro complex is due to traces of HCl or $Cl^{\bullet}$ radical always present in CD_2Cl_2 solvent.

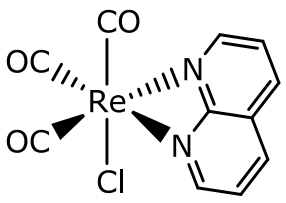

Chart 3.

As already observed for α-substituted pyridazines in preliminary experiments, the high steric hindrance of naphthyridine seems to cause the inhibition of all the fragmentation pathways of the parent cluster **1** but the formation of the monomeric species depicted in Chart 3.

5.2.2 Preliminary photophysical characterization

The experimental (electrochemical, photophysical) and computational characterization of these new complexes is still in progress. The absorption and emission spectra of the *trans*-square clusters **4b** and **4c** are shown in Figure 3. The available spectroscopic data are summarized in Table 3. As in the previously reported tetranuclear clusters with pyridazine,[3] the absorption band at 395 ÷ 420 nm are ascribed to be ^{1}MLCT transitions $d\pi$ (M) $\rightarrow$ π^*(N,N). The higher energy bands around 250-300 nm are can be ascribed to the superposition of *d-d* excitations from the t_{2g} to the e_g set of the two Re atoms and π–π^* intraligand transitions localized on the diazine ring.[8,9]

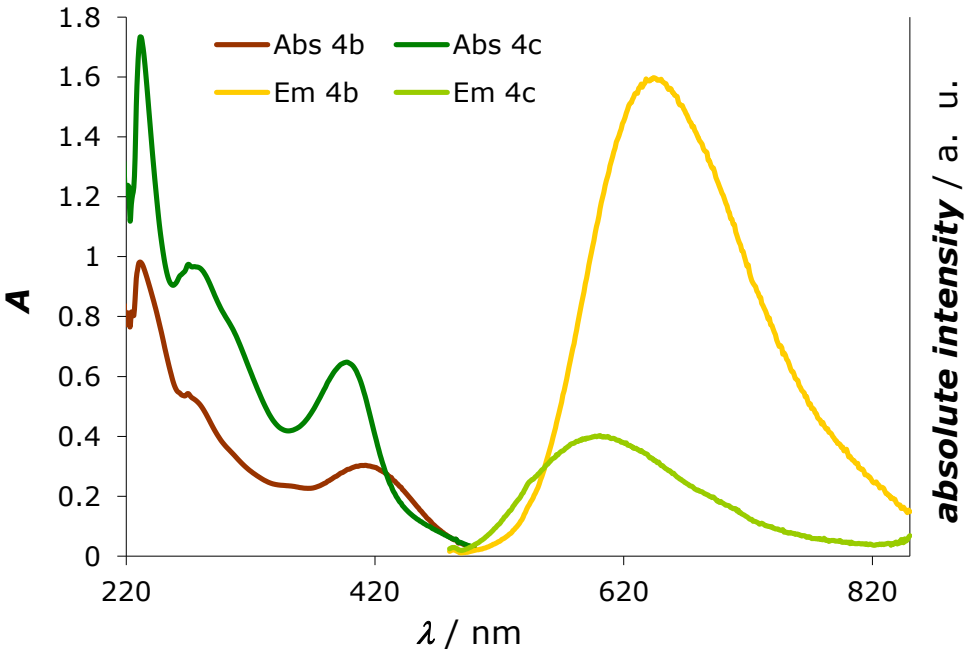

Figure 3. Absorption and emission spectra of the *trans*-square clusters **4a** with **L1** and **L2** in CH_2Cl_2 at 293 K.

In CH_2Cl_2 solution at 293 K, the novel complexes emit in the range 600 ÷ 650 nm. A blue shift is observed for the 6,7-dihydro-5*H*-cyclopentapyridazine derivative with respect to 4,5-bis(trimethylsilyl)pyridazine, due to the presence of the $SiMe_3$ groups, that allows a partial delocalization of the electron density on the silicon atoms, resulting in a small HOMO-LUMO gap of the corresponding complex. Photo luminescent quantum yields of the *trans*-square complexes **4b** and **4c**, measured in CH_2Cl_2 solution at 293 K, are lower than the corresponding *trans*-square **4a** with pyridazine.[**Errore. Il segnalibro non è definito.**3]

Complex	**X**	**λ_{abs} [nm]**	**λ_{em} [nm]**	**$\Phi_{em} \times 10^2$**
4b	**L1**	412	644	0.80
4c	**L2**	397	601	0.20
4a	**pydz**	401	611	1.7

Table 3. Preliminary absorption and emission data of *trans*-square complexes **4b**, **4c** and **4a** in (deoxygenated) CH_2Cl_2 solution at room temperature.

5.3 Conclusions

The reaction pathways of the tetranuclear clusters $[Re_4(\mu_3\text{-}H)_4(CO)_{12}]$ with β-substituted 1,2-diazine (4,5-bis(trimethylsilyl)pyridazine and 6,7-dihydro-5*H*-cyclopentapyridazine) have been investigated. The behavior is similar to those observed for the nude pyridazine, and the *trans*-square clusters are already the main species, easily isolable by precipitation. However, the presence of substituents has an influence on the fragmentation pathway of the parent cluster, due to the steric hindrance of the substituents. This behavior is very evident in the case of 1,8-naphthyridine, in which only the formation of the dimeric species has been observed, together with small amount of the mononuclear complex $[ReCl(CO)_3(1,8\text{-naphthyridine})]$.

Both the new two *trans*-square complexes are weaker emitters than the corresponding *trans*-square with pyridazine. Therefore the observed variation of luminescence does not follow the same trend of the $[Re_2(\mu\text{-}Cl)_2(CO)_6(\mu\text{-}1,2\text{-diazine})]$ compounds, indicating that no straightforward transfer of information from one class to another is possible, since the factors affecting the photophysical properties are well different in the two classes of complexes.

The electrochemical investigation of the complexes is under investigation, in order to determine the HOMO-LUMO gap of such complexes and the redox properties. The completion of the photophysical analyses is also in progress, especially in the solid state, to verify if also in this case a deep difference is present between the emission properties measured in solution and in solid, as previously reported in the case of the dichloro complexes.[4]

(1) Horng, H. C.; Cheng, C. P.; Yang, C. S.; Lee, G.-H. *Organometallics* **1996**, *15*, 2543-2547;

(2) Beringhelli, T.; D'Alfonso, G. *J. Chem. Soc., Chem. Commun*. **1994**, 2631-2632;

(3) Panigati, M.; Donghi, D.; D'Alfonso, G.; Mercandelli, P.; Sironi, A.; Mussini, P.; D'Alfonso, L. *Inorg. Chem.* **2006**, *45*, 10909-10921;

(4) Quartapelle Procopio, E.; *Mauro*, M.; Panigati, M.; Donghi, D.; Mercandelli, P.; Sironi, A.; D'Alfonso, G.; De Cola, L. *J. Am. Chem. Soc*. **2010**, *132*, 14397-14399;

(5) Mauro, M.; Quartapelle Procopio, E.; Sun, Y.; Chien, C.H.; Donghi, D.; Panigati, M.; Mercandelli, P.; Mussini, P.; D'Alfonso, G.; De Cola, L. *Adv. Funct. Mater*. **2009**, *19*, 2607-2614;

(6) Sauer, J.; Heldmann, D. K.; Hetzenegger, J.; Krauthan, J.; Sichert, H.; Schuster, J. *Eur. J. Org. Chem.* **1998**, 2885-2896;

(7) Monkowius, U.; Svartsov, Y. N.; Fischer, T.; Zabel, M.; Yersin, H. *Inorg. Chem. Commun.* **2007**, 1473-1477;

(8) Halverson, F.; Hirt, R. C. *J. Chem. Phys.* **1951**, *19*, 711-718;

(9) Hirt, R. C.; King, F. T.; Cavagnol, J. C. *J. Chem. Phys.* **1956**, *25*, 574-576.

Chapter 6

EXPERIMENTAL SECTION

In this chapter the mainly experimental characterization methodologies used in this thesis are described. These techniques comprise steady-state absorption and emission spectroscopies, time-resolved fluorescence spectroscopy and electrochemical analysis (cyclic voltammetry). The syntheses of the complexes reported in chapters 3-5 are also reported, together with the experimental details of the investigated reactions.

6.1 Experimental techniques

6.1.1 Steady-state absorption and emission spectroscopy

Considering a dilute solution of a given chromophore, which is not giving any aggregation phenomena: its absorbance $A(\lambda)$ is defined as the efficiency of light absorption at a due wavelength λ by an absorbing medium. In dilute solutions and in absence of aggregation phenomena, the absorbance follows the Lambert-Beer law, expressed by equation 1:

$$A(\lambda) = \log_{10} \frac{I_0}{I} = \varepsilon l c \qquad \text{(eq. 1)}$$

where I_0 is the intensity of the incident light, I is the intensity of the light absorption process, ε is the molar absorption coefficient (in L mol^{-1} cm^{-1}), l is the absorption path length (in cm) and c is the concentration of the absorbing species (in mol L^{-1}).

Electronic absorption spectra were recorded on Agilent 8543 spectrophotometer, at room temperature.

Emission spectra are normally recorded at a fixed excitation wavelength using a spectrofluorometer. In this thesis, steady-state emission spectra were recorded on a HORIBA Jobin-Yvon IBH FL-322 Fluorolog 3 spectrometer equipped with a 450 W xenon arc lamp, double grating excitation and emission monochromators (2.1 nm mm^{-1} dispersion; 1200 grooves mm^{-1}) and a Hamamatsu R928 photomultiplier tube or a TBX-4-X single-photon-counting detector. Figure 1 describes a general setup for measuring emission spectra.

The excitation light, generated by a Xenon lamp, passes through a monochromator: part of the light is reflected by a beam splitter to a reference channel, while the rest of the light reaches the sample. Luminescence of the sample, collected at 90° with respect to the incident light, passes through a second monochromator before reaching the detector. Emission and excitation spectra were corrected for source intensity (lamp and grating) and emission spectral response (detector and grating) by standard correction curves.

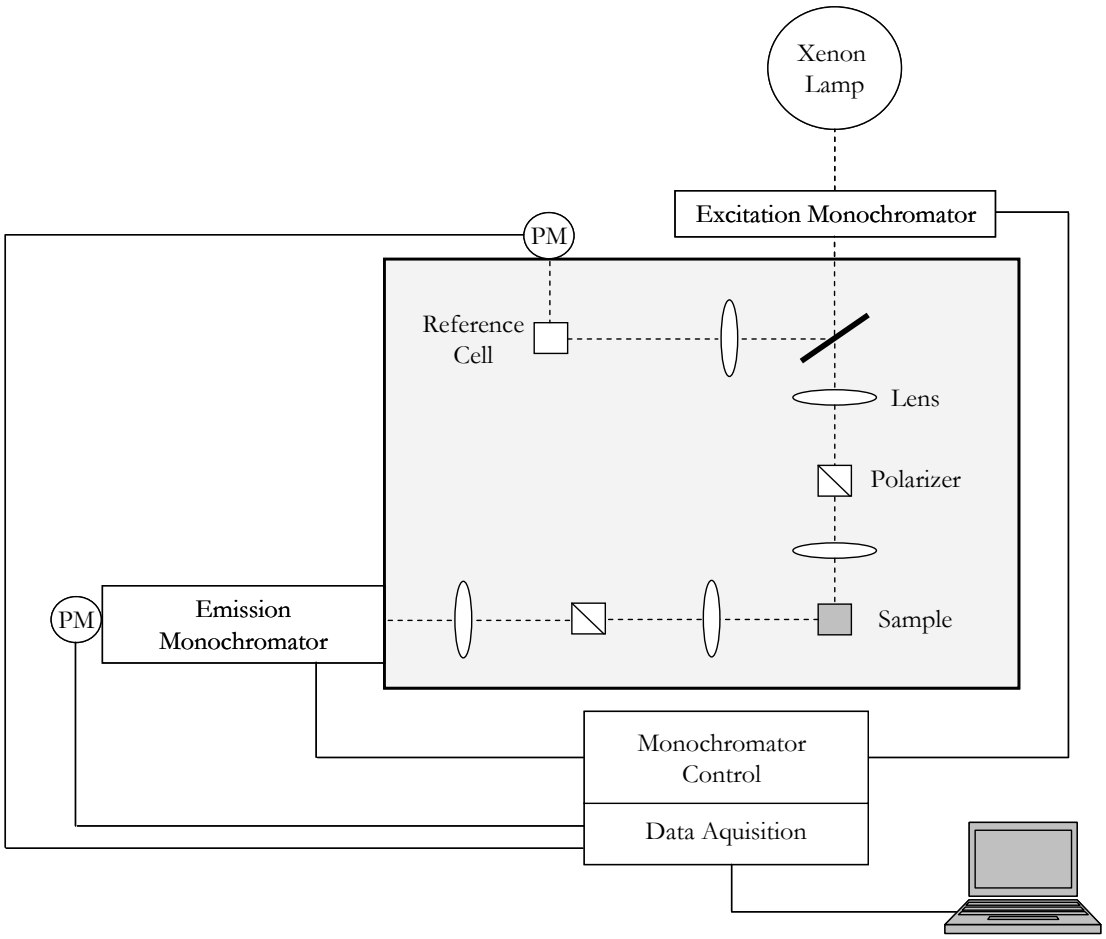

Figure 1. General scheme of a spectroflurometer with PC interface.

Luminescence quantum yields (Φ_x) were measured in optically dilute solutions (O.D. < 0.1 at excitation wavelength) and compared to reference emitters by using the Crosby and Demas method,[1] equation 2:

$$\Phi_s = \Phi_r \left[\frac{A_r}{A_s}\right]\left[\frac{n_s^2}{n_r^2}\right]\left[\frac{D_s}{D_r}\right] \qquad \text{(eq. 2)}$$

where A_r and A_s are the absorbance of the reference and the unknown sample respectively, at a given excitation wavelength λ; D_r and D_s are the integrated emission intensity the excitation wavelength λ, n_s and n_r are the refractive index of the solvents used for unknown and reference sample respectively. This equation is valid only when the reference and the sample are excited with light of the same wavelength; otherwise it has to be corrected for the relative intensities of the incident light at different wavelengths.

All solvents were spectrometric grade. The solutions have been prepared under nitrogen directly in the quartz cuvettes, by the Schlenk technique, and were further deoxygenated by bubbling N_2 for 20 minutes just before measurements. The emission intensities have been normalized to an absorption value of 0.1. Quantum yields have been determined by comparison with the emission of $[Ru(bpy)_3]Cl_2$ in water (Φ = 0.04).[2]

6.1.2 Time-resolved fluorescence spectroscopy

Dynamic fluorescence measurements have been performed with a frequency modulated phase fluorometer (Digital K2, I.S.S., Urbana IL). The excitation was accomplished by the 9 mW output of a 378 nm diode laser (I.S.S., Urbana IL). At least fifteen data at logarithmically spaced frequencies in the range 0.3 ÷ 30 MHz with a cross-correlation frequency of 400 Hz (A2D, ISS Inc., USA) have been acquired for lifetime measurements. The convenient accuracy for phase angles and modulation ratios has been of 0.2° and 0.004, respectively. Lifetime measurements have been performed under the magic angle conditions[3] and a 535 nm long pass filter (Andover Co.) has been employed in order to cut light scattering. A solution of glycogen in doubly distilled water has been used as reference sample.[4] Lifetime data fitting has been accomplished by an I.S.S. routine based on the Marquardt least squares minimization, with a two exponentials decay scheme in order to take into account the scattering contribution to the overall signal. The fit of the fluorescence intensity decay *F(t)* yields the lifetime values τ_i together with the corresponding fractional intensities f_i: $F(t) = \sum \alpha_i \, e^{-t/\tau_i}$ and $f_i = \alpha_i \tau_i / \sum \alpha_i \tau_i$ where α_i represent the pre-exponential factors.

6.1.3 Electrochemical measurements

The cyclovoltammetric analysis were carried out using an AUTOLAB PGSTAT potentiostat (EcoChemie, The Netherlands) run by a PC with GPES software. The experiments has been performed at scan rates typically ranging 0.02 to 10 V s^{-1}, in HPLC-grade acetonitrile solutions at 0.00025–0.001 M concentration in each substrate, deareated by N_2 bubbling, with tetrabutylammonium hexafluorophosphate $TBAPF_6$ (Fluka) 0.1 M as the supporting electrolyte, at 298 K. The ohmic drop has been compensated by the positive feedback technique.[5] The working electrode was a glassy carbon one (AMEL, diameter = 1.5 mm) cleaned by diamond powder (Aldrich, diameter = 1 μm) on a wet cloth (STRUERS DP-NAP); the counter electrode was a platinum wire; the reference electrode was an aqueous saturated calomel electrode, having in our working medium a difference of -0.385 V vs. the $Fc^+|Fc$ couple (the intersolvental redox potential reference currently recommended by IUPAC)[6] and +0.032 V vs. the $Me_{10}Fc^+|Me_{10}Fc$ couple (an improved intersolvental reference under investigation).[7] The normalized convoluted peak currents have been computed by the relationship $i_L/c = I_L/Ac = nFD^{1/2}$, where I_L = limiting current; i_L = limiting current density; A = electrode surface; c = substrate concentration in the bulk; n = number of transferred electrons; F = Faraday's constant = 96485 C mol^{-1} e^{-1}; D = diffusion coefficient. The pseudo first-order k' constants for the chemical reaction of the P product of the first monoelectronic oxidation step have been estimated from the following equation 3:

$$\ln\frac{[P]_t}{[P]_0} = -k't = \ln\frac{I_{p,b}}{I_{p,f}}, \text{ where } t = \frac{(E_\lambda - E_{p,f}) + (E_\lambda - E_{p,b})}{v} \qquad \text{(eq. 3)}$$

where $E_{p,f}$ and $I_{p,f}$ are the peak potential and current of the forward peak, $E_{p,b}$ and $I_{p,b}$ the peak potential and current of the backward peak, E_λ the inversion potential in the positive potential scan and v the potential scan rate.

6.1.4 Other techniques

All the reaction were performed under N_2 using the Schlenk technique and solvents deoxygenated and dried by standard methods.

Elemental analyses were performed on a Perkin Elmer CHN2400 instrument.

^{1}H NMR and ^{19}F spectra were recorded on Bruker DRX300 or DRX400 spectrometers.

IR spectra were acquired on Bruker Vector22 FT instrument.

6.2 Experimental section of Chapter 3

Pyridazine (pydz) was used as received from Aldrich. $[Re(CO)_5(OTf)]$,[8] $[Re_2(\mu\text{-}OMe)_3(CO)_6][NEt_4]$,[9] and $[Re_4(\mu_3\text{-}OH)_4(CO)_{12}]$[10] were prepared according to literature methods.

Synthesis of $[Re_2(\mu\text{-}SC_6H_5)_2(CO)_6(\mu\text{-pydz})]$ (2). A sample of $[Re(CO)_5(OTf)]$ (50 mg, 0.105 mmol) dissolved in freshly distilled THF was treated with 0.5 equivs of pyridazine (4.2 mg, 0.053 mmol) and then with 1 equiv of C_6H_5SH (12 mg, 0.105 mmol) and 1 equiv of bis(dimethylamino)naphthalene (DMAN) (22.9 mg, 0.105 mmol). The reaction mixture was refluxed for 2.5 h. A white precipitate was separated and the supernatant solution was evaporated to dryness. Separation by column chromatography on SiO_2 using ethyl acetate/dichloromethane 1:19 afforded spectroscopically pure **2** (R_F = 0.90). Isolated yield: 13 mg, 30%. IR ν(CO), CH_2Cl_2: 2035w, 2018s, 1936m, 1912m cm^{-1}. ^1H NMR (δ, CD_2Cl_2): 9.96 (pseudo t, 2H), 7.90 (pseudo t, 2H), 7.18-7.12 (m, 10H). Anal. Calcd: C, 31.50; H, 1.68; N, 3.34. Found: C, 31.42; H, 1.74; N, 3.41. Red crystals suitable for X-ray analysis were grown by slow evaporation from a CH_2Cl_2 solution at 300 K.

Synthesis of $[Re_2(\mu\text{-}OC_6F_5)_2(CO)_6(\mu\text{-pydz})]$ (3). A sample of $[Re(CO)_5OTf]$ (50 mg, 0.105 mmol) dissolved in freshly distilled CH_2Cl_2 was treated at room temperature with 1.5 equivs of C_6F_5OH (30 mg, 0.160 mmol) and 1.5 equivs of DMAN (34 mg, 0.160 mmol). After refluxing for 5 h, IR monitoring showed two

ν(CO) bands at 2023s, 1913vs cm^{-1}, attributable to $[DMANH]^+[Re_2(\mu\text{-}OC_6F_5)_3(CO)_6]^-$. The colorless solution was evaporated to dryness, dissolved in freshly distilled toluene, treated with 0.5 equiv of pyridazine (4.3 mg, 0.054 mmol) and refluxed for 3 h. The color of the solution turned to dark yellow and IR monitoring showed the disappearance of the bands of the intermediate species, substituted by the bands of **3**. ^1H NMR analysis in CD_2Cl_2 of the reaction mixture showed the presence mainly of **3**, accompanied by minor amounts of unidentified species. Separation by column chromatography on SiO_2 using dichloromethane/*n*-hexane 9:1 afforded spectroscopically pure **3** (R_F = 0.64). Isolated yields: 22 mg (47%). IR ν(CO), CH_2Cl_2: 2047w, 2033s, 1944s, 1916s; ^1H NMR (δ, CD_2Cl_2): 9.85 (pseudo t, 2H), 8.27 (pseudo t, 2H); ^{19}F NMR (α, CD_2Cl_2, 173 K): -156.7 (pseudo d, *ortho*), -161.8 (pseudo d, *ortho*), -163.7 (pseudo t, *meta*), -164.3 (pseudo t, *meta*), -164.3 (pseudo t, *para*). Anal. Calcd: C, 26.78; H, 0.41; N, 2.84. Found: C, 26.92; H, 0.48; N, 2.89. Yellow crystals suitable for X-ray analysis were grown by slow diffusion of *n*-hexane into a CH_2Cl_2 solution, at 248 K.

Synthesis of $[Re_2(\mu\text{-}OC_6H_5)_2(CO)_6(\mu\text{-pydz})]$ (4). Molten phenol was used as solvent, as follows: a sample of $[Re(CO)_5OTf]$ (60 mg, 0.126 mmol) was treated in a Schlenk tube with C_6H_5OH (6 g), 0.65 equivs of pyridazine (6.6 mg, 0.082 mmol,), 0.9 equivs of Na_2CO_3 (12 mg, 0.113 mmol), and then heated at 55°C, causing melting of phenol. The orange mixture was maintained at this temperature for 20 h, and then unreacted C_6H_5OH was sublimed under vacuum, leaving a yellow-orange residue. The solid was

suspended in THF, then the mixture was filtered and chromatographed on SiO_2, with dichloromethane/ethyl acetate 9:1. The expected product **4** was eluted first (R_F = 0.73, isolated yield 11 mg, 20%.) IR ν(CO), CH_2Cl_2: 2036w, 2021s, 1927s, 1903s cm^{-1}; ^1H NMR (δ, CD_2Cl_2): 9.83 (pseudo t, 2H), 8.20 (pseudo t, 2H), 7.31-7.26 (m, 4H), 7.00-6.92 (m, 6H). Anal. Calcd: C, 32.75; H, 1.75; N, 3.47. Found: C, 32.58; H, 1.59; N, 3.53. Yellow crystals for X-ray analysis were obtained by slow diffusion of *n*-hexane into a CH_2Cl_2 solution, at 248 K.

Synthesis of $[Re_2(\mu\text{-}OMe)_2(CO)_6(\mu\text{-}pydz)]$ (5). A sample of $[Re_2(\mu\text{-}OMe)_3(CO)_6][NEt_4]$ (43 mg, 0.057 mmol) dissolved in 5 mL of freshly distilled CH_2Cl_2, was treated with 1 equiv of pyridazine (4.4 mg, 0.057 mmol) and 1 equiv of triflic acid CF_3SO_3H (8.5 mg, 0.057 mmol). The mixture was stirred at room temperature for 6 h, than the orange-red solution was evaporated to dryness. Separation by column chromatography on SiO_2 using dichloromethane/ethyl acetate 9:1 afforded, besides the expected $[Re_2(\mu\text{-}OMe)_2(CO)_6(\mu\text{-pydz})]$ (R_F = 0.71, compound **5**), also two other species in which the methoxo groups had been in part or completely replaced by OH groups: $[Re_2(\mu\text{-OMe})(\mu\text{-OH})(CO)_6(\mu\text{-pydz})]$ (R_F = 0.24) and $[Re_2(\mu\text{-}OH)_2(CO)_6(\mu\text{-pydz})]$ (RF = 0.14, compound **6**: it was isolated by elution with neat ethyl acetate). $[Re_2(\mu\text{-}OMe)_2(CO)_6(\mu\text{-pydz})]$ (**5**). Isolated yield: 16 mg (41%). IR ν(CO), CH_2Cl_2: 2027w, 2010s, 1915s, 1892s cm^{-1}; ^1H NMR (δ, CD_2Cl_2): 9.69 (pseudo t, 2H), 8.06 (pseudo t, 2H), 4.22 (s, 6H). Anal. Calcd: C, 21.11; H, 1.48; N, 4.10. Found: C, 21.60; H, 1.61; N, 4.10.

Synthesis of $[Re_2(\mu\text{-}OH)_2(CO)_6(\mu\text{-}pydz)]$ (6). A sample of $[Re_4(\mu_3\text{-}OH)_4(CO)_{12}]$ (150 mg, 0.131 mmol) dissolved in 3 mL of water was treated with 2 equivs of pyridazine (21.0 mg, 0.262 mmol) and heated at 100°C for 4 h in a microwave oven, affording an orange precipitate and a yellow solution. The whole suspension was chromatographed on a SiO_2 column, with ethyl acetate/dichloromethane 1/1, affording spectroscopically pure **6**. Isolated yield: 111 mg, 65%. IR ν(CO), CH_2Cl_2, 2029w, 2013s, 1917s, 1892s cm^{-1}; ^1H NMR (δ, CD_2Cl_2): 9.75 (pseudo t, 2H), 8.07 (pseudo t, 2H), 1.14 (s, 2H). HR-EI MS: m/z 655.923460, calcd for $C_{10}H_6N_2O_8Re_2$:655.923945. Anal. Calcd: C, 18.35; H, 0.92; N, 4.28. Found: C, 18.83; H, 0.86; N, 3.98.

Single-Crystal X-Ray Diffraction Analysis: *Crystal data for* **2**·CH_2Cl_2. $C_{23}H_{16}Cl_2N_2O_6Re_2S_2$, M_r = 923.80, orthorhombic, space group *Pbca* (No. 61), a = 18.041(2), b = 14.442(2), c = 20.886(2) Å, V = 5441.8(11) $Å^3$, Z = 8, d_{calc} = 2.255 g cm^{-3}, T = 100(2) K, crystal size = 0.35 × 0.27 × 0.23 mm^3, μ = 9.281, λ = 0.71073 Å. Refinement of 334 parameters on 7883 independent reflections out of 68104 measured reflections (R_{int} = 0.0346, R_σ = 0.0191, $2\theta_{max}$ = 60.0°) led to R_1 = 0.0231 ($I > 2\sigma(I)$), wR_2 = 0.0545 (all data), and S = 1.087, with the largest peak and hole of 0.940 and −0.610 e $Å^{-3}$.

Crystal data for **3**. $C_{22}H_4F_{10}N_2O_8Re_2$, M_r = 986.67, orthorhombic, space group *Fdd*2 (No. 43), a = 19.395(2), b = 25.618(2), c = 10.262(2) Å, V = 5098.8(12) $Å^3$, Z = 8, d_{calc} = 2.571 g cm^{-3}, T = 150(2) K, crystal size = 0.14 × 0.11 × 0.11 mm^3, μ = 9.613, λ = 0.71073 Å. Refinement of 199 parameters on 3694 independent reflections out of 27975 measured reflections (R_{int} =

0.0606, R_σ = 0.0374, $2\theta_{max}$ = 60.0°) led to R_1 = 0.0243 ($I > 2\sigma(I)$), wR_2 = 0.0507 (all data), and S = 1.017, with the largest peak and hole of 0.894 and −0.635 e Å^{-3}.

Crystal data for **4**·½CH_2Cl_2. $C_{22.5}H_{15}ClN_2O_8Re_2$, M_r = 849.21, monoclinic, space group $P2_1/c$ (No. 14), a = 8.860(2), b = 12.518(2), c = 23.094(2) Å, β = 96.10(2)°, V = 2546.8(7) Å^3, Z = 4, d_{calc} = 2.215 g cm^{-3}, T = 295(2) K, crystal size = 0.19 × 0.07 × 0.05 mm^3, μ = 9.650, λ = 0.71073 Å. Refinement of 325 parameters on 7447 independent reflections out of 57778 measured reflections (R_{int} = 0.0540, R_σ = 0.0303, $2\theta_{max}$ = 60.0°) led to R_1 = 0.0313 ($I > 2\sigma(I)$), wR_2 = 0.0635 (all data), and S = 1.019, with the largest peak and hole of 0.985 and −0.731 e Å^{-3}.

CCDC-830740–830742 contains the crystallographic data for **2**–**4**. These data can be obtained free of charge from The Cambridge Crystallographic Data Centre.

Computational Details: Ground state geometries were optimized by means of density functional calculations. The parameter-free hybrid functional PBE0[11] was employed along with the standard valence double-ζ polarized basis set 6-31G(d,p) for C, H, Cl, N, and O. For Re and S the Stuttgart-Dresden effective core potentials were employed along with the corresponding valence triple-ζ basis set.

All the calculations were done assuming C_{2v} (for **3**–**6**) or C_2 (for **2**) symmetry. The nature of all the stationary points was checked by computing vibrational frequencies and all the species were found to be true minima.

In order to simulate the absorption electronic spectrum down to 230 nm the lowest 50 singlet excitation energies were computed by means of time-dependent density functional calculations. Calculations were done also in presence of solvent (toluene, used in most of the photophysical characterizations) described by the conductor-like polarizable continuum model (CPCM).[12]

All the calculations were done with Gaussian 03.[13]

6.3 Experimental section of Chapter 4

Pyridazine (pydz) was used as received from Aldrich. $[Re(CO)_5Cl]$,[14] $[Re(CO)_5Br]$,[15] $[Re_4(\mu_3\text{-}H)_4(CO)_{12}]$[16] and $[Re_4(\mu_3\text{-}OH)_4(CO)_{12}]$[10] were prepared according to literature methods.

Synthesis of $[Re_2(\mu\text{-}OMe)_3(CO)_6][NEt_4]$. A sample of $[Re_2(CO)_{10}]$ (230 mg, 0.30 mmol) dissolved in freshly distilled THF was treated with 8 mL of methanolic NaOMe (0.2 M). The reaction was concentrated under vacuum to eliminate the THF; the reaction mixture was allowed to release CO overnight. The solution was evaporated to dryness. The white solid was dissolved in MeOH, treated with an aqueous solution of NEt_4Cl (1.5 g, 9.05 mmol), after which a white solid was reformed again. The reaction was stored at 277 K for 2 days. The mixture was filtered and the solution was concentrated and stored at 300 K in order to further crystallize. The precipitate was washed with H_2O until the mother liquors were neutral. Isolated yield: 119.6 mg, 52%. IR ν(CO), CH_2Cl_2: 1996s, 1876s cm^{-1}.

Synthesis of $[Re_2(\mu\text{-}OH)_3(CO)_6][NEt_4]$. A sample of $[Re(CO)_5Br]$ (402 mg, 0.99 mmol) dissolved in freshly distilled THF was treated with 16 mL of NaOH (0.3 M). The reaction was concentrated under vacuum to eliminate the THF; the reaction mixture was allowed to release CO overnight. The solution was concentrated to 1/5 of the original volume, treated with NEt_4Cl (1.6 g, 9.6 mmol): a white solid was formed immediately. The reaction was stored at RT for 5 days, to allow the complete metathesis of the cation. Then the mixture

was filtered and the solution was concentrated and stored at 300 K in order to further crystallize. The precipitate was washed with H_2O until the mother liquors were neutral. Isolated yield: 110 mg, 31%. IR ν(CO), CH_2Cl_2: 1995s, 1876s cm^{-1}.

Synthesis of N,N'-diformylhydrazine $C_2H_4N_2O_2$. An slight excess (4.4 eqvs.) of formic acid (30 mL, 0.914 mmol) was added slowly to hydrazine monohydrate (10 mL, 0.206 mmol). The reaction mixture was heated at 373 K overnight. The excess of formic acid was distilled under vacuum by a gentle warming (323 K). The desired product, a white gluey solid, was suspended in EtOH, filtered and then washed with EtOH. ^{1}H NMR spectrum showed the resonance of the amidic and formylic protons at 10.05 (2H) and 8.01 (2H) ppm respectively. The splitting of these two signals and the appearance of new signals at 9.42, 8.15 and 7.92 ppm are due to the different resonance structures of the N,N'-diformylhydrazine, as reported in Scheme 1.[17]

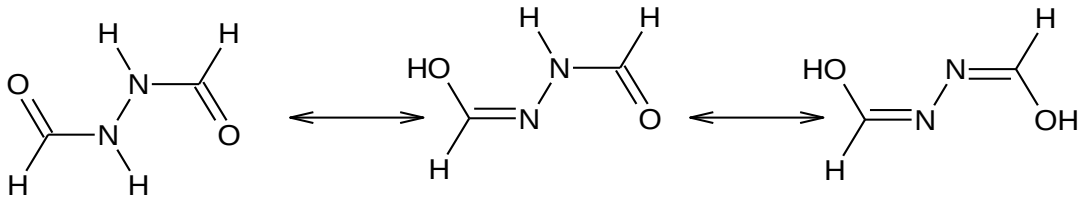

Scheme 1. Resonance structures of N,N'-diformylhydrazine.

Isolated yield: 9 mg, 50%. IR, ν, KBr: 3111 (NH), 2918s (CH), 1619 (CO) cm^{-1}. ^{1}H NMR (δ, $(CD_3)_2SO$): 10.05 (s, 2H: N*H*), 7.90-8.01 (d, s, 2H: C*H*O). Anal. Calcd: C, 27.28; H, 4.58; N, 31.81. Found: C, 27.36; H, 4.69; N, 32.01.

Synthesis of 4-(*p*-tolyl)-4*H*-1,2,4-triazole (L1). N,N'-diformylhydrazine was formed directly in situ, by reacting N-formylhydrazine (770 mg, 12.83 mmol) with triethyl orthoformate (TEOF) (3.2 mL, 19.24 mmol) in MeOH. The solution was refluxed for 3.5 h, then the solvent was removed under reduced pressure, leaving a crude orange oil. 1 equiv of *p*-toluidine (1.374 g, 12.83 mmol) was then added, and the reaction mixture was heated to 463 K for 2 h. The excess of TEOF was distilled under vacuum by warming at 353 K. The desired product, a white solid, was obtained by treating the brown residue with anhydrous Et_2O. The white precipitate is washed with Et_2O until the mother liquors were colorless. A further purification was performed by sublimation (433 K, 10 mbar). Isolated yields: 1.396 g (68%). ^{1}H NMR (δ, $CDCl_3$): 8.50 (d, 2H), 7.35 (d, 2H), 7.31 (d, 2H), 2.45 (s, 3H). Anal. Calcd: C, 67.91; H, 5.70; N, 26.40. Found: C, 65.86; H, 5.56; N, 27.56.

Synthesis of 4-(*n*-propyl)-4*H*-1,2,4-triazole (L2). N,N'-diformylhydrazine was formed directly in situ, by reacting N-formylhydrazine (770 mg, 12.83 mmol) with triethyl orthoformate (TEOF) (3.2 mL, 19.24 mmol) in MeOH. The solution was refluxed for 3.5 h, then the solvent was removed under reduced pressure, leaving a crude orange oil. 1 equiv of *n*-propylamine (1.06 mL, 12.84 mmol) was then added, and the reaction mixture was refluxed for 20 h. The excess of TEOF was distilled under vacuum by warming at 353 K. The resulting yellow oil was purified by distillation under reduced pressure. By this way the purification was not complete, as confirmed by the presence, in ^{1}H NMR spectrum, of the unreacted amine together with other unidentified signals,

responsible of about 15% of the integration. Also the position of the signals was slightly different from the literature data[18], although after addition of three drops of D_2O the signals recovered their usual position. The product was not further purified. ^{1}H NMR (δ, $CDCl_3$): 8.40 (s, 2H), 4.07 (t, 2H); 1.88 (m, 2H); 0.99 (t, 3H). ^{1}H NMR (δ, $CDCl_{3(+\ D2O)}$): 8.16 (s, 2H), 4.07 (t, 2H); 1.85 (m, 2H); 0.98 (t, 3H).

Synthesis of 4-(4'-nitrophenyl)-4*H*-1,2,4-triazole (L3). N,N'-diformyl-hydrazine was formed directly in situ, by reacting N-formylhydrazine (770 mg, 12.83 mmol) with triethyl orthoformate (TEOF) (3.2 mL, 19.24 mmol) in MeOH. The solution was refluxed for 3.5 h, then the solvent was removed under reduced pressure, leaving a crude orange oil. 1 equiv of p-nitroaniline (1.77 g, 12.83 mmol) was then added, and the reaction mixture was heated to 463 K for 2.5 h. The excess of TEOF was distilled under vacuum by warming at 353 K. The resulting yellow oil was purified by distillation under reduced pressure. The desired product, a yellow solid, was obtained by treating the orange residue with hot EtOH. Isolated yields: 1.112 g (45%). ^{1}H NMR (δ, $(CD_3)_2CO$): 9.08 (s, 2H), 8.47 (d, 2H); 8.08 (d, 2H). Anal. Calcd: C, 50.53; H, 3.18; N, 29.46. Found: C, 50.20; H, 3.24; N, 29.00.

Synthesis of [Re_2(μ-Cl)$_2$(CO)$_6$(μ-4-(*p*-tolyl)-4*H*-1,2,4-triazole)] (1). A sample of $[Re(CO)_5Cl]$ (80.6 mg, 0.221 mmol) and 4-(*p*-tolyl)-4*H*-1,2,4-triazole (17.6 mg, 0.111 mmol) was suspended in freshly distilled toluene. The reaction mixture was refluxed for 2 h, leading to a formation of a brownish

solid and an orange supernatant solution. FTIR spectrum showed the disappearance of the carbonylic band of the rhenium precursor and the appearance of four new carbonylic bands attributable to the desired complex (IR ν(CO), Toluene: 2049w, 2034s, 1943s, 1912s cm^{-1}). The supernatant solution was separated and the solvent was removed under reduced pressure. The solid thus obtained was washed two times with a small amount of CH_3Cl, leading to the formation of a grey precipitate and an orange supernatant solution that was collected with the previous one. The resulting supernatant solutions were dried again, and the precipitate underwent the same treatment previously described. Isolated yields: 51.4 mg (60%). IR ν(CO), CH_2Cl_2: 2049w, 2033s, 1940s, 1914s cm^{-1}; ^{1}H NMR (δ, $(CD_3)_2CO$): 10.38 (s, 2H), 7.94 (d, 2H); 7.55 (d, 2H); 2.48 (s, 3H). Anal. Calcd: C, 23.38; H, 1.65; N, 5.54. Found: C, 22.13; H, 1.65; N, 4.71.

Synthesis of $[Re_2(\mu\text{-}Cl)_2(CO)_6(\mu\text{-}4\text{-}(n\text{-propyl})\text{-}4H\text{-}1,2,4\text{-triazole})]$ (2). A sample of $[Re(CO)_5Cl]$ (80.1 mg, 0.216 mmol) and 4-(*n*-propyl)-4*H*-1,2,4-triazole (10 µL, 0.096 mmol) was suspended in freshly distilled toluene. The slight excess of $[Re(CO)_5Cl]$ with respect to the stoichiometric was due to the presence of an estimated 15% of impurity in the triazole reagent. The reaction mixture was refluxed for 2 h, after which the solution remained clear and colorless. FTIR spectrum showed the disappearance of the carbonylic band of the rhenium precursor and the appearance of four new carbonylic bands attributable to the desired complex (IR ν(CO), Toluene: 2048w, 2033s, 1942s, 1911s cm^{-1}). The solution was evaporated to dryness. Separation by column

chromatography on SiO_2 using ethyl acetate/dichloromethane 8:2 afforded spectroscopically pure the desired product (R_F = 0.90). Isolated yields: 29 mg (41%). IR ν(CO), CH_2Cl_2: 2049w, 2033s, 1940s, 1914s cm^{-1}; ^1H NMR (δ, $(CD_3)_2CO$): 9.93 (s, 2H), 4.56 (t, 2H); 2.21 (m, 2H); 1.11 (t, 3H). Anal. Calcd: C, 18.29; H, 1.26; N, 5.82. Found: C, 18.95; H, 1.26; N, 5.56.

Synthesis of $[Re_2(\mu\text{-}Cl)_2(CO)_6(\mu\text{-}4\text{-}(4'\text{-nitrophenil})\text{-}4H\text{-}1,2,4\text{-triazole})]$ (3). A sample of $[Re(CO)_5Cl]$ (50.1 mg, 0.139 mmol) and 4-(4'-nitrophenil)-4*H*-1,2,4-triazole (17.6 mg, 0.111 mmol) was suspended in freshly distilled toluene. The reaction mixture was refluxed for 1 h, after which the solution turned clear blue with a yellow precipitate. FTIR spectrum showed the disappearance of the carbonylic band of the rhenium precursor and the appearance of four new carbonylic bands attributable to the desired complex (IR ν(CO), Toluene: 2050w, 2035s, 1945s, 1913s cm^{-1}). The supernatant solution was separated and the solvent was removed under reduced pressure. The yellow solid thus obtained was collected together with the initial precipitate Separation by column chromatography on SiO_2 using ethyl acetate /dichloromethane 8:2 afforded spectroscopically pure the desired product (R_F = 0.90). Isolated yields: 57 mg (52%). IR ν(CO), CH_2Cl_2: 2050w, 2035s, 1944s, 1917s cm^{-1}; ^1H NMR (δ, $(CD_3)_2CO$): 10.63 (s, 2H), 8.61 (d, 2H); 8.46 (d, 2H). Anal. Calcd: C, 20.98; H, 0.75; N, 6.99. Found: C, 21.63; H, 0.95; N, 6.99.

Synthesis of $[Re_2(\mu\text{-}1,2,4\text{-triazolate})_3(CO)_6][NEt_4]$. Molten triazole was used as solvent, as follows: a sample of $[Re_2(\mu\text{-}OH)_3(CO)_6][NEt_4]$ (60.3 mg, 0.084 mmol) was treated in a Schlenk tube with 1,2,4-triazole (300 mg) and then heated at 140°C, causing melting of triazole. The colorless mixture was maintained at this temperature for 5 h, after which the formation of a white precipitate was observed. Then unreacted triazole was sublimed under vacuum, affording spectroscopically pure the desired product. Isolated yields: 22 mg (30%). IR ν(CO), CH_2Cl_2: 2016s, 1908s cm^{-1}; ^1H NMR (δ, $(CD_3)_2CO$): 8.25 (s, 6H), 3.46 (q, 8H); 1.41 (tt, 12H); ^{13}C NMR (δ, $(CD_3)_2CO$): 155.9 (N*C*N), 52.1 (*C*H_2); 6.7 (*C*H_3). Anal. Calcd: C, 27.46; H, 2.99; N, 16.01. Found: C, 27.00; H, 2.98; N, 17.18.

Alternative synthesis of $[Re_2(\mu\text{-}OH)_2(CO)_6(\mu\text{-pydz})]$. A sample of $[Re_4(\mu_3\text{-}OH)_4(CO)_{12}]$ (150 mg, 0.013 mmol) was dissolved in water, then pyridazine (19 µL, 0.026 mmol) was added. The solution was heated at 100°C in a microwave oven for 4 h, after which a white precipitate was formed. The entire solution was evaporated to dryness, leading to a white solid. Separation by column chromatography on SiO_2 using ethyl acetate/dichloromethane 1:1 afforded spectroscopically pure the desired product. Isolated yields: 111 mg (65%). IR ν(CO), CH_2Cl_2: 2029m, 2012s, 1916s, 1892s cm^{-1}; ^1H NMR (δ, CH_2Cl_2): 9.80 (t, 2H), 8.07 (t, 2H).

Synthesis of $[Re_2(\mu\text{-}OMe)(\mu\text{-}1,2,4\text{-triazolate})_2(CO)_6][NEt_4]$. Molten 1,2,4-triazole was used as solvent, as follows: a sample of $[Re_2(\mu\text{-}OMe)_3(CO)_6][NEt_4]$ (63.4 mg, 0.083 mmol) was treated in a Schlenk tube with 1,2,4-triazole (350 mg) and then heated at 140°C, causing melting of triazole. The colorless mixture was maintained at this temperature for few minutes, then rapidly cooled to RT. The resulting solid was suspended in H_2O, the solution was filtered and the solid was abundantly washed with water to eliminate the excess of triazole, affording spectroscopically pure the desired product. Isolated yields: 53 mg (76%). IR ν(CO), CH_2Cl_2: 2017m, 2006s, 1899s, 1885s cm^{-1}; ^1H NMR (δ, $(CD_3)_2CO$): 8.10 (s, 4H), 4.44 (s, 3H), 3.51 (q, 8H), 1.44 (tt, 12H) Anal. Calcd: C, 27.24; H, 3.25; N, 11.70. Found: C, 27.29; H, 3.29; N, 11.75.

Reaction between $[Re_4(\mu_3\text{-}H)_4(CO)_{12}]$ and 4-(*p*-tolyl)-4*H*-1,2,4-triazole)] (1). A sample of $[Re_4(\mu_3\text{-}H)_4(CO)_{12}]$ (5.8 mg, 4.6 μmol) was dissolved in 1.2 mL of CD_2Cl_2 directly in a NMR tube, then $[Et_4N][BF_4]$ (1.7 mg, 7.8 μmol) was added as internal standard. The solution was cooled at 195 K and **1** (1.8 mg, 10 μmol) was added. After a rapid stirring at RT, the reaction was followed by ^1H NMR spectroscopy. The reaction has been monitored by ^1H NMR spectroscopy (Figure 2).

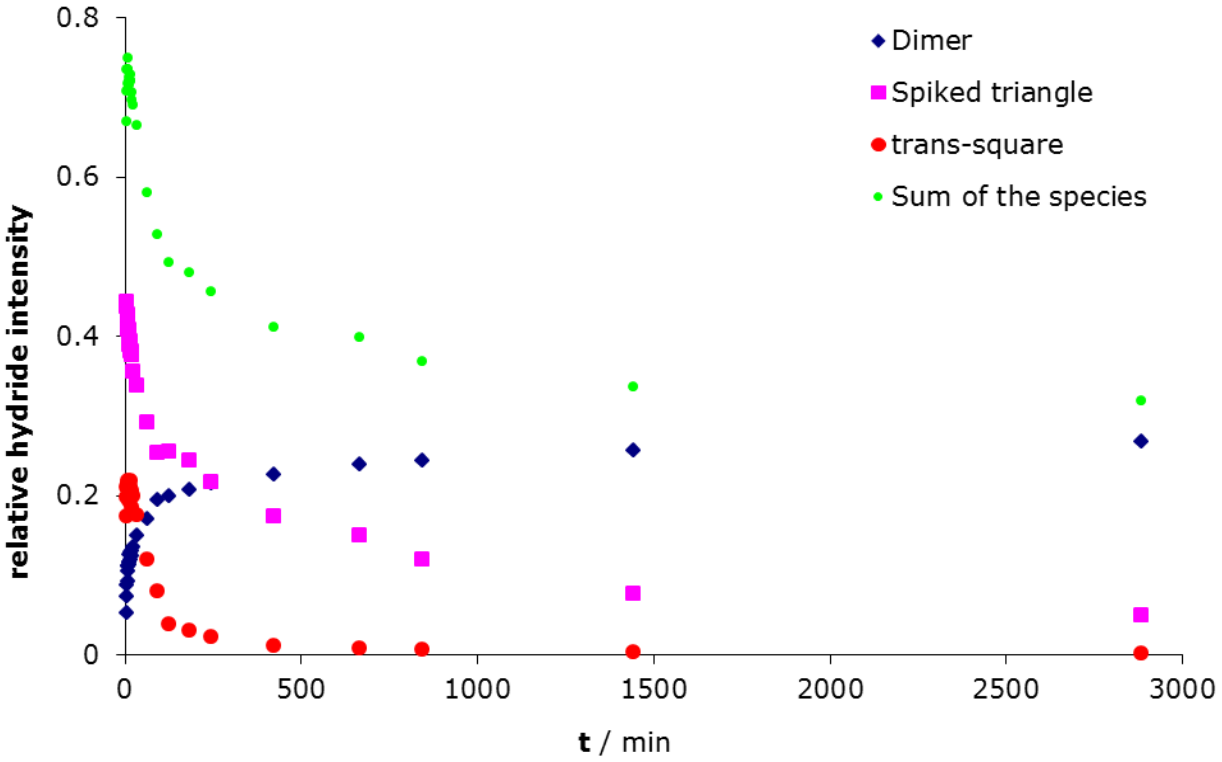

Figure 2. ^{1}H NMR monitoring of the course of the reaction of $[Re_4(\mu_3\text{-}H)_4(CO)_{12}]$ with 4-(*p*-tolyl)-4*H*-1,2,4-triazole) (CD_2Cl_2, 298 K). In the ordinate, the fraction of the overall hydride intensity for each species is reported.

As in the case of 1,8-phthalazyne (see chapter 5.2.1.3), at the end of the reaction only the dimeric species is present, confirming the role of the substituents on the aromatic ring in the fragmentation path of the parent Re(I) cluster.

Stability of [$Re_2(\mu\text{-}Cl)_2(CO)_6$(μ-4-(*p*-tolyl)-4*H*-1,2,4-triazole)] (1) in CD_3CN. Few milligrams of **1** was dissolved in 500 μL of CD_3CN directly in a NMR tube. The stability of the complex was followed by ^1H NMR spectroscopy (Figure 3). After few hours the appearance of new peaks showed the partial degradation of the dimer.

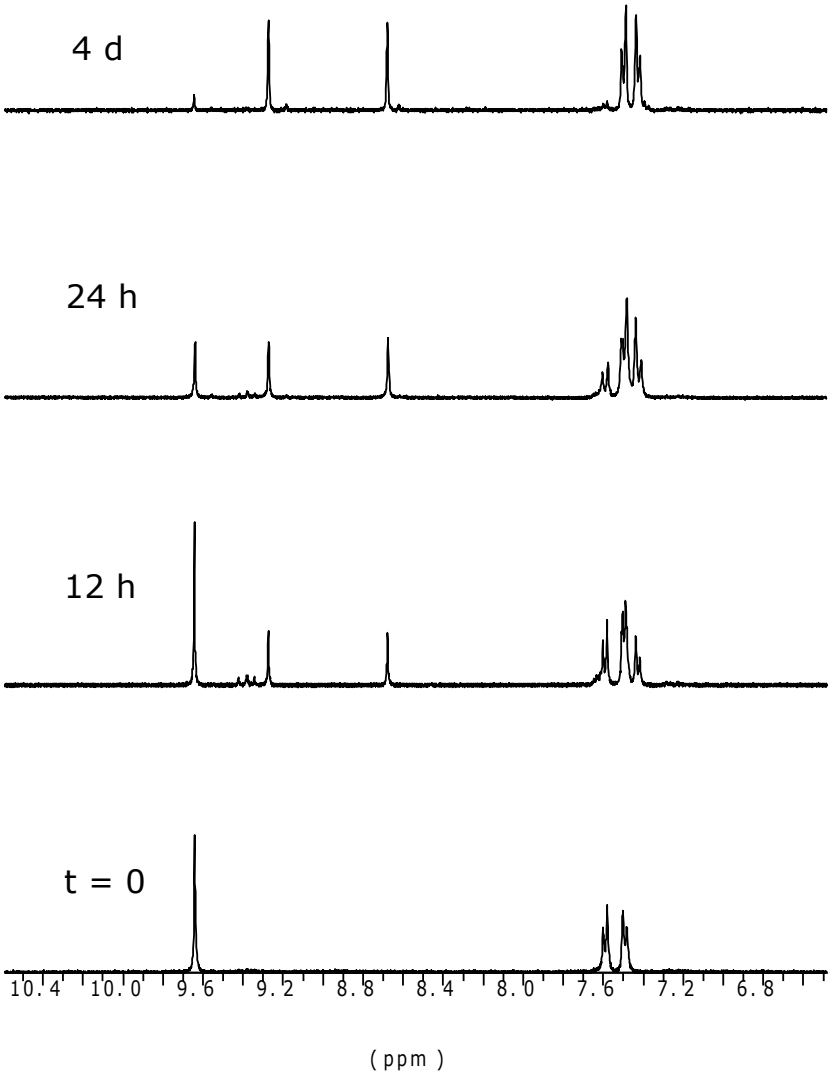

Figure 3. Aromatic region of the protonic spectrum of **1** in CD_3CN at different times. The appearance of new signals indicates the degradation of the product.

The reaction was also monitored by IR spectroscopy, performed in CH_3CN. After 4 days the carbonylic bands assumed the typical pattern of a mononuclear complex, confirming the instability of the dimer in acetonitrile (Figure 4).

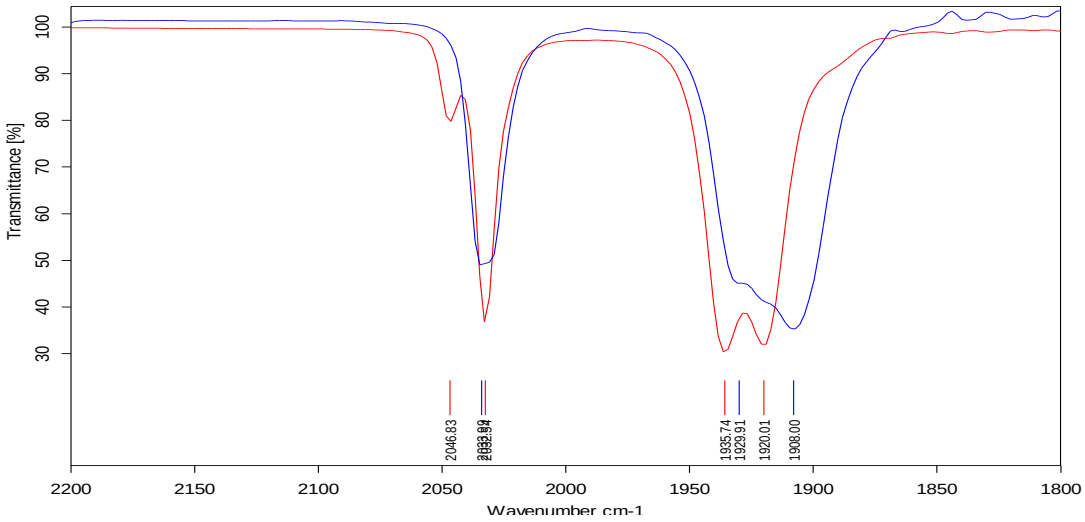

Figure 4. IR spectra of **1** in CH_3CN at t = O (red) and after 4 days (blue). A clearly degradation of the product is visible.

Attempts of substitution of triazole with pyridazine in [Re_2(μ-Cl)$_2$(CO)$_6$(μ-4-(*p*-tolyl)-4*H*-1,2,4-triazole)] (1). A sample of **1** (5 mg, 6.5 μmol) was dissolved in CH_2Cl_2, then pyridazine (0.9 μL, 13.0 μmol) was added. The solution was stirred overnight, than an IR spectra was recorded. No difference could be observed with respect to the initial spectrum of the complex, indicating that, at RT, no substitution occurred. The solution is then evaporated to dryness, dissolved in toluene and refluxed. After 5 h the colorless solution turned pale yellow; an IR spectrum showed new carbonylic bands at 2048w, 2026s, 1942s, 1920s, 1906s cm^{-1}. ^1H NMR spectrum ($(CD_3)_2CO$) showed the presence of signals in the

aromatic region at 8.92 and 9.37 ppm, ascribed to a terminal triazole. The presence of a small resonance at 10.39 ppm is attributable to a μ_2-coordinated triazole, while two resonances at 7.95 and 9.74 ppm are characteristic of pyridazine rings symmetrically coordinated.

The same reaction was performed with an excess of pyridazine. A sample of **1** (5 mg, 6.5 μmol) was dissolved in toluene, then pyridazine (2.0 μL, 22.6 μmol) was added. The solution was refluxed for 5 h. No difference appeared in the IR spectra with respect to the previous reaction.

Synthesis of tetrazole complexes. A sample of 5-phenyl-3-*t*-butyl-tetrazole (**L4**) (6.0 μL, 0.028 mmol) was dissolved in 1 mL of toluene-d^8 directly in a NMR tube, then $[Re(CO)_5Cl]$ (20.4 mg, 0.055 mmol) was added. The solution was refluxed for 5 h, and a formation of a white crystalline precipitate was observed. An IR monitoring of the reaction showed a variation of the carbonylic bands with respect to the rhenium precursor. Crystals were isolated from the solution, but their geminate nature prevented the possibility to obtain a XRD crystal structure. ^{1}H NMR characterization of the white crystals was performed, showing the presence of multiple overlying resonances in the aromatic region.

The toluene supernatant solution and the crystals were collected again and evaporated to dryness. Separation by column chromatography on SiO_2 using dichloromethane/hexane 6:4 afforded two main fraction, both constituted by two different species (in different ratio). Because of the difficulty of further purification, both the fraction were crystallized by slow diffusion of *n*-hexane into a CH_2Cl_2 solution, at 248 K, obtaining crystals suitable for X-ray analysis.

The same reaction was performed with an excess of $[Re(CO)_5Cl]$ in order to investigate the capability of the tetrazole to act as bridge between two $Re(\mu\text{-}Cl)_2Re$ units. **L4** (2.1 mg, 0.010 mmol) was dissolved in 1 mL of toluene-d^8 directly in a NMR tube, then $[Re(CO)_5Cl]$ (19 mg, 0.050 mmol) was added. The solution was refluxed for 2 h, after which a formation of a beige precipitate was observed. ^1H NMR spectrum of the supernatant solution showed the absence of the tetrazolic signals, meaning that all the tetrazole was in the precipitate. The precipitate was isolated, and crystals suitable for XRD analysis were obtained by slow diffusion of *n*-hexane into a CH_2Cl_2 solution, at 248 K, showing the presence, among the other products, of the tetranuclear complex **6**.

6.4 Experimental section of Chapter 5

1,8-naphthyridine (**L3**) was used as received from Aldrich. $[Re_4(\mu_3\text{-}H)_4(CO)_{12}]$[16] (**1**), 4,5-bis(trimethylsylil)pyridazine (**L1**) and 6,7-dihydro-5*H*-cyclopentapyridazine (**L2**)[19] were prepared according to literature methods.

Reaction between 1 and L1. A sample of **1** (9.5 mg, 7.6 μmol) was dissolved in 500 μL of CD_2Cl_2 directly in a NMR tube, then **L1** (3.6 mg, 16.1 μmol) was added. The color of the solution immediately turned from brownish red to orange. The reaction was monitored by ^1H NMR spectroscopy for one week. The intensity of the signals in the hydride region of the spectrum (from 0 to -20 ppm) was chosen as parameter to investigate the course of the reaction and to evaluate the amount of the different species. After 2 h the reaction was almost complete and did not further evolve. After 5 days an orange precipitate was separated and the supernatant solution was evaporated to dryness. The precipitate was almost exclusively constituted of the *trans*-square species **4b**. Separation of the residue of the supernatant solution by column chromatography on SiO_2 using dichloromethane/*n*-hexane 7:3 afforded spectroscopically pure the dimeric species **3b** (RF = 0.66). ^1H NMR data of all the species are discussed in Table 1 of Chapter 5. Orange crystals of **4b** were obtained by slow diffusion of *n*-hexane into a CH_2Cl_2 solution, at 248 K.

Synthesis of $[Re_4(\mu\text{-}H)_4(CO)_{12}(\mu\text{-}L1)_2]$ (4b). A sample of **1** (57 mg, 46 μmol) was dissolved in 5 mL of CH_2Cl_2, then **L1** (21 mg, 92 μmol) was added. The solution was stirred overnight; then the precipitate was separated from solution. The orange precipitate was dried without further purification, affording spectroscopically pure **4b.** Isolated yield: 33 mg (46%). IR ν(CO), CH_2Cl_2: 2040s, 2017vs, 1984vs, 1925s cm^{-1}.

Reaction between 1 and L2. A sample of **1** (12.1 mg, 9.75 μmol) was dissolved in 700 μL of CD_2Cl_2 directly in a NMR tube, then **L2** (2.3 mg, 19 μmol) was added. The color of the solution turned yellow and then brown after vigorous stirring. The reaction was monitored by ^1H NMR spectroscopy for 30 h. The intensity of the signals in the hydride region of the spectrum (from 0 to -20 ppm) was chosen as parameter to investigate the course of the reaction and to evaluate the amount of the different species. The presence of unreacted **1** (~ 15%) after 20 h suggested that a sub-stoichiometric amount of diazine **L2** was present; then a second addition of **L2** was performed (0.6 mg, 5 μmol). After 10 h the reaction was almost complete and did not further evolve. An orange precipitate was separated. The precipitate was almost exclusively constituted of the *trans*-square species **4c**. ^1H NMR data of all the species are discussed in Table 2 of Chapter 5.

Synthesis of $[Re_4(\mu\text{-}H)_4(CO)_{12}(\mu\text{-}L2)_2]$ (4c). A sample of **1** (79 mg, 64 μmol) was dissolved in 10 mL of CH_2Cl_2, then **L2** (15 mg, 128 μmol) was added. The solution was stirred overnight, then the yellow precipitate was separated from solution. The precipitate was dried without further purification, affording spectroscopically pure **4c.** Isolated yield: 51 mg (60%). IR ν(CO), CH_2Cl_2: 2038s, 2015vs, 1983vs, 1920s cm^{-1}.

Reaction between 1 and L3. A sample of **1** (5.0 mg, 4.1 μmol) was dissolved in 500 μL of CD_2Cl_2 directly in a NMR tube, then **L3** (1.1 mg, 8.2 μmol) was added. The color of the solution immediately turned orange. The solution was stirred overnight. The reaction was monitored by ^1H NMR spectroscopy for 24 h. The intensity of the signals in the hydride region of the spectrum (from 0 to -20 ppm) was chosen as parameter to investigate the course of the reaction and to evaluate the amount of the different species. After 4 h the reaction was almost complete and did not further evolve. A red precipitate was separated and dissolved again in CD_2Cl_2. A mixture of the dimeric species $[Re_2(\mu\text{-}H)_2(CO)_6(\mu\text{-}\eta^2\text{-}\mathbf{L3})]$ (**3d**) and the monomeric species $[Re(CO)_3Cl\mathbf{L3}]$ was present. ^1H NMR data are discussed in Chapter 5 (Paragraph 5.2.1.3).

(1) Crosby, G. A.; Demas, J. N. *J. Am. Chem. Soc.* **1970**, *92*, 7262-7270;

(2) Ishida, H.; Tobita, S.; Hasegawa, Y.; Katoh, R.; Nozaki, K. *Coord. Chem. Rev.* **2010**, *254*, 2449-2458;

(3) Lakowicz, J. R. *Principles of Fluorescence Spectroscopy*, 2nd ed., Kluver Academic/Plenum Publishers, New York, 1999;

(4) Collini, M.; Chirico, G.; Baldini, G.; Bianchi, M. E. *Biopolymers* **1995**, *36*, 211–225;

(5) Bard, A. J.; Faulkner, L. R. *Electrochemical Methods. Fundamentals and Applications*; Wiley, New York, 2002, pp. 648–650;

(6) a) Gritzner, G.; Kuta, J. *Pure Appl. Chem.* **1984**, 56, 461–466; b) Gritzner, G. *Pure Appl. Chem.* **1990**, *62*, 1839–1858;

(7) a) Noviandri, I.; Brown, K. N.; Fleming, D. S.; Gulyas, P. T.; Lay, P. A.; Masters, A. F.; Phillips, L. *J. Phys. Chem. B* **1999**, *103*, 6713–6722; b) Ruiz, J.; Astruc, D. *Comptes Rendus Acad. Sci., Série IIc: Chemie* **1998**, I, 21–27; c) Falciola, L.; Gennaro, A.; Isse, A. A.; Mussini, P. R.; Rossi, M. *J. Electroanal. Chem.* **2006**, *593*, 47–56;

(8) Schmidt, S. P.; Nitschke, J.; Trogler, W. C. *Inorg. Synth.* **1989**, *26*, 113–117;

(9) a) Ciani, G.; D'Alfonso, G.; Freni, M.; Romiti, P.; Sironi, A. *J. Organomet. Chem.* **1978**, *152*, 85–94; b) Jiang, C.; Wen, Y.-S.; Liu, L.-K.; Hor, T. S. A.; Yan, Y. K. *Organometallics* **1998**, *17*, 173–181;

(10) Herberhold, M.; Süss, G.; Ellermann, J.; Gäbelein, H. *Chem. Ber*. **1978**, *111*, 2931–2941;

(11) Called PBE1PBE in Gaussian;

(12) a) Adamo, C.; Barone, V. *J. Chem. Phys.* **1999**, *111*, 6158–6170; b) Perdew, J. P.; Burke, K.; Ernzerhof, M. *Phys. Rev. Lett.* **1996**, *77*, 3865–3868; c) Perdew, J. P.; Burke, K.; Ernzerhof, M. *Phys. Rev. Lett*. **1997**, *78*, 1396;

(13) Gaussian 03 (revision C.02), Gaussian Inc., Wallingford, CT, **2004**;

(14) Appel, M.; Heidrich, J.; Beck, W. *Chemische Berichte* **1987**, *120*, 1087-1090;

(15) Kutal, C.; Weber, M. A.; Ferraudi, G.; Geiger, D. *Organometallics* **1985**, *4*, 2161-2166;

(16) a) Andrews, M.A.; Kirtley, S.W.; Kaesz, H.D. *Inorg. Chem.* **1977**, *16*, 1556-1561; b) Johnson, J.R.; Kaesz, H.D. *Inorg. Synth.* **1978**, *18*, 60-62;

(17) Bhargavi, G.; Sireesha, B.; Devi, C.S. *Proc. Indian Acad. Sci. (Chem. Sci.)* **2003**, *115*, 23-28;

(18) Yasuda, T; Imase, T; Sasaki, S; Yamamoto, T. *Macromolecules* **2005**, *38*, 1500-1503.

(19) Sauer, J.; Heldmann, D. K.; Hetzenegger, J.; Krauthan, J.; Sichert, H.; Schuster, J. *Eur. J. Org. Chem.* **1998**, 2885-2896.